

300yo.

NATIONAL AERONAUTICS AND SPACE ADMINISTRATION

Technical Report No. 32-813

Mariner-Mars Science Subsystem

F. L. Schutz et al

GPO PRICE \$ \_\_\_\_\_

CFSTI PRICE(S) \$ \_\_\_\_\_

Hard copy (HC) 3.00

Microfiche (MF) 175

ff 653 July 65

**N66 36306**  
 (ACCESSION NUMBER)  
105  
 (PAGES)  
CR-77906  
 (NASA CR OR TMX OR AD NUMBER)

**N66 36318**  
 (THRU)  
1  
 (CODE)  
31  
 (CATEGORY)



JET PROPULSION LABORATORY  
CALIFORNIA INSTITUTE OF TECHNOLOGY  
PASADENA, CALIFORNIA


August 15, 1966

NATIONAL AERONAUTICS AND SPACE ADMINISTRATION

*Technical Report No. 32-813*

***Mariner-Mars Science Subsystem***

*F. L. Schutz et al*



---

Robert V. Meghrebian, Manager  
Space Sciences Division

**JET PROPULSION LABORATORY  
CALIFORNIA INSTITUTE OF TECHNOLOGY  
PASADENA, CALIFORNIA**

August 15, 1966

Copyright © 1966  
Jet Propulsion Laboratory  
California Institute of Technology  
Prepared Under Contract No. NAS 7-100  
National Aeronautics & Space Administration

## CONTENTS

<b>I. The Mariner-Mars Science Subsystem</b> by Frank L. Schutz . . . . .	1	✓
A. Introduction . . . . .	1	
B. The Mission . . . . .	1	
C. The Spacecraft . . . . .	6	
<b>II. Science Subsystem</b> by W. G. Fawcett . . . . .	11	✓
A. General Description . . . . .	11	
B. Physical Characteristics . . . . .	11	
C. Functional Characteristics and Constraints . . . . .	11	
D. Preassembly and Prelaunch Testing . . . . .	14	
E. Operation . . . . .	14	
F. Data Format . . . . .	17	
<b>III. Cosmic-Ray Telescope</b> by J. A. Simpson and J. J. O'Gallagher . . . . .	19	✓
A. Purpose and Objectives . . . . .	19	
B. Theory . . . . .	19	
C. Procedure . . . . .	20	
D. Description of Equipment . . . . .	22	
<b>IV. Cosmic-Dust Detectors</b> by D. K. Schofield . . . . .	23	✓
A. Purpose . . . . .	23	
B. Description . . . . .	23	
C. Function . . . . .	24	
D. Summary . . . . .	24	
<b>V. Trapped-Radiation Detectors</b> by D. K. Schofield, D. Chinburg, and D. Enemark . . . . .	26	✓
A. Purpose . . . . .	26	
B. Description and Function . . . . .	26	
<b>VI. Ionization Chamber</b> by I. G. Despain and H. A. Andersen . . . . .	29	✓
A. Introduction . . . . .	29	
B. Scientific Objectives . . . . .	29	
C. Constraints and Requirements . . . . .	29	
D. Functional Description . . . . .	30	
E. Physical Description . . . . .	32	
F. Design Evolution . . . . .	34	
G. Calibration . . . . .	34	
H. Instrument Failure . . . . .	35	

**CONTENTS (Cont'd)**

<b>VII. Plasma Probe</b> by R. A. Graham . . . . .	36 ✓
A. Experimental Objectives . . . . .	36
B. General Theory of Operation . . . . .	36
C. Instrument Program . . . . .	38
D. Construction . . . . .	43
E. Results on <i>Mariner IV</i> . . . . .	43
<b>VIII. Magnetometer</b> by David D. Norris, James L. Lawrence, and James S. Bunn . . . . .	45 ✓
A. Instrument Objectives . . . . .	45
B. Description . . . . .	45
C. Design Evolution . . . . .	50
D. Subsystem Operation . . . . .	55
<b>IX. Television System</b> by J. Denton Allen and L. Malling . . . . .	58 ✓
A. Introduction . . . . .	58
B. TV System Parameters . . . . .	58
C. Camera Mechanization . . . . .	58
D. Camera Electronics . . . . .	61
E. Summary . . . . .	67
<b>X. Data-Automation System</b> by W. J. Schneider and D. L. Nay . . . . .	68 ✓
A. Description of Mission . . . . .	68
B. Real-Time Data Handling . . . . .	69
C. Encounter Sequence . . . . .	69
D. Video Data Handling . . . . .	69
E. Packaging . . . . .	73
F. Testing . . . . .	75
<b>XI. Planetary-Scan System</b> by R. Y. Wong . . . . .	76 ✓
A. System Objectives and Requirements . . . . .	76
B. Functions . . . . .	76
C. Components of the System . . . . .	78
D. Physical Characteristics . . . . .	82
E. System Performance . . . . .	82
<b>XII. Science Data Processing</b> by Stephen Z. Gunter and Michael J. Sander . . . . .	86 ✓
A. Introduction . . . . .	86
B. Test-Data Processing . . . . .	86
C. Flight-Operations Support Processing . . . . .	88
D. Master Data Library . . . . .	91
E. Summary . . . . .	92

## I. THE MARINER-MARS SCIENCE SUBSYSTEM

Frank L. Schutz

Jet Propulsion Laboratory  
Pasadena, California

### A. Introduction

The *Mariner-Mars '64* project was the most complex mission conducted by the United States in its program of unmanned exploration of the Moon and planets. This difficulty stems from several factors: the communication distance, the extended operating lifetime requirements, and the guidance accuracy required from the launch vehicle.

The primary objective of the mission was to make meaningful scientific measurements during the planetary encounter. A series of 22 pictures was taken by a slow-scan television system and measurements were made by a group of energetic-particle detectors, a magnetometer, and a micrometeorite detector. An additional experiment was conducted when the radio signal was bent by the Martian atmosphere as the spacecraft was occulted by the planet.

The *Mariner-Mars '64* spacecraft was, in a general sense, related to its predecessor, the *Mariner-Venus '62* spacecraft. However, the resemblance was only superficial because all of the spacecraft's major subsystems either have been modified and improved or were designed for this particular mission.

This project was initiated in the fall of 1962 by the National Aeronautics and Space Administration of the United States. This was the second project of a two-part program to send highly integrated spacecraft past the near planets, Venus and Mars, to obtain scientific information concerning these planets and to extend the state of the art in the design of deep-space probes. The first project was successfully concluded when *Mariner II* reached Venus in December 1962. The second project was successfully concluded when *Mariner IV* encountered Mars on July 14, 1965, and transmitted the results of the measurements.

In each of these projects, the first launch of a two-launch opportunity was aborted because of a launch-vehicle problem. The *Mariner I* booster was destroyed from the ground when it deviated from the prescribed launch plan because of an error in the launch vehicle's

guidance equation. The first launch of the *Mariner-Mars '64* project was aborted when the shroud failed to separate from the spacecraft and the solar panels could not be opened. The second launch was delayed until a metal shroud, similar to those used in the *Ranger* project could be built and tested. In spite of the fact that the shroud did not separate, the spacecraft operated for 8½ hr before its battery failed. The analysis of the data obtained during this period of operation aided in the determination of the failure mode.

The second *Mariner-Mars '64* spacecraft was successfully launched on November 28, 1964, after a flawless countdown.

### B. The Mission

The *Mariner 1964* project included the development of a spacecraft capable of meeting the mission objectives within specific constraints and requirements. Additional effort was expended in developing the operational capability of the ground support facilities to meet the mission profile requirements.

#### 1. Objectives

The primary objective of the *Mariner-Mars 1964* project was to conduct scientific observations of the planet Mars during the 1964-1965 opposition and to transmit the results of these measurements to Earth. The planetary observations should, to the greatest practical extent, provide maximum information about Mars. To meet these requirements, a television system, a micrometeorite detector, and a number of field and particle instruments were carried.

A secondary objective was to provide experience and knowledge about the performance of the basic engineering equipment of an attitude-stabilized spacecraft during an extended flight from the Earth in the antisolar direction. An additional objective was to perform magnetic-field, energetic-particle, and micrometeorite measurements during the period between launch and Mars encounter.

**2. Characteristics and Constraints**

Two standard *Atlas-D*/improved *Agena-D* launch vehicles and two launch pads were provided at the Air Force Eastern Test Range, Cape Kennedy, Florida, to launch two spacecraft during the 29-day launch period. A third flight spacecraft, but not a third launch vehicle, was prepared in case difficulties developed in either of the first two spacecraft before launch. Launches were to be conducted on a minimum separation of 48 hr, depending upon the success of the first launch.

The extended duration of the mission required that the spacecraft be capable of an operational lifetime of greater than 6000 hr, twice that required for the earlier *Mariner II* Venus mission. This reliability had to be met in spite of an increase in the number of piece parts from 54,000 on *Mariner II* to 138,000 on *Mariner IV*.

The trajectory was selected so

1. The Sun-probe-Mars (SPM) angle could not equal zero, or Sun acquisition would be lost.
2. The Canopus-probe-Mars (CPM) angle could not equal 36 deg, or Canopus acquisition could be lost.
3. The probability of either the spacecraft or the second stage of the launch vehicle impacting the planet was less than  $10^{-4}$ .
4. The area of the planet covered during the television picture-taking sequence contained both light and dark areas.
5. The spacecraft would pass the planet at a distance not to exceed 40,000 km.

The actual trajectory of *Mariner IV* meets these constraints. Figure 1 is the overall trajectory and Fig. 2 is the near-Mars trajectory. The area actually covered by the television pictures is indicated by the small rectangles in Fig. 3.

**3. Mission Profile**

The mission profile consists of the planned sequence of events between launch and mission termination.

**a. Launch Phase.** The launch phase lasts from launch-vehicle lift-off through to separation of the spacecraft from the second stage *Agena-D*.

From lift-off to shroud ejection the spacecraft transmitter radiated at low power (1 w instead of 10) through

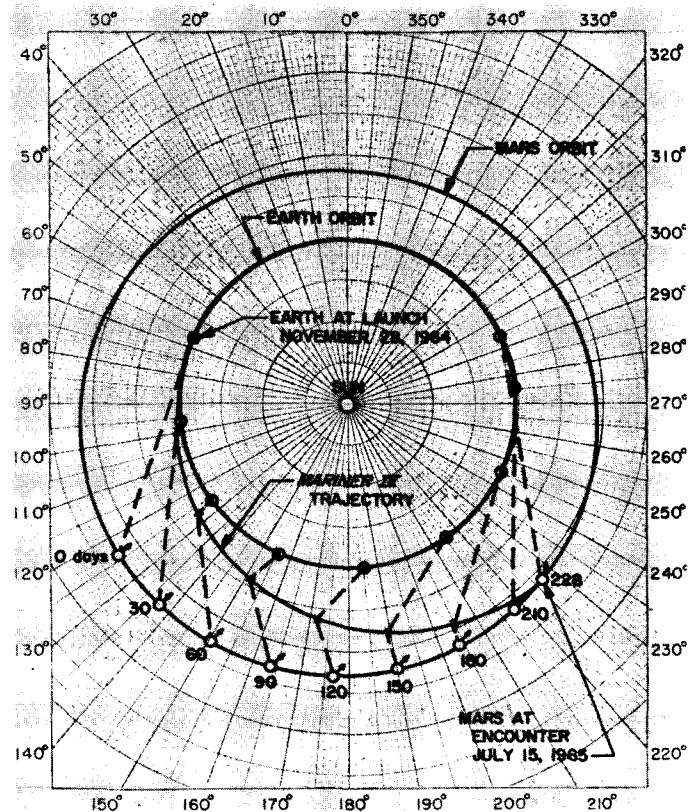


**Fig. 1. Mariner IV trajectory**

a parasitic antenna located on the shroud. After the shroud was ejected, the transmitter radiated through the low-gain antenna. When the spacecraft separated from the *Agena-D* the pyrotechnic system was armed, the science subsystem (except for the television and planetary sensors) energized, and the radiated power increased to 10 w.

The launch phase included the entire first stage, *Atlas*, motor burn, the first and second motor burns of the *Agena-D*, and the period spent in a parking orbit before the second *Agena-D* motor burn.

**b. Acquisition Phase.** Upon separating from the *Agena-D*, the spacecraft began a series of operations designed to establish solar-attitude stabilization. The solar panels were deployed and the search for the Sun begun. Solar acquisition can require as long as 30 min. Power was supplied by the battery until acquisition was completed. After acquisition, the spacecraft rolled about the Sun-spacecraft axis at a controlled rate until the star tracker was activated 997 min after lift-off. This period was required to minimize the chance of acquiring a

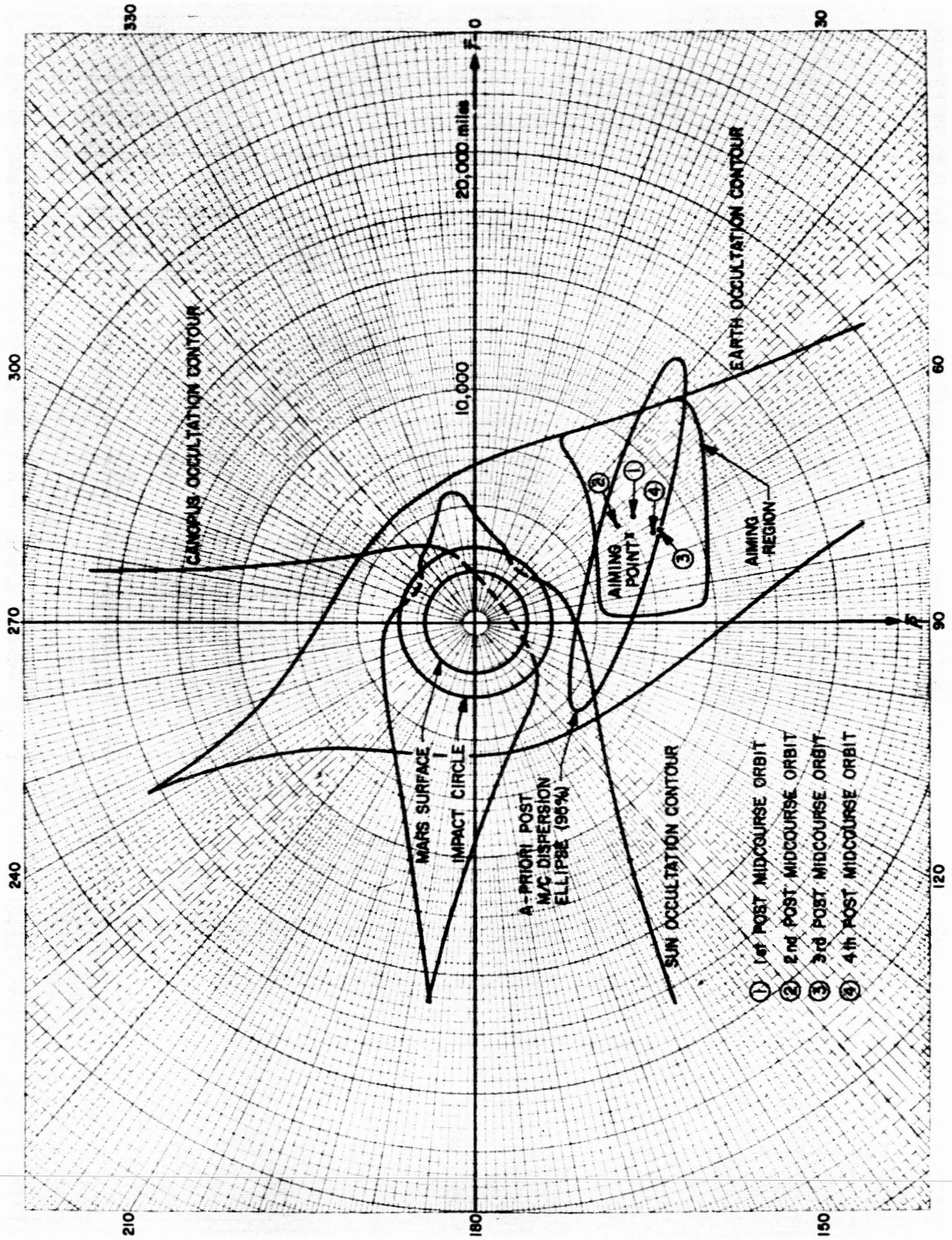


Fig. 2. Near-Mars trajectory



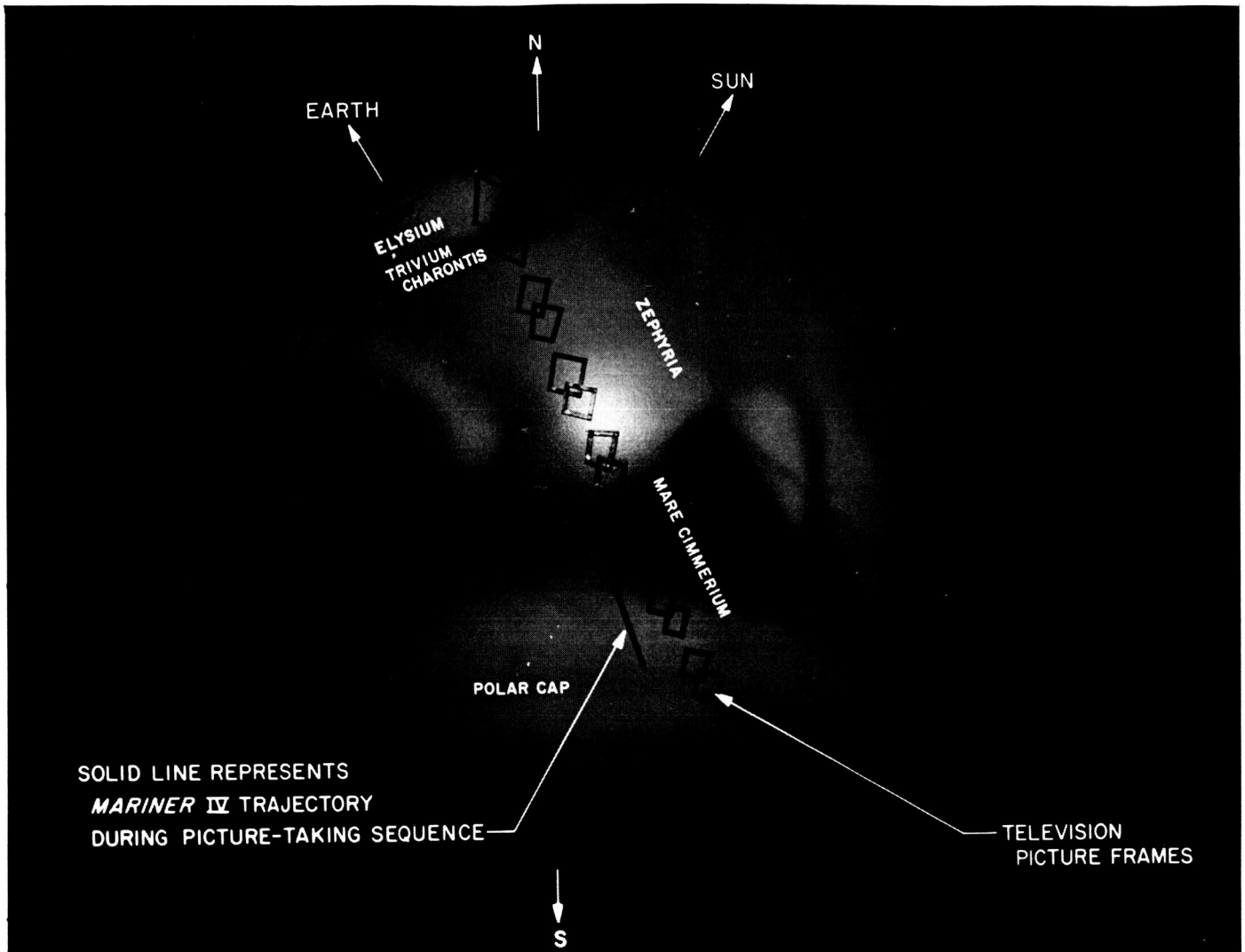


Fig. 3. Television picture coverage

celestial body other than the star Canopus, to calibrate the X and Y axes of the spacecraft magnetic field, and to keep the Canopus star tracker deenergized during the period the spacecraft spent in the radiation belts near Earth.

As soon as the spacecraft acquired Canopus, the acquisition phase was completed and the cruise phase begun.

**c. Cruise Phase.** The period between completion of the attitude-stabilization process and the beginning of the encounter with Mars is called the cruise phase. At pre-selected times during this portion of the mission, several discrete events occurred:

1. The data-transmission rate was changed from the launch rate of  $33\frac{1}{2}$  bits/sec to  $8\frac{1}{2}$  bits/sec.

2. The star-tracker cone angle was changed four times to ensure that the star Canopus remained in its field of view.

3. The spacecraft transmitter was changed from the low-gain to the high-gain antenna.

The only events that could have disrupted the cruise mode were failures, trajectory correction maneuvers, or special ground controlled tests, such as the early planetary platform cover removal that was performed.

During the majority of the mission, communications with the *Mariner IV* were one-way, that is, "down-link" only from the spacecraft transmitter to a ground station

receiver. Two-way communications were scheduled periodically to obtain precision doppler data for orbit determination. For such operations, a signal was sent from a Deep Space Instrumentation Facility station ground transmitter "up-link" to the spacecraft receiver and retransmitted by the spacecraft transmitter to the station ground receiver. At such times, the spacecraft transmitter was coherent (synchronized) with the ground-transmitter frequency and the difference between the frequency of the ground-transmitter output and ground-receiver input was the doppler shift from which spacecraft position information was obtained.

*d. Maneuvers.* Seven days after launch, the cruise phase was interrupted and a trajectory-correction maneuver performed. This spacecraft had the capability of performing two maneuvers, but the second was not required.

*e. Encounter Phase.* During the actual encounter of the spacecraft with the planet, defined as the period beginning about 9 hr before and ending about 4 hr after closest approach, the encounter instruments were energized. After the planet was located by the planetary-scan system, the television pictures were sequenced and then recorded by the tape recorder. Approximately 1 hr after closest approach, the spacecraft was occultated from the Earth by the planet and an occultation experiment performed. Analysis of the data acquired during this period should yield information relative to the scale height and pressure of the Martian atmosphere.

*f. Post-Encounter Phase.* At the end of the encounter, the stored science data were transmitted. Engineering data was inserted between each picture to establish the condition of the spacecraft. Picture transmission required  $8\frac{1}{3}$  hr per picture.

*g. Termination.* The mission was terminated when the combined effects of increased range and antenna pointing error exceeded the communication capability.

#### 4. Mission Operations

The mission operations were conducted using the facilities of the Deep Space Network (DSN). These facilities include the Space Flight Operations Facility (SFOF), Deep Space Instrumentation Facility (DSIF) and the DSN Ground Communication System.

The Deep Space Network (DSN) is a precision communication system that is designed to communicate

with, and permit control of, spacecraft designed for deep-space exploration.

#### 5. Space Flight Operations Facility (SFOF)

The role of the SFOF was to provide operational and technical support during the planning and execution of the mission. The operational functions included were mission operations, Deep Space Instrumentation Facility control, and data processing. The technical functions included analysis and interpretation of the data obtained to evaluate the spacecraft operation. No analysis or evaluation of the scientific data was attempted except to define the interrelationship between it and the engineering data.

All mission flight operation, direction, and control originated in the SFOF. Each of the technical disciplines was provided with separate areas in the SFOF to analyze and evaluate its data. The Space Sciences Analysis Area was used by the scientists and engineers associated with the science subsystem. Facilities were also provided for the Spacecraft Performance and Analysis Group, the Flight Path Analysis Group, and the Mission Support Area.

The data input to the SFOF from the spacecraft was processed in the following three categories:

1. Real-time operational monitoring and processing which comprise all the IBM 7040 computer programs.
2. Near-real-time operational space-flight analysis programs which were processed in the IBM 7094 computer for operational flight-path analysis and for spacecraft-and scientific-instrument performance and analysis.
3. Non-real-time space-flight analysis and research programs which have multiple options and functions.

The real-time operational data were used to establish the condition of the spacecraft and scientific instruments. Continuous plots of specific scientific data were available to principal investigators or their representatives. A representative of the science subsystem was stationed in the SFOF continuously from spacecraft launch to mission termination.

The near-real-time analysis programs were used to give a composite picture of a specific block of data. This enabled the principal investigators or their representatives to obtain scientific data that were a reduced version of the real-time or raw data.

The final non-real-time data reduction is accomplished by off-line computers. Their output consists of data which

is cross-correlated with spacecraft position and attitude as a function of time, the scientific data from other instruments, and an integrated summary of the scientific data from a particular instrument.

Some special science real-time data processing was required to ensure that an operational failure occurring during the critical encounter mode would not jeopardize the mission. This involved preparation of a sequence of ground commands that could be sent to the spacecraft to back up the on-board commands or to overcome actual operational malfunctions.

## 6. Deep Space Instrumentation Facility (DSIF)

The function of the DSIF was to obtain angular position, doppler, and telemetry data from the spacecraft during the post-injection phase of the mission. Ranging data could have been obtained as a backup to two-way doppler. Additionally, the DSIF sent commands to the spacecraft when required.

Data obtained by the DSIF are transmitted by teletypewriter and wide-band Data-Phone circuits to the Space Flight Operations Facility (SFOF) at the Jet Propulsion Laboratory (JPL), Pasadena, California, as they are received. These data are also recorded at the receiving station and dispatched to the SFOF by airmail.

The DSIF commitment to the *Mariner-Mars* 1964 project included the Pioneer Site, Goldstone, California; the Woomera, Australia, station; and the Johannesburg, South Africa, station. Later the Tidbinbilla station replaced Woomera.

The DSIF provided 24-hr coverage except during some *Ranger* and *Surveyor* operations. The critical portions of the mission were afforded continuous coverage. Tracking overlap between stations gave assurance that no data would be lost.

Each DSIF station was connected via the DSN Ground Communication System to the SFOF by one voice line, a voice-quality (3-kc bandwidth) data line, and two teletypewriter lines.

## C. The Spacecraft

The launched weight of the *Mariner IV* spacecraft (Fig. 4 and 5) was 575 lb. It is 9½ ft tall, has a span of 22 ft 7½ in., was fully attitude-stabilized, with the Sun and Canopus as reference objects. It derived power from a battery and from photovoltaic cells mounted on

panels having a body-fixed orientation. The battery provided power during launch, trajectory correction maneuvers, and acted as a backup to the solar cells in case solar acquisition was lost. A communication system, in addition to its command capability to the spacecraft and telemetry capability to Earth, provided, in conjunction with the DSIF, angle tracking and doppler for orbit determination. The guidance system design permitted trajectory correction maneuvers using a propulsion system capable of executing two such maneuvers. Figure 6 is a functional block diagram of the spacecraft.

### 1. Attitude Control Subsystem

Stabilization of the spacecraft during the mission was provided by 12 cold-gas (nitrogen) jets mounted at the outer ends of the solar panels. These jets are logically controlled by signals from three gyroscopes or from the Canopus star tracker and two Sun sensors. The attitude-control system responds to these signals by turning on the appropriate jet nozzle and allowing nitrogen gas to escape, thereby imparting a reaction force to the spacecraft to correct its angular position. Pitch-and-yaw control was provided by the primary and secondary Sun sensors and roll control was provided by the Canopus star tracker.

There is also an auxiliary attitude-control system that corrects for unbalances in solar pressure. This was accomplished by positioning solar vanes mounted at the end of each solar panel to control the pitch-and-yaw axes within the limit cycles of the gas-jet system. The vanes were initially deployed electromechanically and then positioned thermomechanically.

If the attitude of the spacecraft was disturbed beyond the limits set for control by the gas jets, three gyroscopes were energized to return the spacecraft to the correct attitude. The nominal accuracy of this subsystem was  $\pm 0.5$  deg with respect to each axis.

During trajectory-correction maneuvers, the subsystem was capable of pointing the propulsion-subsystem thrust axis to any desired orientation with a  $1-\sigma$  accuracy of  $\pm 0.5$  deg from the nominal reference attitude and with a drift rate of less than 0.5 deg/hr. This stability was maintained during the propulsion-subsystem operation through the use of an auto-pilot-jet-vane actuation system.

### 2. Central Computer and Sequencer Subsystem

The central computer and sequencer provided the basic timing signals for the spacecraft. This subsystem

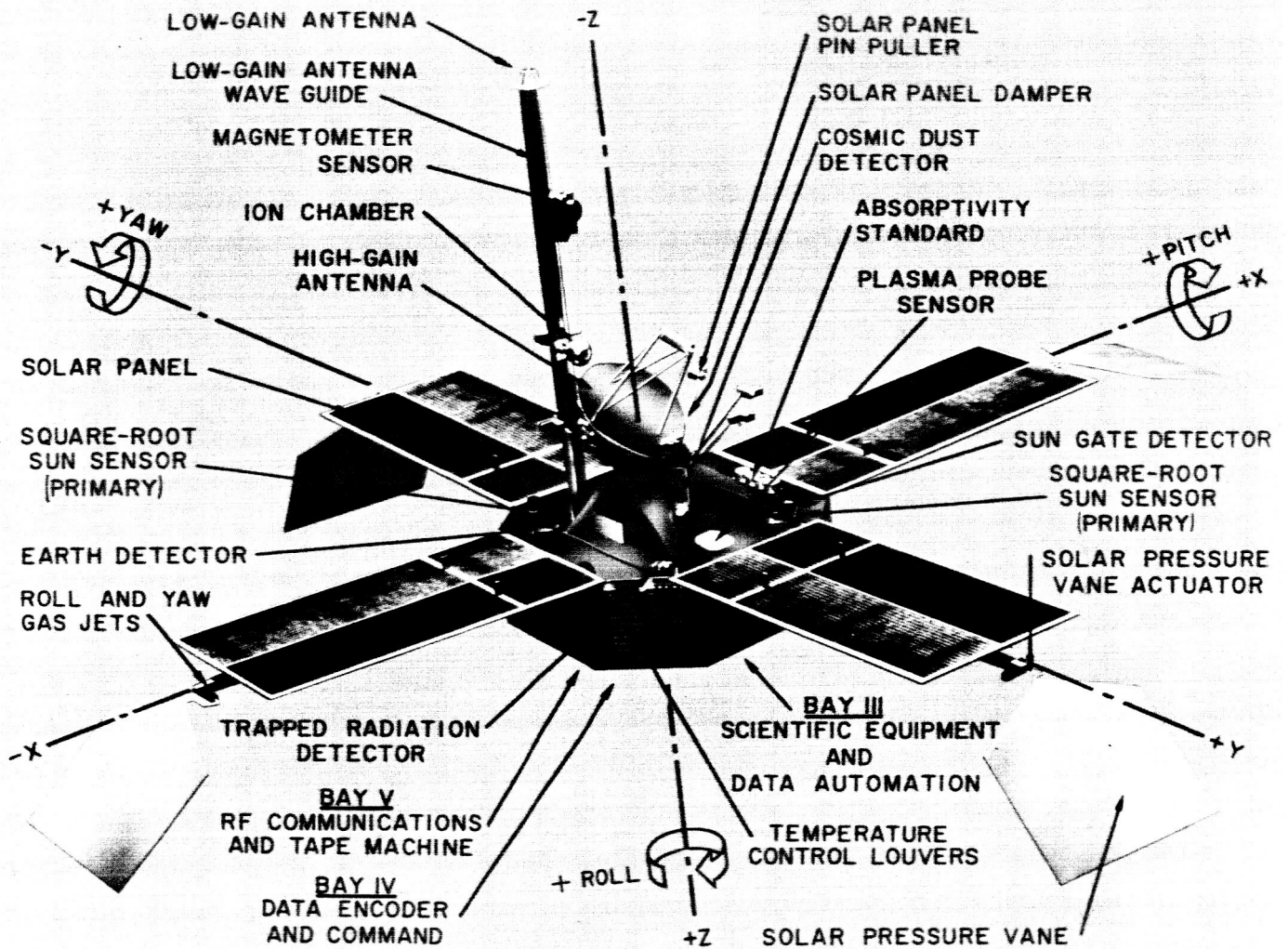


Fig. 4. Mariner spacecraft, top view

also provided the timing for events such as solar-panel deployment, trajectory corrections, attitude-control system activation, planetary-encounter related events, spacecraft data-rate changes, switching the communication system between antennas, and changing the Canopus star tracker's cone angle. The propulsion-subsystem motor burn time was controlled to an accuracy of  $\pm 0.08$  seconds by the central computer and sequencer.

### 3. Command Subsystem

Radio commands transmitted to *Mariner IV* were decoded and routed to their destination by the command subsystem. There were 30 possible commands that could be transmitted to the spacecraft. However, the spacecraft was designed so that if every operation was performed

correctly from launch to mission termination, there would be no need for using these commands. They serve primarily as redundant control of the spacecraft. Twenty-nine of the commands were fixed, direct commands which perform a single function. The remaining command was used to establish the attitude of the spacecraft and period of motor ignition during the trajectory correction. The command data-rate was 1.0 bits/sec.

### 4. Data-Encoder Subsystem

Data telemetered from the spacecraft consisted of a data frame containing both engineering and science measurements which were alternately sequenced by the data-encoder subsystem. This frame consisted of 420 data bits, the first 140 of which contained engineering data, with

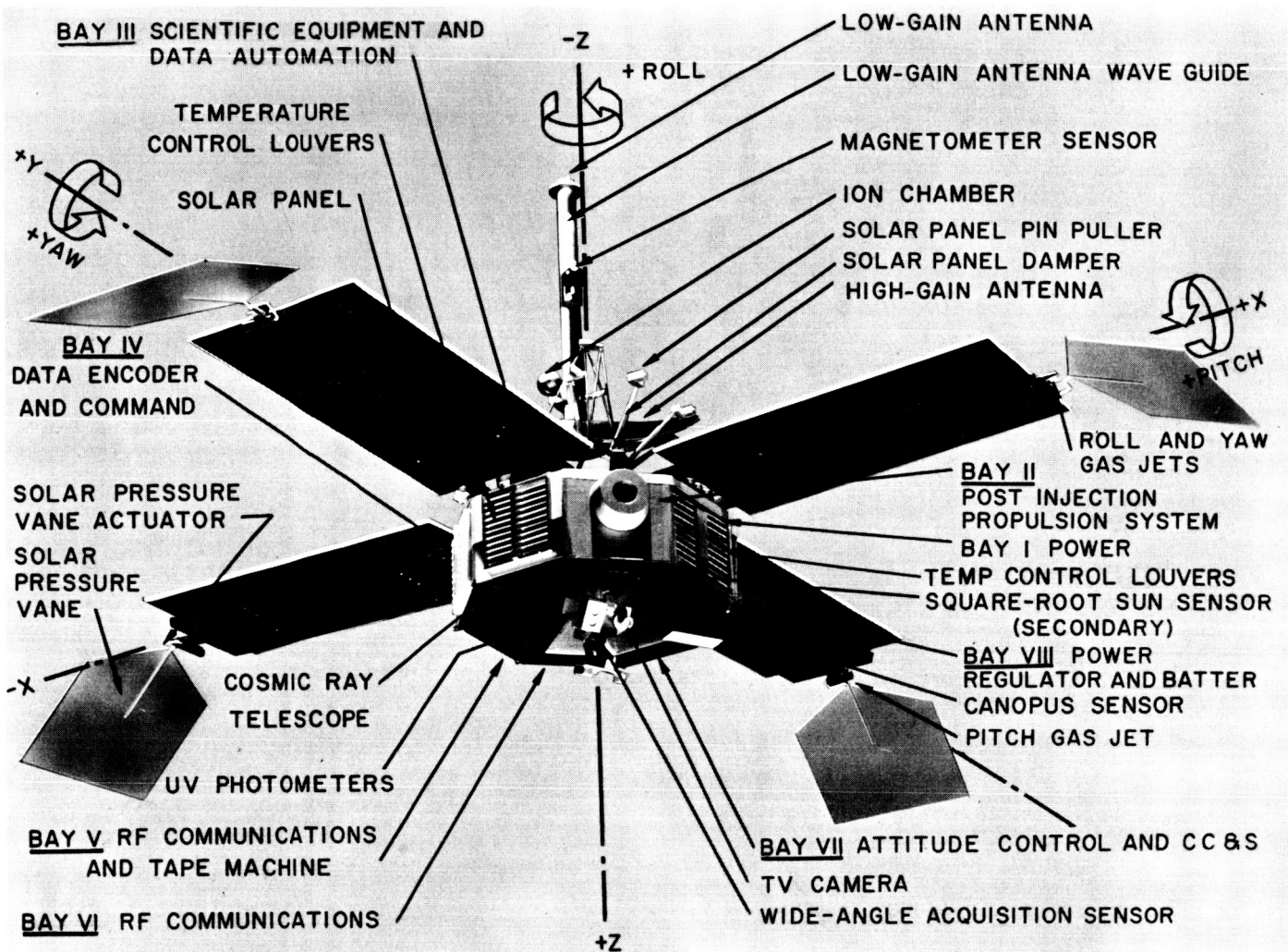


Fig. 5. Mariner spacecraft, bottom view

the remaining 280 bits being used by the science sub-system.

The data encoder sampled 100 engineering measurements while operating at either of two data-transmission or bit rates,  $8\frac{1}{3}$  or  $33\frac{1}{3}$  bits/sec. It was also required to operate in four data modes or sequences:

- Data Mode 1 Engineering data only.
- Data Mode 2 The normal mode with  $\frac{1}{3}$  engineering and  $\frac{2}{3}$  science each data frame.
- Data Mode 3 Science data only.

Data Mode 4 Playback of data from the tape recorder with insertions of Mode 1 data between television pictures.

These data modes were independent of the spacecraft bit rate and they were selected by logic on the spacecraft or by ground command. The bit rate was changed from  $33\frac{1}{3}$  to  $8\frac{1}{3}$  bits/sec by the central computer and sequencer on January 3, 1965.

### 5. Radio Subsystem

The radio subsystem was composed of a transmitter and receiver operated in conjunction with two antennas.

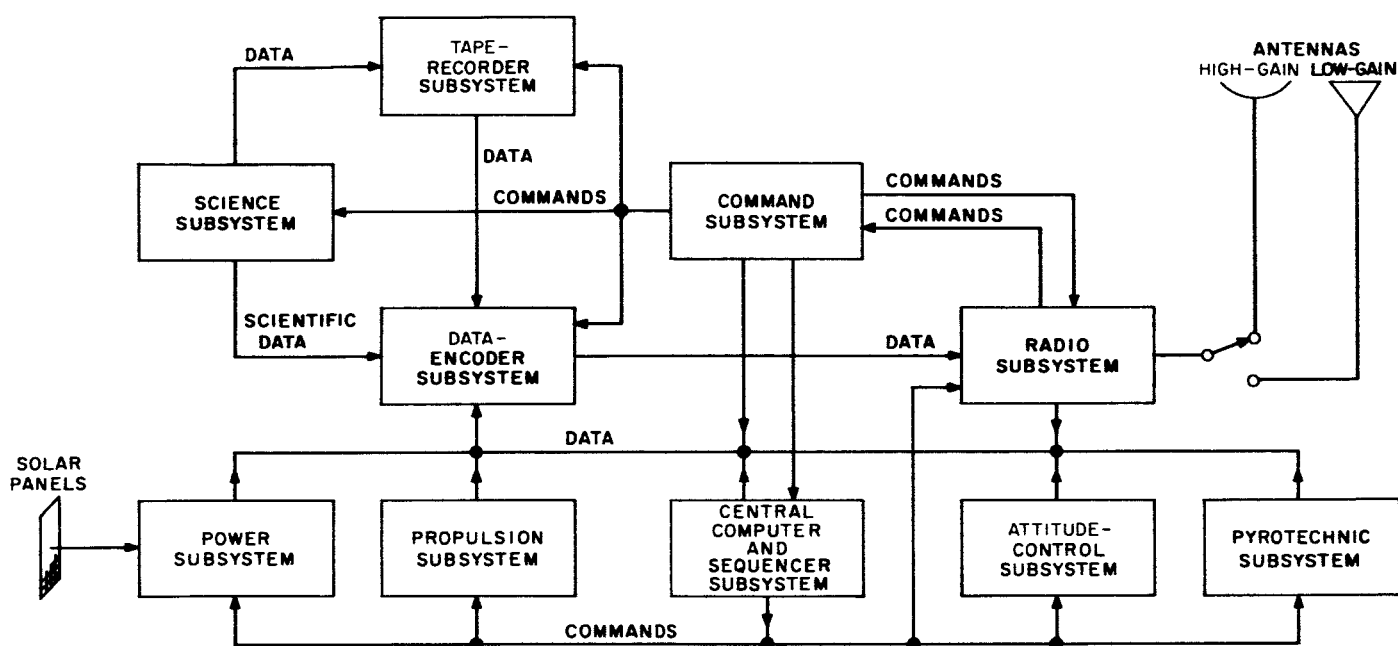


Fig. 6. Spacecraft functional block diagram

**a. Transmitter.** The transmitter consisted of two redundant radio-frequency power amplifiers and two redundant exciters. A transmitter made up of an exciter and power amplifier operated coherently with the receiver and with either of two antennas. Selection of the transmitter-receiver-antenna combination was by the central computer and sequencer with ground command backup. The transmitter operated at 2295 MHz with a power output of 10 w.

**b. Receiver.** The receiver operated with either of the two spacecraft antennas at a frequency of 2113 MHz. The receiver could be switched between these two antennas by ground command. If the receiver was connected to the high-gain antenna and the gyros were turned on, the receiver would automatically be switched to the low-gain antenna. If the receiver lost lock (signal from Earth) it would be automatically switched between the high- and low-gain antennas every 66% hr if lock was not reacquired for two 66%-hr cyclic intervals.

**c. High-Gain Antenna.** The high-gain antenna was a fixed (relative to the spacecraft), on-axis fed, elliptical sector of a paraboloid measuring  $21 \times 46$  in. This antenna was used by the spacecraft during the second half of the mission because of the small change in the Earth-Sun-spacecraft reference angle. Use of a fixed antenna eliminated pointing control (as on *Mariner II* and *Ranger*), thereby increasing the reliability of the spacecraft.

**d. Low-Gain Antenna.** The low-gain antenna provided the primary Earth-to-spacecraft (receiver) link throughout the mission in addition to providing telemetry during the first half of the mission. It provided essentially uniform coverage in the forward (solar direction) hemisphere of the spacecraft.

## 6. Power Subsystem

The primary power source on the spacecraft consisted of four solar panels containing 28,224 individual photovoltaic solar cells oriented normal to the Sun-probe-line and covering 70 sq ft. A secondary power source was a rechargeable silver-zinc 1200-watt-hr battery that provided power to the spacecraft during launch, trajectory correction, or other maneuvers where the spacecraft's solar-panel output voltage fell below that of the battery.

The power subsystem contained redundant power regulators, either of which could handle the full spacecraft load in the event one was automatically switched out because of a failure. The input to these regulators varied from a nominal 640 w near Earth to 310 w at Mars encounter. The power demands were a 260 w maximum during maneuvers and 140 w during the post-encounter playback of data from the tape recorder.

The output from the power regulators was distributed to the other spacecraft subsystems in the form of 50 v rms,

2400-cps square waves. A separate 28-v, 400-cps, 3-phase supply was used to power the gyros. One phase of the latter supply was also used to supply the tape recorder and planetary platform drive motors. Only the radio subsystem received unregulated direct-current power to operate the cavity radio-frequency amplifier.

Users were required to transformer-isolate their loads from the spacecraft power source.

### 7. Propulsion Subsystem

A trajectory correction was performed by changing the attitude of the spacecraft as required and firing a small 50-lb-thrust motor. The ability to perform two of these maneuvers was designed into the spacecraft through the use of two sets of explosive valves. The second motor burn was not required because the first one placed the spacecraft on a near-perfect trajectory.

The motor burned anhydrous hydrazine and used nitrogen tetroxide as the starting fluid. It could burn for a minimum of 50 ms and a maximum of 100 sec, which resulted in an incremental speed of 0.125 to 188 mph.

Jet vanes capable of deflecting the motor jet stream provided thrust-vector control through  $\pm 5$  deg.

### 8. Pyrotechnic Subsystem

The spacecraft employed a number of squib-actuated devices, such as solar-panel latches, and propulsion-system valves. These devices were fired by commands from other spacecraft subsystems at the appropriate time.

The pyrotechnic subsystem was not armed until the spacecraft separated from the launch vehicle. This was a precaution against an inadvertent or spurious command causing premature operation in the subsystem.

### 9. Tape-Recorder Subsystem

It was a requirement that the television pictures be stored on magnetic tape because the spacecraft's data-transmission rate was only  $8\frac{1}{2}$  bits/sec and the data acquired at 83,333 bits/sec. The tape recorder, in conjunction with the buffers contained in the data-automation system, provided a 10,000-to-1 data-rate conversion. The data enter the tape recorder at 10,700 bits/sec and are synchronously played back at  $8\frac{1}{2}$  bits/sec.

The tape recorder was a two-track machine with a tape loop of 330 ft. The record cycle was controlled by the data-automation system and the playback cycle by internal tape-recorder logic. The data were put onto the tape in RZ format. The maximum storage capability of the subsystem was  $5.24 \times 10^6$  bits of data.

### 10. Science Subsystem

The science subsystem was composed of instruments and ancillaries selected to meet the mission objectives, namely, to make planetary observations and to perform field and particle measurements throughout the mission. The observations and measurements were intended to investigate the topography of Mars, its possible magnetic field and radiation belts, and the dust particles that may be trapped in close proximity to the planet.

All of the instruments except the television were capable of making measurements during the cruise portion of the flight; they were programmed to take interplanetary data concerning the solar plasma, micrometeorites, magnetic fields, and energetic-particle distribution in space. The ancillary equipment consisted of the data-automation system, the planetary-scan system, and the narrow-angle Mars gate.

## II. SCIENCE SUBSYSTEM

W. G. Fawcett

Jet Propulsion Laboratory  
Pasadena, California

### A. General Description

The *Mariner-Mars* 1964 science subsystem consists of the following:

1. Instruments, including cosmic-dust detector, helium magnetometer, plasma probe, cosmic-ray telescope, trapped-radiation detectors, ion chamber, and television.
2. Ancillaries, including data-automation system (DAS), planetary-scan system, and narrow-angle Mars gate.

All but one of the instruments, i.e., the television, were designed to operate and collect scientific data in interplanetary space as well as in the vicinity of Mars. Accordingly, the data-automation system consists of two functionally independent portions: the real-time DAS, which operated throughout the mission and performed all of the functions necessary for the proper collection and sequencing of data from the so-called "cruise science" instruments and putting data into format, and the non-real-time DAS which operated only in the vicinity of Mars for the purpose of controlling the planetary-scan and television subsystems and providing for the transfer of television picture data to the spacecraft tape recorder. The planetary-scan system has a wide-angle optical sensing device mounted on a movable platform to search for, acquire, and track the planet so that the television camera would be correctly oriented toward the desired portions of the planet's surface. The narrow-angle Mars gate provided a signal that caused the DAS to inhibit the scan-platform motion and initiate the picture-recording sequence just before the near limb of the planet entered the television camera field of view.

### B. Physical Characteristics

Although the science subsystem weighs only 51.25 lb—less than 10% of the total spacecraft weight—it contains half of the spacecraft's 34,000 electronic component parts. Science power consumption was 21.56 w during interplanetary cruise and 37.02 w during the planet-encounter phase of the mission.

Table 1 contains a summary of the more important characteristics of each instrument and ancillary, and Table 2 lists the corresponding principal investigators.

### C. Functional Characteristics and Constraints

Of necessity, interplanetary/planetary scientific payloads must inevitably accept weight, volume, and power constraints resulting from whatever is left over after the needs of all mission-critical elements (such as the power, radio, data-encoder, and attitude-control subsystems) have been satisfied.

There were other constraints on the *Mariner-Mars* 1964 science subsystem design, in addition to those placed by the science subsystem on the rest of spacecraft. These constraints played a large part in determining the ultimate spacecraft design.

#### I. Operating Lifetime

Inasmuch as the nominal mission lifetime was approximately 6,000 hr and all science equipment would be required to undergo many hundreds of hours of pre-launch testing, an electronic-component-part screening program was required for each instrument (and ancillary). The purpose of this program was twofold. First, there would be assurance that every part installed in an instrument would have been tested well beyond the normal regions of infant mortality. This not only prevented in-flight failures but also reduced the costly delays that result from failures during the instrument and spacecraft test phases. Second, and equally important, it was designed to reveal basic inadequacies in part types or manufacturing processes which would not otherwise be immediately apparent.

A typical JPL screening process for transistors consists of the following for each and every part:

1. Visual inspection under a 20-power microscope for cracked glass-to-metal seals, tarnished or corroded leads, nicked or broken leads, signs of mishandling, etc.



Table 1. Mariner-Mars 1964 instruments and ancillaries

Description	Spacecraft unit number	Weight, lb	Power, w	Look angle	Purpose	Number of sensors	Output data
Instrument							
Cosmic-ray telescope	21	2.58	0.598	30 deg 1/2 angle cone along + z axis	To detect and measure trapped corpuscular radiation in the vicinity of Mars. To measure the flux and energy of alpha particles and protons as a function of position and time in interplanetary space.	1 sensor, 3 detectors in telescope	Digital (4)
Cosmic-dust detector	24	2.10	0.201	Into plane of ecliptic in direct and retrograde motion	To make direct measurements of the dust-particle momentum and mass distribution in the Earth-Moon, Mars-Deimos-Phobos, and interplanetary regions.	2 sensors	Digital (1)
Trapped-radiation detectors	25	2.20	0.350	3 sensors 70 deg to probe-Sun line, 30 deg 1/2 angle cone  1 sensor 135 deg to probe-Sun line, -30 deg 1/2 angle cone	To search for magnetically trapped particles in the vicinity of Mars and, if found, make a preliminary estimate of their distribution, energy spectra, and identity. To monitor solar cosmic rays and energetic electrons in interplanetary space, to determine their angular distribution, energy spectra, and time history.	4 sensors	Digital (5)
Ionization chamber	26	2.71	0.460	Omnidirectional	To detect and measure the average omnidirectional flux of corpuscular radiation in regions between the Earth and Mars. To measure the average specific ionization attributable to this flux. To measure the omnidirectional flux and specific ionization of charged particles which may be trapped in the vicinity of Mars.	2 sensors	Digital (2)
Plasma probe	32	6.41	2.65 average, 2.90 peak	30 deg 1/2 angle cone 10 deg from probe-Sun line	To measure the spectral distribution, flux density and time history of the positively charged solar plasma traveling outward from the Sun and to correlate their measurements with those from the magnetometer.	1 sensor (3 sections)	Pulse width (1)

Table 1. Mariner-Mars 1964 instruments and ancillaries (Cont'd)

Description	Spacecraft unit number	Weight, lb	Power, w	Look angle	Purpose	Number of sensors	Output data
<b>Instrument</b>							
Magnetometer	33	7.50	7.30	1 sensor along z axis, 1 sensor along y axis, 1 sensor along x axis	To investigate the existence of a Martian planetary field and determine its characteristics as a function of direction, magnitude, multipolarity, and orientation with respect to the planetary rotational axis. To investigate the interaction between planetary and interplanetary magnetic fields. To measure the magnitude and direction of the steady and slowly varying components of the interplanetary magnetic field and to determine its variation with heliographic altitude and longitude.	3 sensors	Pulse width (3)
Television	36	11.28	8.0	1.05 deg x 1.05 deg	To make preliminary topographic reconnaissance of portions of the surface of Mars. To attain an improved knowledge of areas of possible living matter. To obtain additional data on the Martian surface reflectivities so that the design of future systems will be enhanced.	1 sensor, 2 alternate color filters	Digital (3), pulse width (1) sequenced
<b>Ancillary</b>							
Data automation system	20	11.91	6.5 average during cruise, 5.6 average during encounter, 8.0 peak during encounter.		The DAS provides the sequencing, processing, storage, buffering, and encoding necessary to realize the optimum scientific value of each instrument. The DAS also performs certain engineering measurements in addition to those made by the spacecraft data encoder.	None	Non-video real-time digital data-to-data encoder; bit sync and RZ video data to S/C video storage.

Table 1. *Mariner-Mars 1964 instruments and ancillaries (Cont'd)*

Description	Spacecraft unit number	Weight, lb	Power, w	Look angle	Purpose	Number of sensors	Output data
<b>Ancillary</b>							
Planetary-scan system	31	5.65 <sup>a</sup>	4.65 (2400 cps), 2.81 (400 cps)	25 deg ½ angle cone	The scan system is used to point the television camera at a point on the planet that is dependent upon the bisector of radiation and the trajectory of the spacecraft.	1 sensor	Pulse width (1)
Narrow-angle Mars gate	7MG1	0.20 <sup>a</sup>	Included in DAS power requirement (0)	2.5 deg x 1.5 deg	Serves to trigger the DAS into initiating the television picture recording mode. In this sense it serves as a backup to the TV.	1 sensor	None

<sup>a</sup>Measured values *Mariner IV*, no cabling harnesses included.

2. Initial measurements at 25°C of  $I_{CB0}$ ,  $I_{EB0}$ ,  $IV_{CEO}$ ,  $h_{FE}$ ,  $V_{CESat.}$ , and  $V_{BESat.}$  under specified conditions.
3. High-temperature storage: 168 hr at 200°C.
4. Repetition of initial measurements.
5. Operational run-in: 168 hr at 100°C ambient temperature with 280 mw total power dissipation.
6. Repetition of initial measurements.

Acceptance criteria consist both of tolerances on the initial measurements and of acceptable changes in parameter values at subsequent measurements. The program was successful in both aspects. For instance, the rejection rate of one diode suddenly jumped from 10% to 70% because the manufacturer had altered his fabrication process. After this was discovered, the manufacturer corrected his process for subsequent JPL orders. Table 3 shows typical screening yields at one point in the program.

**2. Magnetic Constraints**

Because of the sensitive magnetometer carried as a part of the *Mariner-Mars 1964* payload, severe constraints were imposed on the use of spacecraft materials that could acquire a permanent magnetic field. In those cases where use of magnetic materials was unavoidable, steps were taken to reduce their fields as seen by the magnetometer sensor, either by the judicious use of shielding or by the most favorable location and orientation of these

materials with respect to other magnetic materials as well as with respect to the magnetometer sensor. In addition, of course, the sensor itself was mounted on the low-gain antenna mast at the greatest practical distance from the bulk of the remaining spacecraft components.

Where use of magnetic materials that contributed significantly to the permanent field of the spacecraft was unavoidable, materials were selected that would retain magnetization during launch. This assured that pre-launch magnetic-field mapping results would remain valid after injection from the parking orbit.

**D. Preassembly and Prelaunch Testing**

It was a requirement that each science subsystem undergo a complete subsystem test prior to delivery to the Spacecraft Assembly Facility, and that the spacecraft be designed so that an operating test could be performed on the launch pad prior to launch. The first requirement ensured the integrity of the complete subsystem prior to spacecraft assembly and thereby provided a reference point on which investigations of later performance anomalies could be based. The second requirement provided project officials with last-minute operational information to which launch/hold criteria could be applied.

**E. Operation**

The spacecraft was launched in Data Mode 2 with the science subsystem deenergized. When the spacecraft

**Table 2. Mariner-Mars 1964 experimenters**

Experiment	Principal investigator/affiliation	Co-investigator/affiliation
Television	Dr. R. B. Leighton, CIT	Dr. B. C. Murray, CIT Dr. R. P. Sharp, CIT Mr. R. K. Sloan, JPL Mr. J. D. Allen, JPL
Plasma probe	Dr. H. S. Bridge, MIT	Dr. A. Lazarus, MIT Dr. C. W. Snyder, JPL
Ion chamber	Dr. H. V. Neher, CIT	Dr. H. R. Anderson, JPL
Trapped-radiation detector	Dr. J. A. Van Allen, SUI	Dr. L. A. Frank, SUI Mr. S. M. Krimigis, SUI
Cosmic-ray telescope	Dr. J. A. Simpson, Univ. of Chicago	Mr. J. O'Gallegher, Univ. of Chicago
Cosmic-dust detector	Mr. W. M. Alexander, GSFC	Mr. O. E. Berg, GSFC Dr. J. L. Bohn, Temple Univ. Mr. C. W. McCracken, GSFC Mr. L. Secretan, GSFC
Magnetometer	Dr. E. J. Smith, JPL	Mr. P. J. Coleman, Jr., UCLA Dr. L. Davis, Jr., CIT Dr. D. E. Jones, Brigham Young Univ.
Occultation	Dr. A. J. Kliore, J.P.L.	Dr. Von Eshleman, Stanford Mr. D. L. Cain, JPL Dr. G. S. Levy, JPL Dr. F. D. Drake, Cornell Dr. Gunnar Fjeldbo, Stanford

**Table 3. Electronic component screening summary**

Commercial or JPL preferred components			
	No. of lots	Total quantity	Yield, %
Transistors	254	15,650	64
Diodes	266	20,200	72
Capacitors	659	15,200	75
Resistors	447	114,000	89
E/M Devices	280	2,550	85

separated from the *Agena* launch vehicle, the cruise or real-time data-automation system (RT-DAS) and the interplanetary instruments were energized. The format of the RT-DAS output during Data Mode 2 is shown in Fig. 1a. In spacecraft Data Mode 1 during the trajectory correction, no science data were transmitted, although the RT-DAS continued to sample the instruments.

The initiation of the encounter mode by central computer and sequencer command or command decoder direct command accomplished the following:

1. The television (TV), non-real-time data-automation system (NRT-DAS), narrow-angle Mars gate (NAMG), planetary-scan system (PSS), and tape recorder were energized.

2. The NRT-DAS sequenced the TV, but did not issue start commands to the tape recorder.

3. The protective cover was removed from the TV, NAMG, and PSS sensors. The scan platform moved through 180-deg arcs until the planet was acquired, then the following events occurred:

- a. The PSS tracked the planet to ensure that the platform continued to point at the bisector of brightness defining the location of Mars.
- b. An output from the PSS through the DAS to the data encoder initiated Data Mode 3. The real-time format for spacecraft Data Mode 3 is illustrated in Fig. 1c.

When the edge of the lighted disk came into view of either the television or narrow-angle Mars gate, the DAS tape-recorder "start" circuits were enabled. The DAS then waited until the beginning of the next standard sequence to initiate the recording cycle. All science data acquired during encounter were stored in the spacecraft

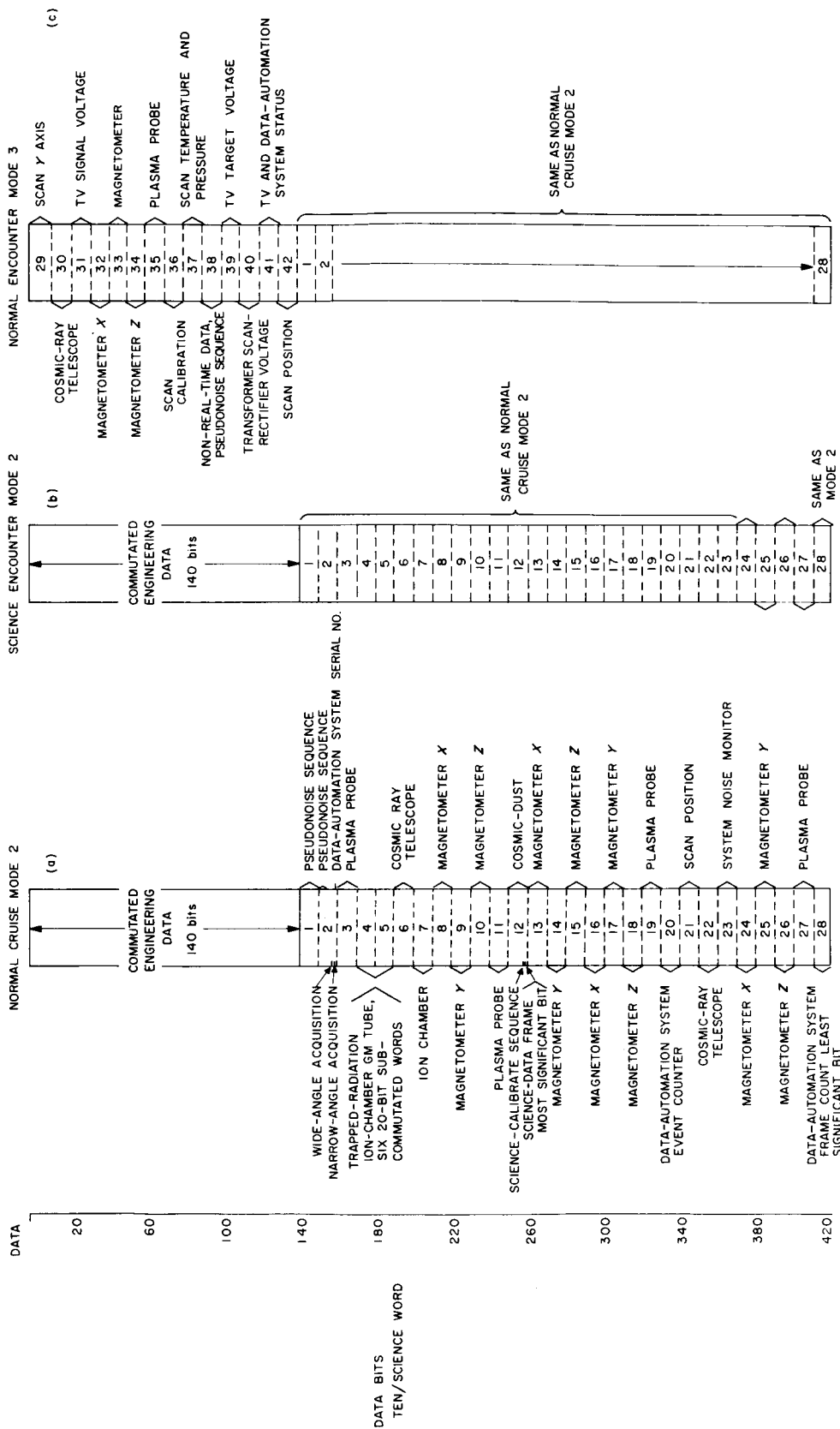


Fig. 1. Real-time data format

tape recorder. The measurements made by the RT-DAS were sent back via the telemetry channel and also transferred to the NRT-DAS for incorporation with the television data and storage in the tape recorder. Scan-platform motion was inhibited during the picture-taking sequence.

The science-encounter mode and spacecraft Data Mode 3 were terminated when the second end-of-tape signal occurred. A backup stop-recording circuit was also included in the DAS. This circuit was set after 18 pictures and reset after 22 pictures had been taken. This reset function activated the "switch to Data Mode 2" command to the data encounter in exactly the same fashion as in the second end-of-tape signal. The spacecraft stayed in Data Mode 2 until a central computer and sequencer (CC&S) or command decoder (CD) command caused the encounter instruments and the NRT-DAS to be deenergized.

The playback of stored science data could be initiated by either CC&S or CD command. The science subsystem was then deenergized, Data Mode 4 was initiated, and the stored data was transmitted to Earth. The pictures were transmitted individually. Between each picture the data encoder was switched to Data Mode 1 so that engineering telemetry could be transmitted and the condition of the spacecraft evaluated.

Upon completion of two picture data transmission cycles, the spacecraft operation reverted to normal cruise mode until mission termination.

## F. Data Format

One of the most important functions of the science subsystem was the arrangement of the data into a coherent form for transmission by the telemetry system. The choice of the format was based on the need for interrelating measurements between instruments to maximize their scientific value. A secondary requirement was to establish a format that would provide the subsystem operational status (engineering) data required to reduce the scientific data.

The data-automation system formats are shown in Fig. 1. Each spacecraft data frame contains 420 bits. During the normal cruise period, the spacecraft was in Data Mode 2 (Fig. 1a), with 140 bits of engineering data and 280 bits of science data. This format was unchanged

by the application of power to the encounter equipment (Fig. 1b). When the planetary-scan system acquired the planet, the data-automation system commanded the data encoder to Data Mode 3. Figure 1c and the science data occupied the entire telemetry-data frame. A close examination of Fig. 1 reveals that

1. The sampling of the three axes of the magnetometer was always followed by a sample of plasma data. This was done to obtain the closest correlation possible between the output data of the two instruments.
2. The particle counters, because of their relatively low counting rates, were subcommutated in words 4 and 5.
3. The first 16 bits of each of the science-data frames were a pseudonoise sequence. This provided a fixed reference point for data reduction and analysis.
4. The serial number of the data-automation system was included in the format to prevent data from one spacecraft from being confused with that of another.
5. A data-frame counter having a maximum capacity of 2048 frames was used to provide a measure of spacecraft time. This was possible because each frame has an equal length, in number of bits, dependent only upon the spacecraft data-transmission or bit rate.
6. The engineering data included in the data-automation system format contained internal subsystem housekeeping functions such as
  - a. An indication of planetary wide- and narrow-angle acquisition and the source of the acquisition.
  - b. An indication of when calibration sequences were in process.
  - c. A system noise monitor, the output of which was zero when no noise existed in the system.
  - d. A non-real-time (encounter) data pseudonoise sequence.
  - e. An event register for the events that occur only during encounter.

Two redundant methods were used to ensure that the data frame always started at the correct time. The data encoder sent a science gate or start-science-data-frame

command and the data-automation system counted 42 words (420 bits) and then reset its word counter. If, however, the two methods became asynchronous, only the science-gate signal would be acted upon.

The spacecraft (data encoder) word length was 7 bits. This was unsatisfactory from the science subsystem point

of view since compression of data, particularly analog data, into 7 bits would compromise the scientific value of the measurement. The word length selected for the science subsystem was 10 bits. All analog-to-digital conversions were 9 bits plus 1 bit to indicate signal polarity. This longer word length also simplified the subcommunication of the energetic-particle detector data.

### III. COSMIC-RAY TELESCOPE

J. A. Simpson and J. J. O'Gallagher

University of Chicago

#### A. Purpose and Objectives

The cosmic-ray telescope (CRT), shown in Fig. 1, was designed to measure the absolute and relative flux levels, and the energy spectra of the two main components of primary radiation, namely protons and helium nuclei, in the energy range from 1 to 170 Mev/nucleon. In addition, the telescope identified He nuclei in the 170 Mev/nucleon- $\infty$  range and electrons over a small range of energies with low efficiency. These measurements, which were made in interplanetary space during the cruise phase, as well as in the vicinity of Mars, included (1) measurement of the radial gradient in the low-energy cosmic-ray intensity between 1 and 1.5 A.U., (2) search for trapped radiation at Mars, and (3) study of the time and spatial dependence and the composition and spectra of solar-flare particles in interplanetary space.

The separation of spatial from temporal variations in the proton and helium spectra and fluxes is based on data obtained from instruments from the University of Chicago launched into Earth orbits September, 1964 (OGO-A and IMP-II), and in May, 1965 (IMP-III), and from the Neutron Intensity Monitor network.

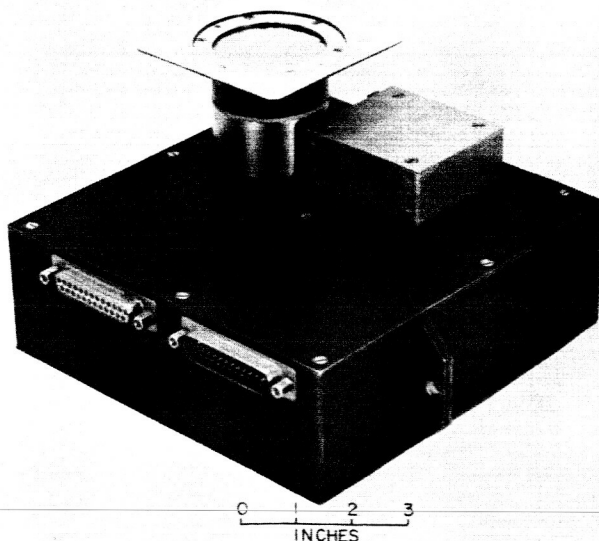


Fig. 1. Cosmic-ray telescope

#### B. Theory

To meet these objectives, a small three-element energy-loss-vs-range telescope was designed. This consists of three gold-silicon surface-barrier detectors, labeled  $D_1$ ,  $D_2$ , and  $D_3$ , arranged coaxially with absorbers between the first and second and second and third detectors as shown in Fig. 2. A particle must have at least 1 Mev/nucleon to penetrate the protective windows and produce a count in  $D_1$ . A particle that does penetrate  $D_1$  must have at least 15 Mev/nucleon to penetrate to  $D_2$  and at least 70 Mev/nucleon to penetrate to  $D_3$  through the intervening absorbers. Thus,  $D_1$  and  $D_2$  define an acceptance cone for producing coincidences of 20 deg half angle. The corresponding geometrical factor is  $0.25 \text{ cm}^2 \text{ steradian}$ .

Figure 3 shows the relation between energy loss in the  $D_1$  detector and particle energy and charge. The absorbers divide the response curve into three ranges, namely, 1 to 15 Mev/nucleon, 15 to 70 Mev/nucleon, and greater than 70 Mev/nucleon. Two points are worth noting:

1. For all particles with sufficient range to produce double or triple coincidence, the energy loss *decreases* with increasing energy to a minimum value, thus setting an upper limit of 170 Mev for protons.
2. The energy loss is proportional to  $Z^2$  so that He nuclei with  $Z = 2$  are completely separated from protons

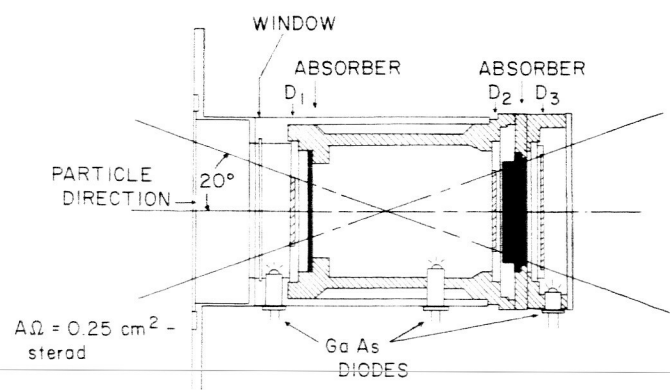


Fig. 2. Cosmic-ray telescope sensor



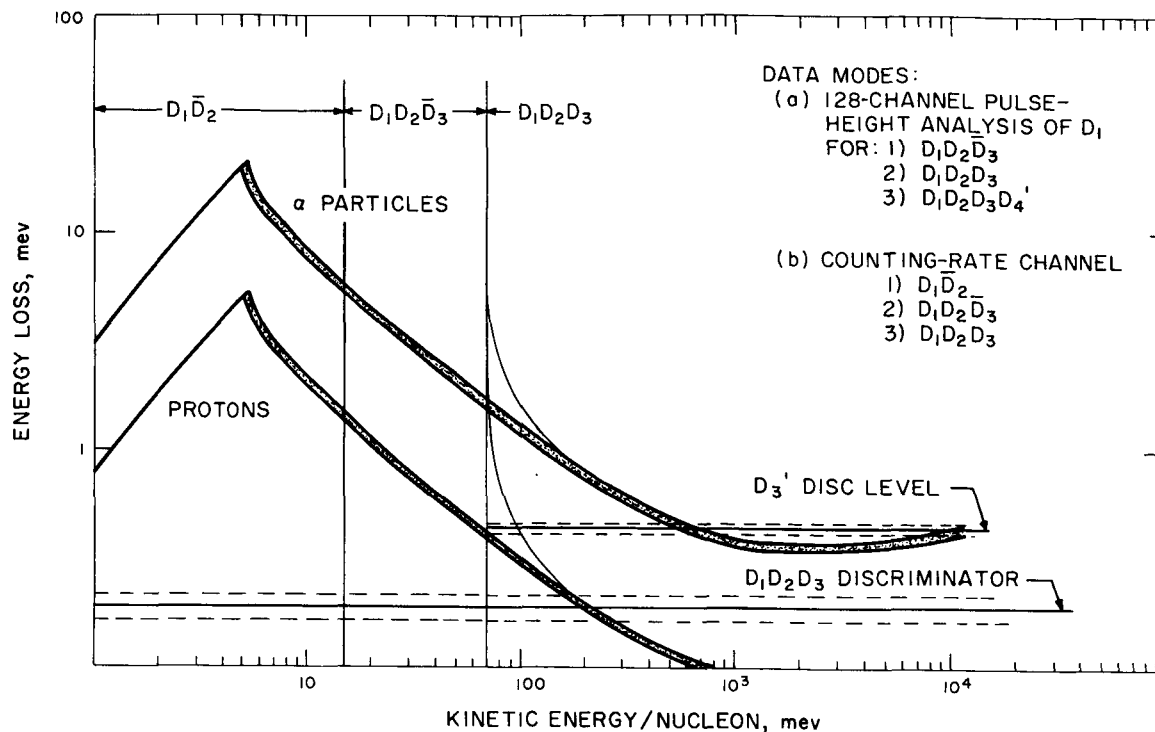


Fig. 3.  $D_1$  energy loss

in the 15-70 Mev/nucleon range by energy-loss measurement and have no upper limit of energy for detection in the greater-than-70 Mev/nucleon range.

**C. Procedure**

**1. Measurements**

Figure 4 is a simplified block diagram of the telescope circuits. Two entirely different types of measurement are made. After amplification by charge-sensitive amplifiers, the signals from the detectors are fed to a set of discriminators. These discriminators in turn lead into coincidence-anticoincidence circuits which have as an output the three counting rates corresponding to the three aforementioned ranges, namely, the singles counting rate of the  $D_1$  detector  $D_1 D_2$  (" $D_1$  and not  $D_2$ ") and two coincidence rates  $D_1 D_2 D_3$  and  $D_1 D_2 D_2$ . These rates with small prescaling are stored in one 10-bit register. The energy loss in the  $D_1$  detector is sampled for  $D_1 D_2 D_3$  and  $D_1 D_2 D_2$  events by recording the pulse height corresponding to the  $D_1$  energy loss for the first  $D_1 D_2$  coincidence produced after each readout in a 128-channel pulse height analyzer.

In addition, indicator bits record whether the event was a double or triple coincidence and, if triple, whether

the energy loss in  $D_3$  was high or low. This second discrimination level on the  $D_3$  detector ( $D_3'$ ) is used to help determine the contribution due to particles entering from the back of the telescope and to separate He nuclei and protons in this higher energy range. This information is stored in a second 10-bit register.

These two registers are each read out serially by the DAS, which supplies a train of 110-kHz pulses to the register, and in parallel into a register within the DAS. The eventual overflow of the CRT register generates a pulse which, when received in the DAS, shuts off the pulse train leaving the DAS register containing a number which is one more than the one's complement of the CRT binary register.

The DAS reads out the particle analysis and count-rate registers in even- and odd-numbered frames, respectively and in any given frame, words 6 and 22 (and 30 during encounter mode at Mars) are CRT data from the corresponding register. This results in accumulation times of 72 and 19.2 sec for words 6 and 22, respectively, at the  $8\frac{1}{2}$  bit/sec transmission rate and one quarter of these times at the  $33\frac{1}{2}$  bit/sec rates. These times are short enough to insure that the storage capacity of the coincidence rate channels exceeds the observed count rates of  $\sim 2.0$  c/min by at least a factor of 10 under normal

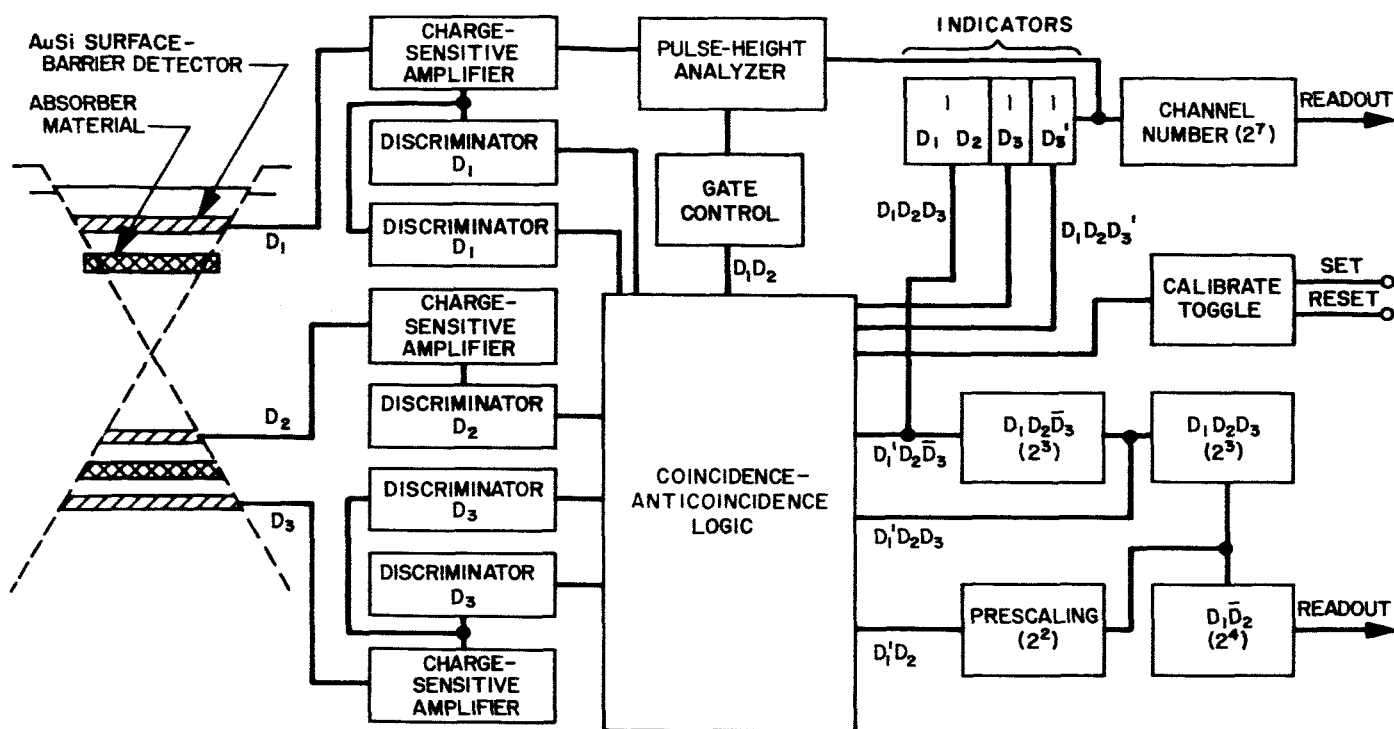


Fig. 4. Cosmic-ray telescope, simplified block diagram

conditions. Statistical analysis is used to extend this range for flare conditions.

## 2. Calibration

The three means of calibration used for the cosmic-ray telescope include both artificial pulse generation and energetic particle measurements using natural radioactive sources or accelerated particles from laboratory accelerators. The most accurate measurements are made using a pulse generator to feed voltage pulses through a calibrated probe input to each of the three charge-sensitive preamplifiers. This deposits at these inputs an amount of charge corresponding to a known energy. The thresholds of the five discriminators and the input response curve of the pulse-height analyzer are measured in terms of energy, with an accuracy of  $\pm 0.5\%$ , by the varying amplitude of the pulse.

For operation in flight and during spacecraft testing, a calibrate mode of instrument operation has been incorporated in the CRT. Permanently installed low-level  $\text{Am}^{241}$  alpha-particle sources on each of the three detectors are encapsulated between two thin layers of Mylar and the particles have only enough energy to penetrate to the detector on which they are mounted. Hence, in the

data mode of operation they produce no coincidence or pulse-height analysis, but only contribute to the  $D_1\bar{D}_2$  rate. In the calibrate mode of operation the coincidence circuits are disabled, allowing the individual count rates on  $D_2$  and  $D_3$  to be recorded and pulse-height analysis of the  $D_1\bar{D}_2$  events to proceed.

Changes in the counting rates of  $D_2$  or  $D_3$  would indicate shifts in the corresponding threshold. The source on  $D_1$  is constructed so as to provide a peak in the pulse-height distribution of a known energy which would thus reflect any changes in amplifier or ADC gain. The plot of such a distribution is shown in Fig. 5. These measurements are primarily designed to be gross checks since the rate of all of these sources lie between 1 and 10 c/min so that long times would be required to build up statistics for accurate measurements. However, they will provide a continuous monitoring of the gain and threshold levels throughout the mission. In flight, the instrument is put into the calibrate mode by command from the spacecraft DAS for a little more than 1 out of every 27 hr.

In addition to being subjected to the aforementioned measurements, all flight units have been exposed to high-energy proton beams from the University of Chicago

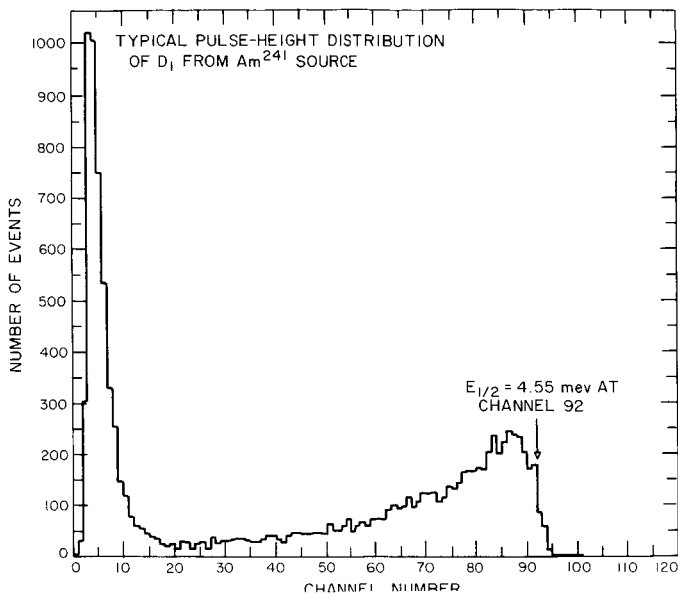


Fig. 5. Calibration pulse-height distribution

170-in synchrocyclotron. The use of penetrating charged particles measures the actual energy ranges produced by the absorbers used in the telescopes. Also the sensitivity of this type of detector to high fluxes of electrons of less than 40 keV and to somewhat lower fluxes of  $> 200$  keV electrons has been measured with the University's small electron accelerator.

Periodic checks of the coincidences and ADC logic assured that the equipment maintained its calibration. Inasmuch as there are no natural radioactive sources of protons or alpha particles with sufficient energy to produce coincidences in the cosmic-ray telescope, a method of artificial stimulation of the individual detectors that simulates coincidences from protons and alpha particles and exercises the logic has been designed at the University of Chicago. This method uses three infrared-producing GaAs diodes mounted so that each diode views one solid-state detector in the telescope as shown

in Fig. 2. These AuSi detectors are sensitive to infrared radiation, producing electron-hole pairs when such radiation is incident on their surface. The three diodes are driven by a program generator capable of delivering to any combination of detectors a preset number of pulses in coincidence at a large number of preset rates. The flexibility of the program generator thus allows the logic and storage to be exercised completely.

A further but somewhat limited logic check was obtained periodically by mounting a  $Sr^{90}$  source on the front radiating fin of the telescope. This source produces 2.2 MeV electrons to which the telescope has a small sensitivity in that a small fraction of the electrons can penetrate the aluminum absorber to  $D_2$  after passing through  $D_1$ , thus producing double (never triple) coincidences at a rate of about 0.5 c/min. This check does not provide any calibration points nor does it exercise all of the logic. It was intended only as a go-no-go check.

#### D. Description of Equipment

The entire instrument weighs 2.6 lb and requires 600 mw of power in continuous operation. It contains 1200 electronic components. Figure 2 is a picture of the instrument with the protective covers for the electronics trays removed. The packaging is of the cordwood module type in which there is nearly a one-to-one correspondence between blocks in the block diagram and modules. The modules are mounted on printed-circuit "mother boards" which essentially "float," i.e., they are not fastened except by the wire connections and are sandwiched between sheets of foam rubber and held in place by the protective cover.

The flight behavior of the electronics of this instrument has been nominal in all respects, showing drifts of less than 1% in the pulse-height analyzer and discriminator thresholds. A number of important scientific results have been published, to be followed by a number of longer-term studies.

## IV. COSMIC-DUST DETECTORS

*D. K. Schofield*

*Jet Propulsion Laboratory  
Pasadena, California*

### A. Purpose

The cosmic-dust detector was designed and manufactured jointly at Goddard Space Flight Center NASA facilities and Marshall Laboratories in Torrance, California. The instrument was used on *Mariner IV* in support of micrometeorite studies conducted by W. M. Alexander of Goddard Space Flight Center.

Dust-particle measurements taken to date have revealed a dust concentration near Earth with a mass distribution somewhat different than that of interplanetary space.

Until the advent of satellites, indirect measurements of dust particles were made using optical and radar techniques.

A single device for direct measurements of the dust-particle characteristics near Earth and in space would be valuable in studying their momentum, mass distribution, flux densities, and time histories. The *Mariner IV* cosmic-dust detector provided just such measurements.

The objectives of the cosmic-dust detector were to continually monitor dust-particle flux and mass distribution from Earth proximity through the Mars encounter and to observe the following:

1. The degree of dust-particle concentration near Earth and near Mars.
2. The rate of change of the dust-particle flux density with respect to distance from Earth.
3. The perturbation effects of large planetary bodies on the dynamic behavior of the dust particles.

With a knowledge of the spacecraft orientation, the instrument will determine whether the dust particles are in direct or retrograde orbits with respect to the spacecraft.

### B. Description

The instrument (Fig. 1) consists of a single assembly containing a sensor and electronics in one chassis. The

plate, seen in the vertical position, is the sensor. Its major dimensions are  $22 \times 22$  cm. The case upon which the sensor is mounted contains the electronic circuits.

The instrument is mounted above the main spacecraft bus, with the case just inside the thermal shield to protect it from the Sun. The sensor, protruding through an opening in the thermal shield, will detect dust particles encountered by the spacecraft.

The sensor is an aluminum impact plate with a crystal acoustical transducer (microphone) bonded to one side. The transducer will detect mechanical vibrations set up in the plate by impacting particles. Both sides of the plate are coated with a nonconducting material over which is evaporated a thin film of aluminum. The impact plate-dielectric-aluminum film combination constitutes a penetration detector in the form of a capacitor.

If a static potential is applied across the capacitor in series with a resistor, any penetrations of the capacitor

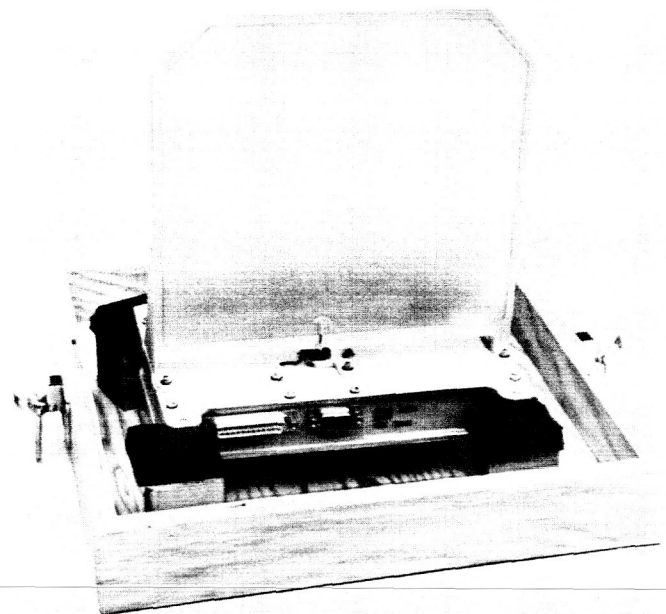


Fig. 1. Cosmic-dust detector

will produce a voltage pulse into the film circuits. The capacitors are more than an order of magnitude more sensitive than the microphone (acoustical sensor) and their use on both sides of the impact plate will provide directional information of the impinging particle.

The instrument memory consists of two 8-bit binary registers called the data-analysis register and the microphone accumulator. Figure 2 is a functional block diagram of the instrument.

The data-analysis register contains

1. Three binary bits (7 levels) of pulse-height analysis data of the impacting particle momentum. (Z121, Z122, Z123)
2. Two binary bits for indication of the particle's incoming directions. (Z124, Z125)
3. Three binary bits for capacitor penetration event accumulation. (Z126, Z127, Z128)

This register is reset after each data readout.

The microphone accumulator is a conventional 8-bit register which records the number of microphone events observed by the instrument. This register is not reset after each data readout because of the low anticipated event rate.

The output of the two registers is in parallel transferred to eight logic modules where "OR" functions are performed, so that upon receipt of a readout command one register is readout. The next readout command reads out the other register and so forth. These outputs are fed through the output modules to the data-automation system.

### C. Function

When a particle impacts the plate, it produces a positive spike to the film circuits and bursts of 100-kc sine waves out of the microphone crystal. This signal from the microphone is amplified, rectified, and detected in the microphone amplifier and fed to a comparator circuit. If the amplitude of this signal is greater than the preset

threshold of the comparator, the output of the comparator circuit will, through associated circuits,

1. Start a 5-kc clock that will dump binary bits into the P.H.A. portion of the analysis register. (The number of bits is a function of the particle momentum.)
2. Inhibit the microphone amplifier for a 30-ms period to prevent circuit excitation at the time of particle analysis.
3. Combine "OR" with the output of the film circuits (through logic circuits) to produce a direction identification in the analysis register.
4. Produce a one-bit increase in the microphone accumulator.

It may be noted that activity has taken place in the microphone accumulator and the direction and pulse-height analysis portions of the analysis register. The only portion not mentioned thus far has been the film accumulator portion of the analysis register.

The film amplifiers are not inhibited with the microphone amplifier. Their outputs are read into the film-accumulation register through "OR" logic and provide an indication of impacts, if any, during the analysis period.

### D. Summary

In summarizing, we have noted data concerning

1. The particle momentum.
2. The incoming-particle direction.
3. Particle impacts below the microphone threshold.
4. Microphone event accumulations.

During the mission, any instrument degradation could be detected by means of an in-flight calibration. The in-flight calibrate command was sent to the instrument once a day. Upon receipt of the calibrate command, a bi-stable multivibrator was toggled. The outputs of the multivibrator were routed through gated circuits to produce high- and low-level signals. These drove the microphone circuits with a high-level signal on one calibrate command and a low-level signal on the next calibrate command. These signals were simulated particle impacts and produced known data in the pulse-height analyzer portion of the analysis register. The film circuits were also activated as a result of the calibrate command.

The in-flight calibrations on *Mariner IV* have all been good and no degradation was detected.

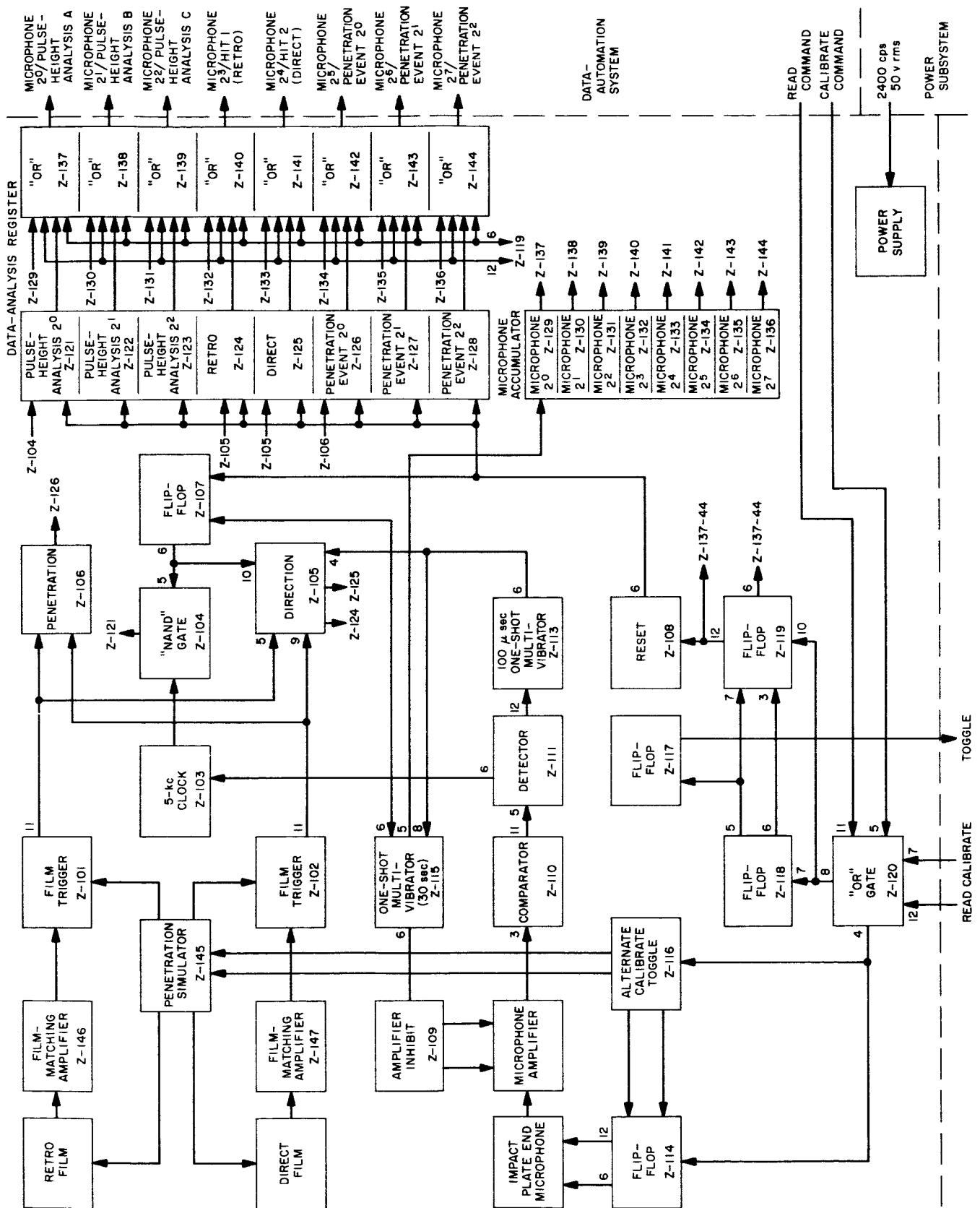


Fig. 2. Cosmic-dust detector, functional block diagram

## V. TRAPPED-RADIATION DETECTORS

D. K. Schofield

Jet Propulsion Laboratory  
Pasadena, California

D. Chinburg and D. Enemark

State University of Iowa

### A. Purpose

The trapped radiation detector was designed and fabricated at the State University of Iowa for the support of further studies on geomagnetically trapped particles by Dr. James Van Allen.

Dr. Van Allen discovered what are now called the Van Allen radiation belts during the early *Explorer* satellite flights. These belts are believed to contain charged particles emanating from solar eruptions which ultimately are trapped in the magnetic field of the Earth.

There are essentially two belts: the inner and outer belts. The inner belt consists primarily of protons and is at a distance of approximately 5,000 km from the Earth at the equator. The outer belt is composed primarily of electrons and is approximately 10,000 to 15,000 km from Earth at the equator.

The prime objective of the trapped-radiation detector was the measurement of similar radiation belts in the vicinity of Mars.

Secondary objectives for the instrument included new measurements of the Van Allen radiation belts taken during the ascent from Earth to the interplanetary medium and measurement of interplanetary cosmic rays while enroute to Mars. These measurements included flux density, energy, directional characteristics, time histories, and the identities of the particles encountered.

### B. Description and Function

The instrument, located on top of bay IV of the spacecraft bus, consists of three Geiger-Mueller (GM) tubes for proton and electron detection, a solid-state detector for proton detection, and a power supply, all in a single magnesium chassis. The device is illustrated in Fig. 1 and 2. Figure 3 is a simplified block diagram of the circuits.

The solid-state detector electronics are contained in a separate RF shielded chassis within the main chassis.

Detectors A, B, and C are type 6213 end-window Geiger-Mueller tubes having nominal energy thresholds of 40 keV for electrons and 500 keV for protons. The tube measures the total number of charged particles passing through its sensitive volume. This volume was shielded so that particles of low and moderate energies may enter only through the window. Particles of much higher energy may penetrate the shield and enter from other directions. However, by allowing for the omnidirectional flux of high-energy particles, a directional measurement of low- and medium-energy particles may be achieved.

Since detector C was to measure higher-energy particles, its energy threshold was increased to 130 keV for

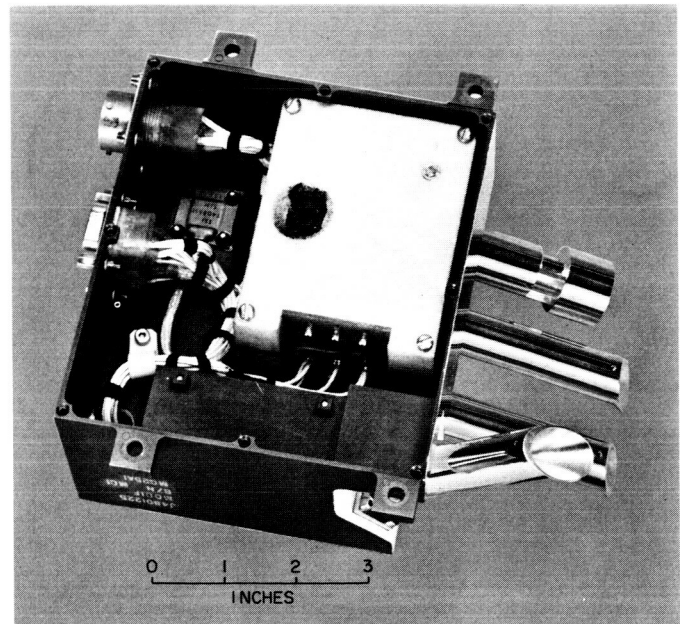


Fig. 1. Trapped-radiation detector, top view

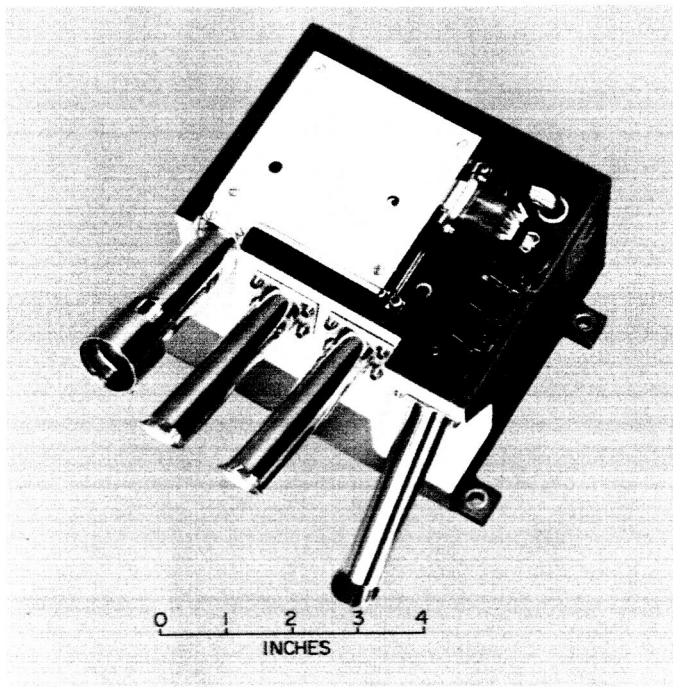


Fig. 2. Trapped-radiation detector, bottom view

electrons and 3 Mev for protons. This was achieved by placing a sheet of aluminum  $\approx 0.0025$  in. thick behind the housing aperture. Thus, with the combination of all

three tubes, data was collected at different view angles on particles falling within the range of 40 kev to 3 Mev.

The output pulses from the three GM tubes are fed into separate complementary NPN-PNP saturating devices which shape and condition them for use in the data-automation system.

Detector D is a two-channel proton spectrometer designated  $D_1$  and  $D_2$ . The energy threshold level of channel  $D_1 = 500$  kev  $\rightarrow$  11 Mev and the threshold level of channel  $D_2 = 880$  kev  $\rightarrow$  4 Mev.

Detector D measures the flux and energy of protons and alpha particles within these given ranges while remaining insensitive to electrons, making it possible to differentiate between the protons and electrons counted by the GM tubes.

Immunity to electrons was accomplished by a combination of three measures:

1. Use of a thin detector to minimize energy loss of penetrating electrons.
2. Use of discrimination levels far above the probable energy loss for individual electrons.

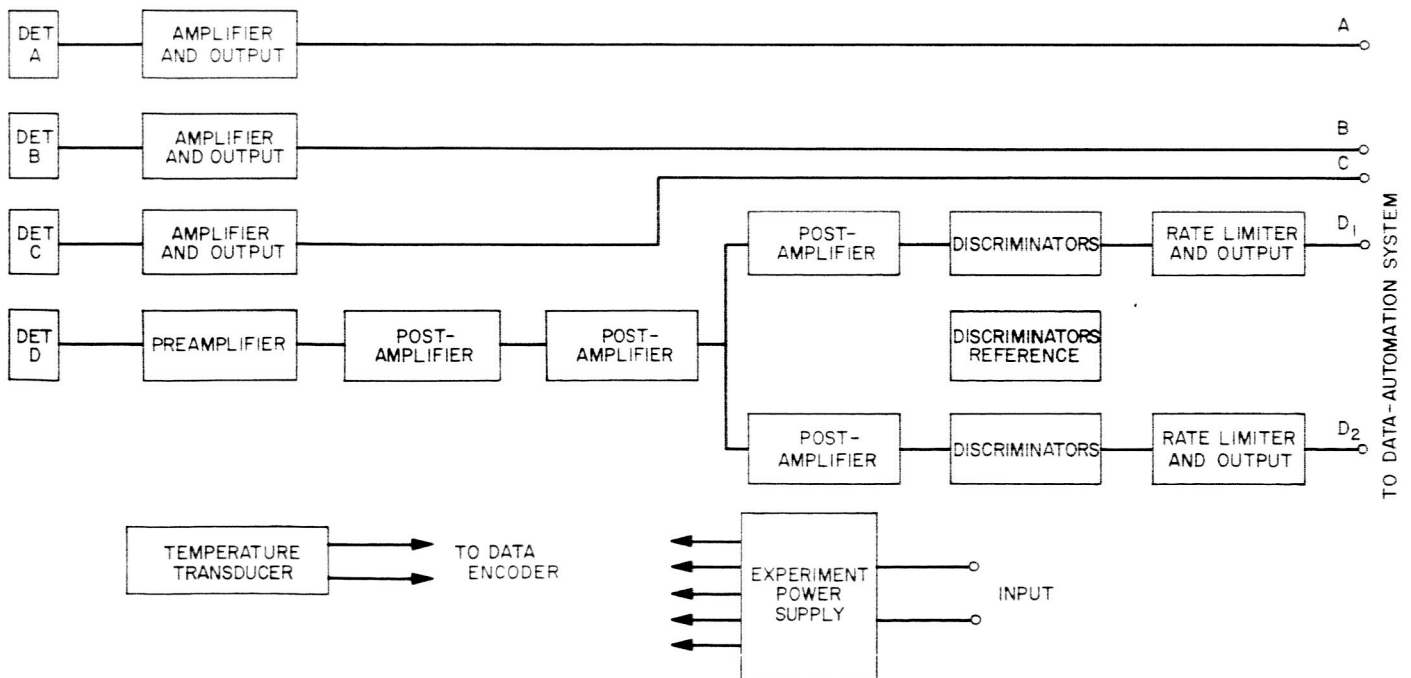


Fig. 3. Trapped-radiation detector, functional block diagram



3. Use of an amplifier with a fast pulse-resolving time to avoid coincidence of low-energy pulses which may pile up to the discrimination level and add counts to the output.

Detector D output is fed into a linear charge-sensitive amplifier. (The main advantage of the charge-sensitive amplifier as opposed to the voltage-sensitive amplifier is that the amplifier output voltage is a function of the particle charge lost in the detector and is therefore insensitive to input capacitance changes in the amplifier.) The preamplifier is followed by a series of highly stable negative-feedback amplifiers (called postamplifiers). The output of the second post-amplifier is fed in parallel to two postamplifiers having different voltage gains. These outputs are transferred to

two identical amplitude discriminators having a common reference supply.

The gains of the postamplifiers were set during instrument calibrations to produce pulses at the discriminators that correspond to the particle detected.

Outputs from the discriminators were fed to the output and rate-limiter circuits that, through the use of a monostable multivibrator and shaping circuits, limit the maximum counting rates below 50,000 c/sec and shape the pulses for use in the data-automation system.

Operation of the unit during the flight of *Mariner IV* has been quite satisfactory in all respects.

## VI. IONIZATION CHAMBER

L. G. Despain and H. A. Andersen

Jet Propulsion Laboratory  
Pasadena, California

### A. Introduction

In recent years considerable emphasis has been placed on determining the energy distribution and the time variation of charged particles in the region that extends from the Earth's surface to the boundary of the magnetosphere. With the advent of unmanned interplanetary exploration, the opportunity is presented to extend the range of investigation beyond the magnetosphere into interplanetary space and even into regions of close proximity to various planets.

Among the many and varied instruments used for making useful measurements regarding charged particles in space are the ionization chamber and the Geiger-Mueller (GM) counter. A particularly stable type of integrating ionization chamber was first developed at the California Institute of Technology in 1950. A modification of this instrument has adapted it for spacecraft use, along with a particularly suited GM tube, on the *Mariner-Mars '64* mission.

### B. Scientific Objectives

The principal objectives of the experiment were

1. To measure ionizing radiation in interplanetary space with such stability and accuracy that changes amounting to only a few percent during a period of several months can be observed. Special interest was focused on
  - a. Dependence of radiation intensity upon distance from the Sun, and
  - b. Dependence of the correlation between changes in radiation at two points upon the distance between the points.
2. To observe the time history of the rise and decay of solar-flare radiation.
3. To observe the relationship between radiation intensity and the plasma and magnetic field measured at the spacecraft.
4. To determine the dependence of items 1, 2, and 3 upon the phase of the solar cycle. This requires that

similar measurements be made on more than one interplanetary spacecraft.

5. To measure energetic, magnetically trapped particles at Mars, if any.

To make these measurements, an integrating ionization chamber was used because of its long-term stability. A single GM counter with similar shielding (Fig. 1) was used as a secondary detector.

### C. Constraints and Requirements

To minimize effects due to shielding and scattering, the detectors had to be mounted on the spacecraft so that the spacecraft components would subtend the minimum possible solid angle at the location of the detectors. This was especially important for the more massive portions of the spacecraft. In addition, the two detectors had to be located as close together as possible so that they would experience the same flux of radiation. For these reasons the instrument was mounted on the omnidirectional antenna away from the body of the spacecraft. In this position the comparatively massive spacecraft body subtends only 8% of  $4\pi$  steradians at the detectors. The instrument chassis, waveguide, and solar panels subtend an additional 20% of the solid angle.

Mounting the instrument on the antenna mast with insulated washers affords the electrical isolation from the spacecraft structure required by the science subsystem.

The time between successive output pulses is the important ionization-chamber parameter to be measured, while, in the case of the GM tube, the number of pulses per unit time is the parameter required. In both cases the respective pulses are transmitted on separate lines to the data-automation system (DAS) for handling. The DAS measures the time interval between the beginning of a frame and the arrival of an ion-chamber output pulse in increments of 1.2 or 0.3 sec, depending on the prevailing bit rate. In addition, the number of ion-chamber pulses per frame is also recorded. If the rate from the ion chamber is one pulse per frame or less (the usual case in

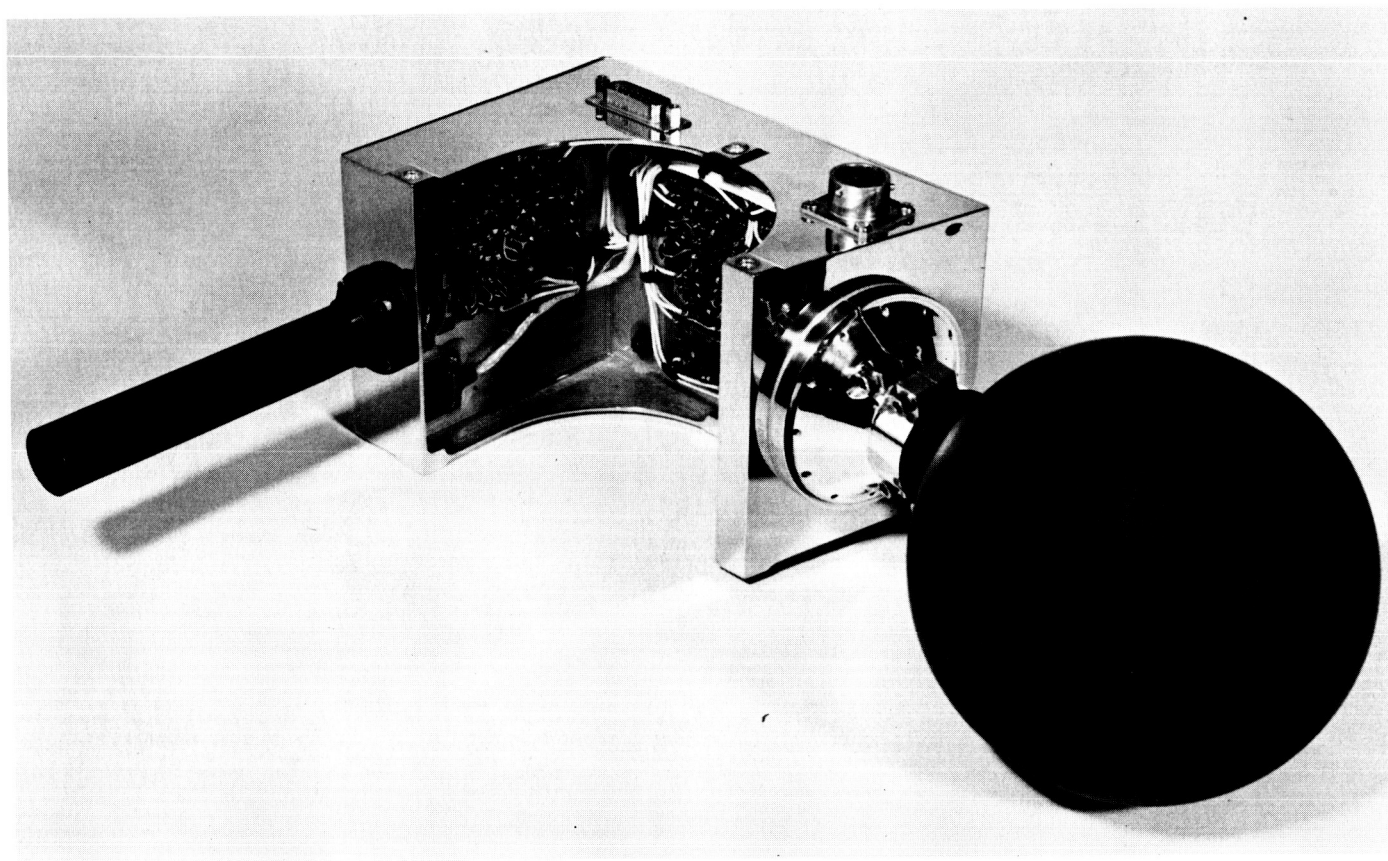


Fig. 1. Ionization chamber

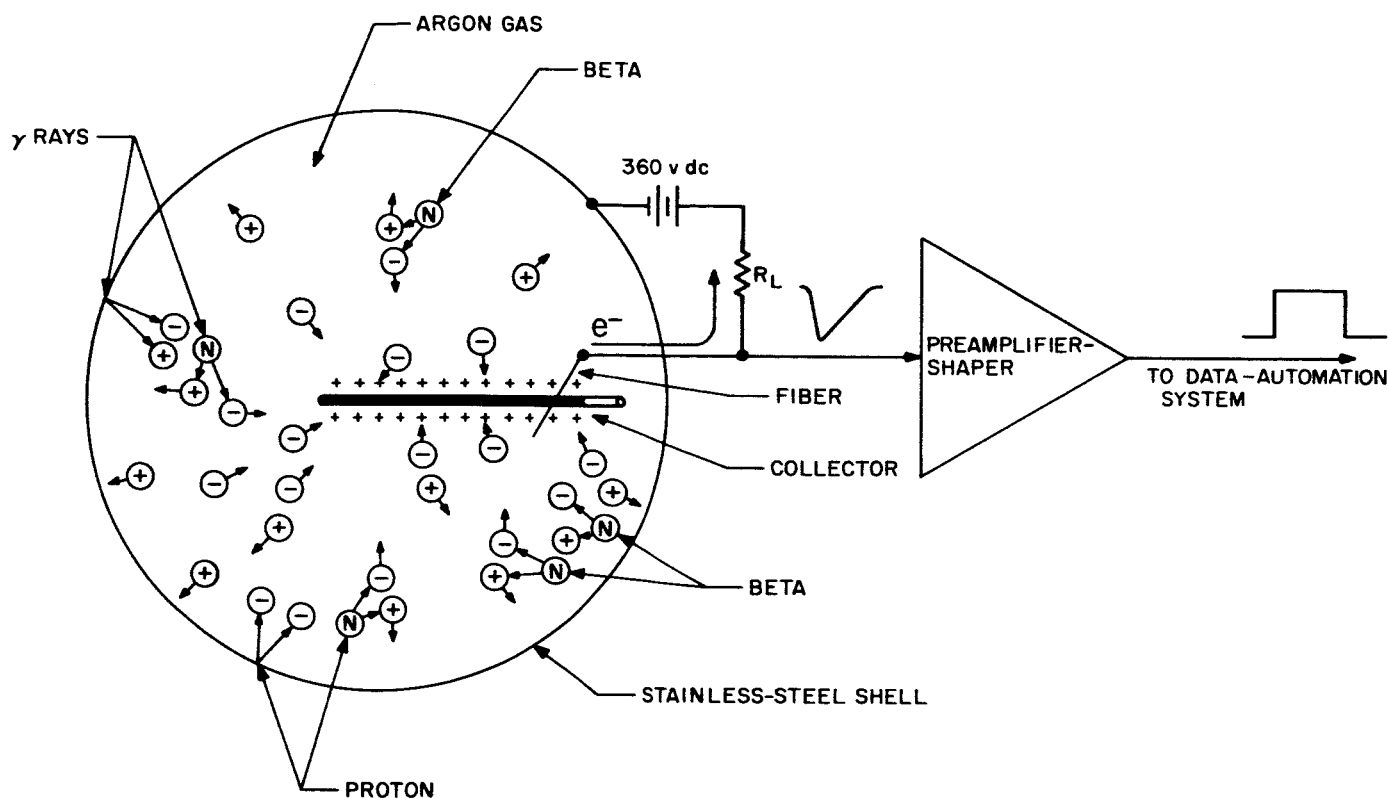
quiescent space), the time between ion-chamber output pulses can be calculated. For more than one pulse per frame the exact time pulses cannot be obtained, but the number of pulses per frame is more significant at these rates and is directly recorded. At rates of 7 or more pulses per frame, all interval-timing bits are reset and the entire ion-chamber data word is devoted strictly to counting pulses. An indicator bit is set by the eighth pulse in any one frame and is useful in reducing the data. In this mode the data register is capable of tabulating as many as  $2^9-1$  pulses per frame. Ion-chamber data are read out once every frame.

The GM tube registers are capable of recording as many as  $5 \times 2^{19}$  pulses per frame. When 19 bits of the 20-bit register are filled ( $2^{19}-1$  pulses per frame), the next pulse triggers a change of tabulating mode. Incoming GM tube pulses are then prescaled by a factor of four before being recorded in the data register. The change to the prescale mode is signalled by an indicator bit to avoid ambiguity. Data from the GM tube are commutated with data from other sensors and consequently are read

out only every fourth frame. Pulses are accumulated for 45 or 11.25 sec when the telemetry bit rates are  $8\frac{1}{2}$  and  $33\frac{1}{3}$  bits/sec, respectively.

#### D. Functional Description

The ionization chamber consists of a stainless-steel sphere filled with argon gas. A quartz electrometer is housed within the sphere and consists of a quartz collector rod and a thin quartz fiber that is separated from the rod by approximately 0.02 in. The collector is coated with Aquadag and the fiber is coated with a thin film of metal. Although the collector is electrically isolated from the fiber and sphere, it is normally positively charged. This charge is produced by a +360 v dc potential on the fiber, which induces a negative image charge on the Aquadag surface of the collector near it. As a result of this image charge, the fiber is attracted to the collector and momentarily contacts it. During contact, electrons pass from the collector to the fiber. When the electron exchange is completed, the fiber springs back to its normal position, leaving the rod positively charged to +360 v.



NOTE: N = NEUTRAL ARGON ATOM

Fig. 2. Ionization chamber radiation detector

When ionizing particles penetrate the sphere, the gas within the chamber becomes ionized (Fig. 2). The resulting positive ions are attracted to the grounded sphere while the electrons are attracted to the collector and tend to neutralize its positive charge. When the collector charge is sufficiently neutralized, the image charge, as previously described, attains sufficient magnitude so that the fiber is pulled to the collector and finally contacts it. A surge of electrons passes from the collector to the fiber and through a load resistor. This current pulse is amplified and presented to the DAS as shown in the block diagram (Fig. 3). Each output represents a fixed amount of charge collected from the gas. Thus, the interval between pulses is inversely proportional to the ionization rate.

The GM sensor consists of a glass tube encased in a stainless-steel cylinder. The anode consists of a tungsten wire stretched along the axis of the tube, while the cathode consists of a thin, transparent, conductive coating on the inner glass wall. Approximately 900 v are maintained between the electrodes. Charged particles which penetrate both the steel shield and the glass wall and enter the sensitive volume of the tube ionize the gas

molecules, as is shown in Fig. 4. The high electric field between the anode and the electrode accelerates the dissociated ions and electrons. The electrons accelerate rapidly because of their low mass and ionize other gas molecules. The ultimate result of the avalanche effect thus produced between electrodes is a momentary current flow through an appropriate load resistor. The resulting pulse is amplified, shaped, and delivered to the DAS as shown in Fig. 3. One output pulse is generated for each charged particle that penetrates the shield and enters the sensitive region of the tube. Thus, the pulse rate is directly proportional to the radiation flux.

Because of a judicious choice of GM tube-shield thickness, both the ionization chamber and the GM tube detect particles of the same energy, i.e., electrons of energy greater than 0.5 Mev, protons of energy greater than 10 Mev, and alpha particles of energy greater than 40 Mev are capable of penetrating the walls of either detector. Both sensors have omnidirectional sensitivity. The ionization chamber measures the average rate of ionization and the GM tube measures the omnidirectional flux.

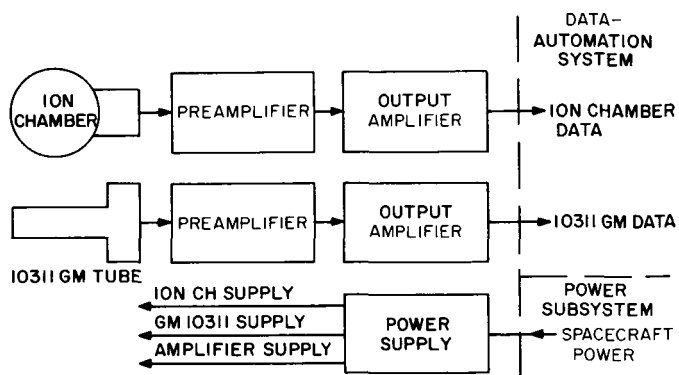


Fig. 3. Ionization chamber, functional block diagram

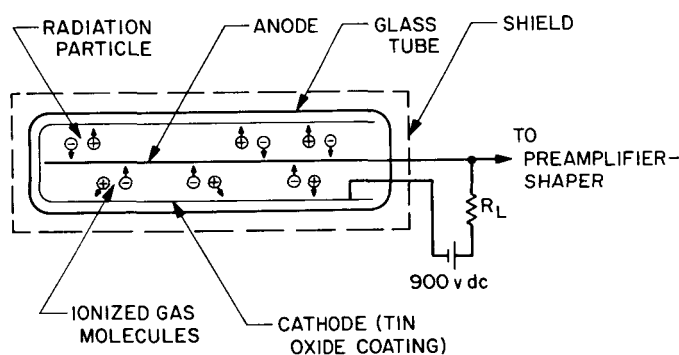


Fig. 4. Geiger-Mueller radiation detector

**E. Physical Description**

The instrument package is made up of four elements: (1) the ionization chamber; (2) a GM tube; (3) electronic circuits consisting of power supply, amplifiers, and pulse shapers; and (4) the chassis to which the foregoing three items are mounted. The overall dimensions of this 2.6 lb assembly are 13.4 x 9.8 x 5.0 in. The assembly system is shown in Fig. 5.

The instrument requires less than 500 mw of raw 2400 Hz, 50 v rms power for its operation. It uses 191 electronic components.

The ion chamber (Fig. 6) consists of a gas-filled 5-in.-diameter sphere, an electrometer, a neck, and a support mechanism for securing the chamber to the electronics subassembly. The surface of the sphere and neck are black oxide to provide the desired thermal emissivity, and the support surface is polished aluminum. The wall thickness of the stainless-steel sphere measures 0.010 in. The overall length of the chamber subassembly is 7.3 in.,

the neck is 1.5 in. in diameter, and the support base is 2.9 in. in diameter. It consumes less than 10 mw of power.

The electrometer consists of a quartz ion collector rod, a quartz fiber, a shielding can, a spider, a spider spring, a cup, and a header. The tapered quartz collector extends through the center of the sphere. The side arm, an integral part of the collector rod, supports the fiber that passes over the collector. The fiber is separated from the collector by 0.02 in. The quartz fiber is welded to the side arm and coated with metal. An Aquadag coating is also placed on the side arm and collector and the uncoated portion of the quartz collector is placed in a silver mounting cup that is held with a spring to a spider plate on the header. The spider is brazed to the header.

The cup is then filled with molten silver chloride, which secures the collector rod to the mounting cup when it solidifies. To prevent the fiber from being affected by variations in supply voltage, the fiber is enclosed by a shielding can which reduces electrostatic forces between the fiber and sphere. This can is spot-welded to the spider skirt. One end of a platinum jumper wire is cemented to the side arm with silver chloride and the other end is welded to a header pin. The header seals the electrometer and argon-filled chamber interior from the atmosphere and it provides electrical contact from the fiber to the preamplifier and high-voltage power supply (+360 v dc).

A filler tube is used to evacuate the chamber during assembly and to fill it with argon. It is threaded for easy removal if the sphere develops a leak. The shell interior, evacuated at bakeout temperature (400°C), is filled with argon gas to an absolute pressure of 4 atm.

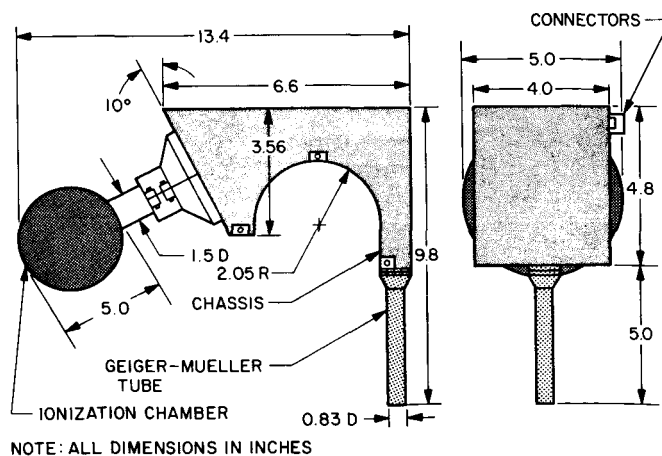


Fig. 5. Dimensional diagram of ionization chamber

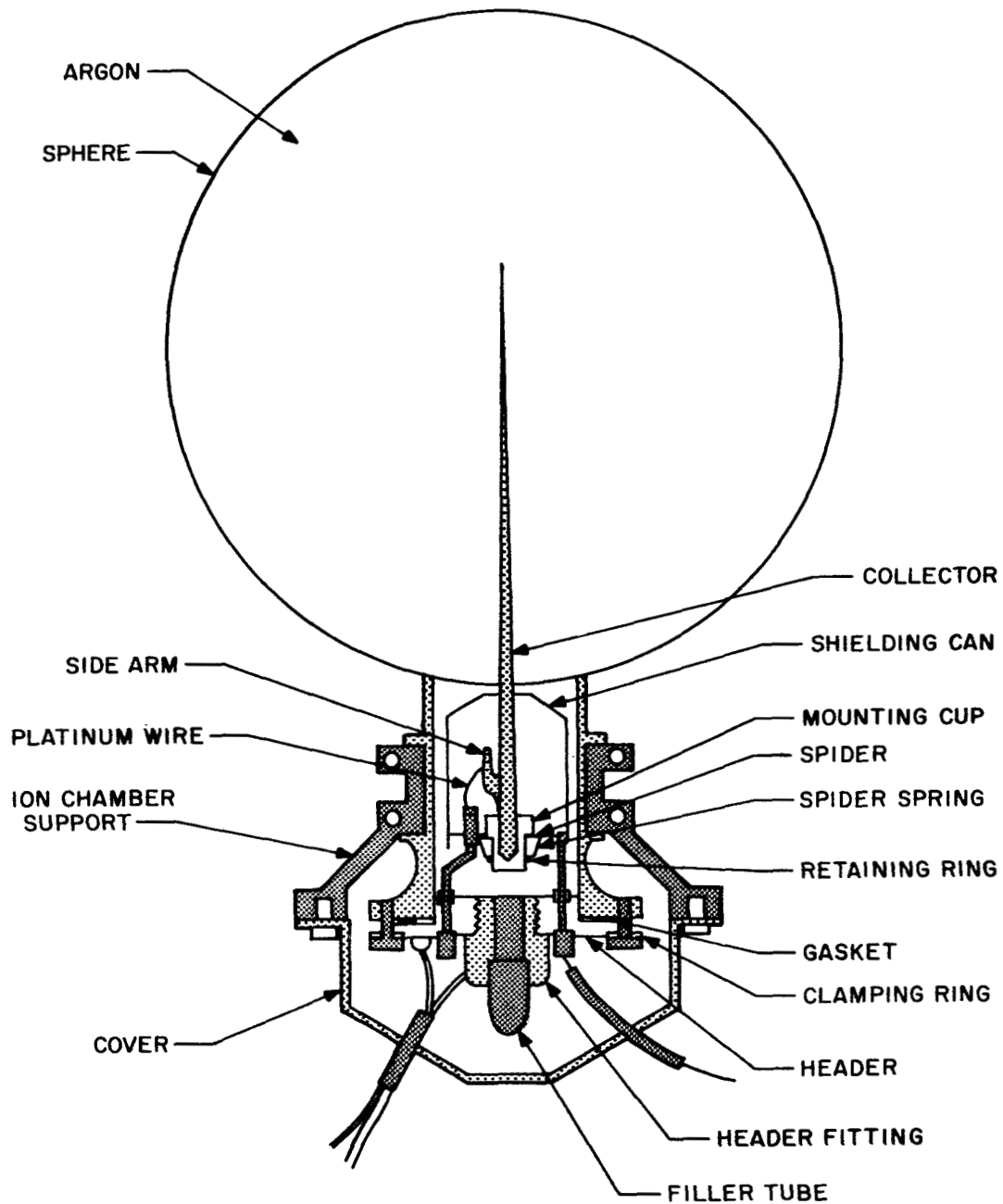


Fig. 6. Cross-section of ionization chamber

The Geiger-Mueller tube subassembly consists of Model 10311 GM tube and a stainless-steel cylindrical shield. The GM tube, manufactured by Radiation Counter Laboratories, is a thin-walled general-purpose instrument filled with neon and halogen gases (Fig. 7). A small amount of halogen gas is used to quickly restore (quench) the ionized neon atoms to their neutral state after the source of radiation is removed. The glass tube is 4.75 in.

long and 0.62 in. in diameter. A 0.003-in.-diameter tungsten anode extends across the tube and is supported on one end by a glass insulator. The cathode, a tin-oxide coating around the inner surface of the glass tube, contacts a metal ring which connects to a short electrode.

The tube is shielded by a 0.83-in.-diameter stainless-steel cylinder 5 in. long. Two RTV (silastic) insulators

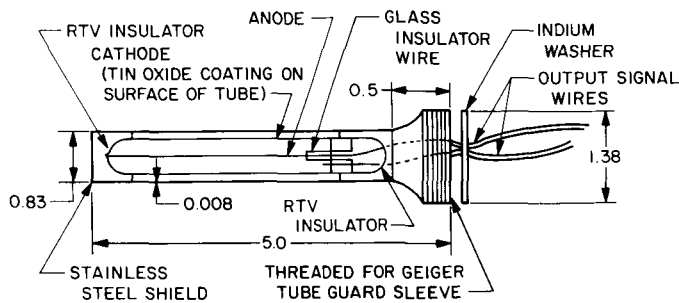


Fig. 7. Cross-section of Geiger-Mueller tube

support the GM tube at its ends. The 0.008-in.-thick cylinder is black oxidized and has four 0.125-in.-diameter holes at its base for mounting to the electronics subassembly. An indium washer is used between the instrument and electronic subassemblies to improve thermal conduction. A threaded metallic sleeve covers the GM tube shield and protects it during transportation and storage.

The power supply and the data-conditioning circuits are fabricated on four printed-circuit boards. All circuit components are mounted on one side of laminated-epoxy circuit boards and are soldered to gold-plated, forked terminals. A conformal coating of epoxy covers the components and circuit board and thus provides protection against shorting, moisture corrosion, and electrical leakage. An insulating board is bonded to the back of each circuit board, and the boards are held to the instrument chassis by screws and an epoxy bonding material.

The instrument chassis was machined from a solid block of magnesium alloy. The chassis surface is gold-plated to provide proper thermal emissivity. The ionization chamber and the GM tube are bolted to the chassis at right angles to each other. This unorthodox configuration contains a semicircular cutout that allows the instrument to be mounted to the cylindrical antenna mast approximately 36 in. above the spacecraft bus. The instrument is mounted between two flanges on the mast structure and is attached to these flanges by means of six screws with insulating inserts.

Two connectors on the instrument chassis provide for (1) input power to the instrument, output signals to telemetry, and a connection to spacecraft ground; and (2) monitor voltages and signals to the Operational Support Equipment (OSE).

## F. Design Evolution

The concept of the instrument is not unique with the *Mariner-Mars '64* program. The concept and design evolved from previous satellite and spacecraft programs, the most recent of which resulted in the *Mariner II* mission. *Mariner II* carried almost identical detectors in a different physical configuration. Minor circuit modifications and repackaging of the detectors to conform to the *Mariner-Mars '64* spacecraft constraints were performed at JPL. Electronic breadboards were built and tested at JPL, but all other units were subcontracted for fabrication.

Design reviews, both at JPL and at the subcontractor facility, resulted in a few minor engineering changes early in the prototype development stages. Such changes included changing the subchassis from aluminum to a magnesium alloy with special heat-conductive properties, and changing the proposed method of ion-chamber mounting to conform more closely to the configuration already proven. Other changes were found necessary later in the environmental testing program and the resulting rework was performed at JPL.

## G. Calibration

The responses of the GM tube and the ionization chamber are determined separately. Absolute calibration of the ion chambers was accomplished by comparing the instruments in a flux of  $\text{Co}^{60}$  gamma rays with a set of standard chambers obtained from the California Institute of Technology. In addition, the response to electrons and the associated *bremsstrahlung* was determined directly by means of an electron accelerator. The X-ray sensitivity of the instruments was measured using a constant-potential X-ray machine as a source. The response to protons has been calculated from theoretical considerations.

The absolute response of the GM tube to penetrating charged particles is determined by the size and shape of the sensitive volume and by the efficiency. It is assumed that the sensitive volume is a right circular cylinder with a diameter ( $d$ ) equal to the internal diameter of the cathode. The effective length ( $l$ ) is determined by the counting rate as a function of the position of a collimated beam of beta particles ( $\text{Sr}^{90}$ ) along the length of the tube. The effective length is set equal to the full width at half maximum of the rate vs position plot. Typical values are  $d = 1.32$  cm,  $l = 6.03$  cm. If  $A$  is the surface area of the

sensitive volume, the omnidirectional geometric factor  $G_o$  is

$$G_o = A/4 \text{ cm}^2, \quad (1)$$

with

$$\frac{\text{Count rate}}{4\pi j} = G_o,$$

where  $j$  is the average unidirectional intensity. With the above values of  $d$  and  $l$ ,  $G_o = 6.9 \text{ cm}^2$ . In a nonisotropic flux, the counting rate depends upon the orientation of the tube.

The efficiency of a tube was measured by forming a coincidence telescope of three parallel tubes denoted A, B, and C, the middle tube being B. The telescope was oriented vertically and exposed to cosmic radiation in the laboratory for 112,000 seconds. The coincidence rates  $ABC$ ,  $\overline{ABC}$ , and the singles rate of A were measured with the following result:

ABC	3175 counts
$\overline{ABC}$	60 counts
Rate of single A	40.7 c/min

If we assume that the tubes are identical and that the inefficiency  $\epsilon \ll 1$ , then  $\epsilon = \overline{ABC}/ABC + 3\overline{ABC} = 1.79\%$ . We conclude that these tubes are 98% efficient for detecting penetrating charged particles.

Thus, it is assumed that protons are detected with an efficiency of 98% if they penetrate the wall of the sensitive volume. This wall may be approximated as follows:

Cylindrical sides	0.2 gm/cm <sup>2</sup> steel . . . area 25 cm <sup>2</sup>
Ends	1.0 gm/cm <sup>2</sup> carbon . . . area 2.75 cm <sup>2</sup>

With these data, the proton response is computed from a consideration of proton range. The electron accelerator

used to calibrate the ion chamber was used also to measure the response of a GM tube to nonpenetrating electrons. Penetrating electrons are detected with an efficiency of 98%. The theoretical mean energy for penetration is 0.5 to 0.55 Mev. The X-ray sensitivity of the GM tube was measured with a constant potential X-ray machine as was done with the ionization chamber.

#### H. Instrument Failure

The *Mariner IV* ionization chamber performed nominally through the first 70 days of the mission. During this period, a profile of radiation intensity was faithfully recorded by the instrument as the spacecraft passed through each of the Van Allen belts, through the boundary of the magnetosphere, and into the relatively stable interplanetary region. Sixty-nine days after the mission began, a solar flare occurred. Both the ion chamber and the Geiger-Mueller tube recorded peak activity of the flare. As the flare subsided and the ion chamber returned to the normal background level, the GM tube indicated a slightly higher rate than was expected over the downward trend, leveling off at a value approximately 30% above the expected pre-flare level. On the 84th day of the mission, after about 10 days of comparatively stable operation at this slightly anomalous level, the rate rose sharply from approximately 40 c/sec to 18,000 c/sec, indicating a spontaneous self-sustained discharge.

On the 109th day of the mission, the GM tube rate dropped to zero and the ion-chamber interval became infinite. No response from either sensor was observed after that time.

The failure mode is now believed to be understood. An almost identical failure has been induced in the life-test model, the only difference being attributable to the considerable difference in operating temperatures between the two units. In addition, the failure symptoms have been reproduced several times on a breadboard unit that is electronically (but not physically) identical to the unit in space. Further tests may prove conclusive.



## VII. PLASMA PROBE

R. A. Graham

Jet Propulsion Laboratory  
Pasadena, California

### A. Experimental Objectives

The plasma instrument aboard *Mariner IV* measures the density, velocity distribution, and bulk direction of the proton-flux component of the solar plasma. The spacecraft telemetry system converts the data to 9-bit digital words and transmits the result to the ground receiving stations.

This mission affords the opportunity of making plasma measurements beyond the influence of Earth's magnetic field and may enable detection of the effect on plasma flow of the magnetic field of Mars. The main aim of data reduction is construction of plasma flow models from profiles of particle velocity, density, and bulk direction taken both in interplanetary space and in the vicinity of Mars. These parameters correspond respectively to mean energy as defined by the modulating electrode voltage, total collector current, and current distribution among the three segments of the collector. The measurements generate histograms of velocity vs density by dividing the proton energy spectrum of interest into 32 windows and taking a set of collector-current measurements for each window.

For direction sensing and energy-window selection, each measurement cycle requires a fairly complex program. In the first half sequence the instrument measures total response at each of the even-numbered energy levels (16 steps), and then samples the individual collector outputs at these energy levels for the direction determination (48 steps). Eight additional self-check steps monitor conditions within the instrument. The second half sequence then fills in the energy spectrum by repeating the above process for the odd-numbered energy level and is identified by modification alterations of the self-check steps.

### B. General Theory of Operation

#### 1. Instrument

The instrument consists of the plasma sensor (Fig. 1), a variable modulating-electrode voltage supply, a measurement chain that converts the small collector currents

to pulse-delay modulation as required by the spacecraft real-time data-automation system (RT-DAS), and logic that interfaces the instrument to the spacecraft and governs the measurement and bookkeeping program.

Figure 2 is the functional block diagram of the instrument. The modulator generates a square-wave signal superimposed on a positive dc voltage. The average voltage output is variable in 32 steps governed by the window voltage control; the ratio of peak-to-peak square-wave amplitude or energy window to mean dc is fixed at 0.25. The gate signal from the timing chain turns on the modulator; synchronization, generated internally, governs the frequency of the ac component.

The modulator output is applied to a grid in the sensor and modulates the particle stream. The resulting ac collector current variations are amplified in three preamplifiers, the outputs of which enter a set of analog gates. In the all-collector measurement mode, the three gates are enabled together. In sequential-collector mode they are selected in the order 2, 3, 1, as governed by the collector

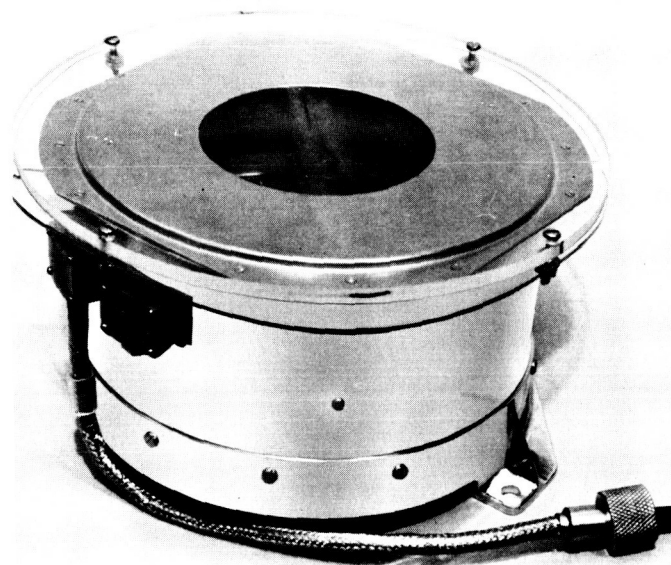


Fig. 1. Plasma probe sensor

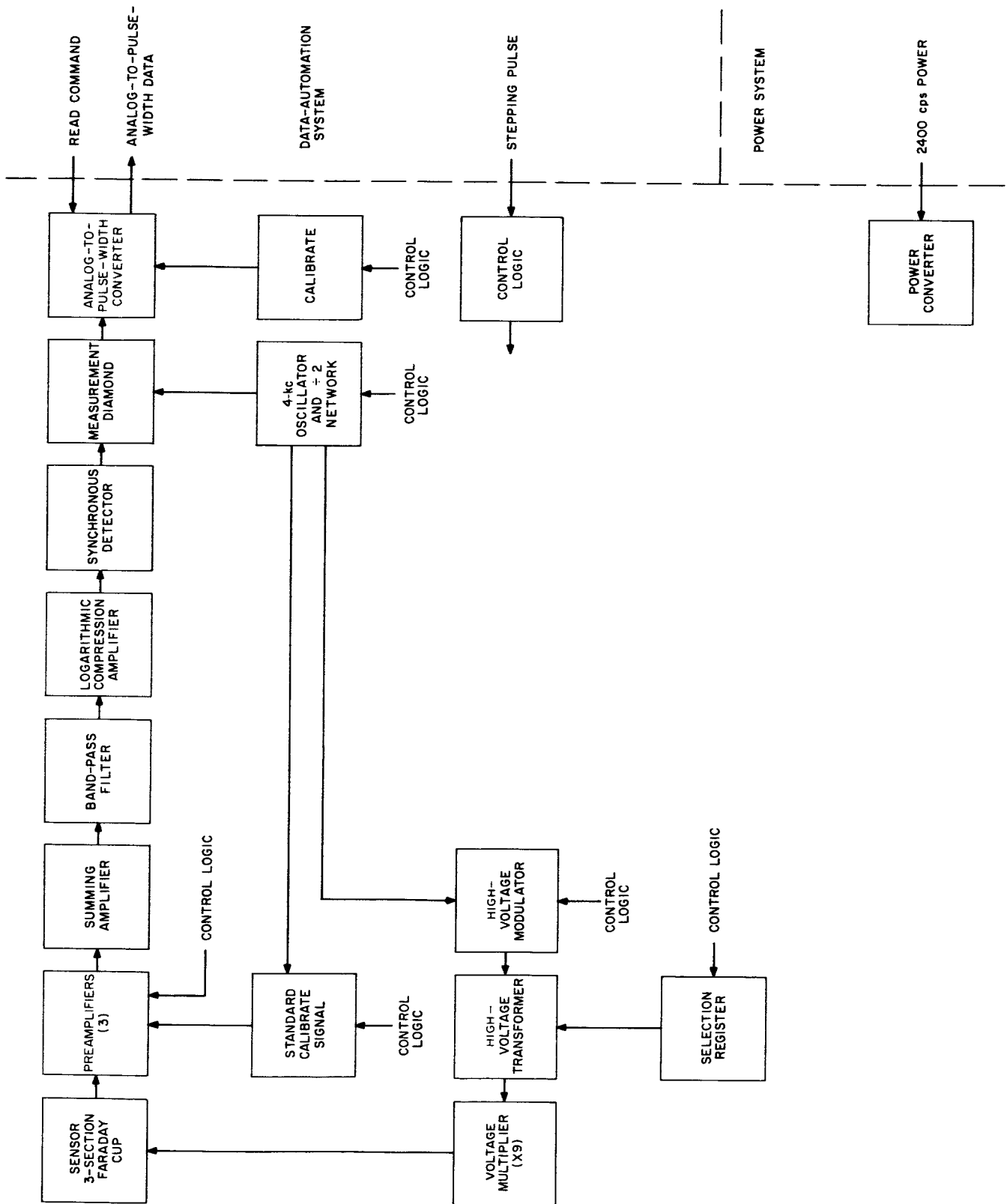


Fig. 2. Plasma probe sensor, functional block diagram

counter. The gate outputs are summed to a single ac signal, amplified, and fed to a bandpass filter. The filter, peaked at the synchronization frequency, attenuates noise outside the passband to produce a relatively pure ac voltage analog of the summed collector currents.

The transfer function of the compression amplifier following the filter closely approximates a logarithmic characteristic over the anticipated four-decade dynamic range of the signal. It accommodates this wide range to the analog-to-pulse-width (A/PW) converter by providing an output change of about 1 v for every decade input change. The synchronous detector receives this compressed ac signal and demodulates it, using synchronization as a reference. An analog diamond circuit transfers the detector dc output to a storage capacitor, which is connected to the analog input of the data converter. The A/PW converter is periodically triggered by a sampling pulse from the spacecraft. At some time interval from the sampling pulse, it returns a pulse to the telemetry equipment; the delay is directly proportional to the analog input voltage.

## 2. Power Supply

The converter supplies all instrument-operating voltages. It consists of a multiple-winding transformer with full-wave diode rectification and capacitor input filtering. Four outputs (+6 v, +20 v, -3 v, and -150 v) use conventional LC or RC filtering; +15 v and -15 v use Zener regulation and are driven by the +20 v and -30 v supplies, respectively. In the remaining power circuits, a Zener-regulated transistor stage replaces the conventional inductive or resistive series element of the filter. The +12-volt supply is actively regulated, using the +15-volt output as a reference; the two actively regulated negative supplies (-6 v and -30 v) use Zeners referenced to ground.

## C. Instrument Program

### 1. Definition of Modes

The 72-step instrument program consists of four measurement and four calibration modes. Measurement modes 0 to 3 involve ac signals only and use the measurement chain; calibration modes 4 to 7 process only dc signals and use separate circuits. In order of occurrence, the eight modes are:

0. All collector (total flux): measurement of the summed outputs of the three cup collectors at each of 16 energy windows (16 steps).

1. Sequential collector (flux direction): measurement of each collector output in turn, also at each of 16 energy windows (48 steps).

2. Standard signal: system gain check with signal fed through each preamplifier in turn (3 steps).

3. Noise: measurement of no-signal output of preamplifier 2 (1 step).

4. High voltage: check of modulator dc output at a selected window (1 step).

5. Temperature: measurement of ambient temperature within the instrument (1 step).

6. Marker: generation of cycle-identification level for use in data reduction (1 step).

7. Reset: redundant counter clears before start of next program cycle to confine any loss of synchronization to one cycle; simultaneous generation of maximum-level marker (1 step).

### 2. Measurement Modes

An entire measurement sequence consists of a two-program cycle. In the second of these the 16 energy windows are decremented by a small factor to provide 32-window resolution, the standard signal is decremented by a large factor, giving a two-point check of measurement chain response, and this program is identified by an increase in the marker amplitude (see calibration section).

The instrument-mode counter executes a complete eight-count once per program or half sequence. The collector counter is a divide-by-3 circuit that enables the analog preamplifier gates individually to provide the sequential-collector measurements. In the all-collector mode, the mode counter overrides these individual selections and gates the three preamplifier outputs together into the summing amplifier. The divide-by-16 window counter drives the window voltage control. It makes two complete counts per half sequence—once in all-collector mode and once at one-third the rate in sequential-collector.

The window voltage control is a logarithmic digital-to-analog converter supplying modulator primary power in

32 logarithmically related steps according to the input count and state-of-sequence flip-flop F10. The mode counter complements F10 once per half sequence. For either state of F10, the window voltage control generates a sequence of 16 windows, each window of which is related to the next higher voltage window by the ratio  $1:\sqrt{2}$ . The lower-level sequence occurs when F10=0; setting F10 then increments the group by the factor  $\sqrt[4]{2}$  or 1.19, so that when the two groups are interlaced to form a single group of 32 (as is done in data reduction to obtain the complete histogram), the voltage ratio of any three adjacent windows is 1:1.19:1.41.

*a. Timing.* The timing chain generates the system clock and measurement gate from the RT-DAS stepping pulse. The chain consists of three one-shot multivibrators: MV1, MV2, and MV3 arranged in cascade with falling-edge trigger circuits for MV2 and MV3. The clock one-shot, MV1, standardizes and stretches the spacecraft stepping signal to a 2-ms pulse that steps the control logic. The clock falling edge triggers MV2, which generates a 200-ms waiting period between the clock and the measurement. The falling edge of the delay level initiates a measurement by triggering MV3, which gates on the modulator and the synchronizer flip-flop (which in turn supplies the modulator input square wave and activates the synchronous detector) for 80 ms.

The instrument generates its own reference frequency (sync) internally. The circuit consists of a free-running multivibrator driving a flip-flop. The multivibrator is temperature compensated and adjusted to run at  $2f_c$ , i.e., twice the center frequency of the bandpass filter in the measurement chain. This flip-flop, complemented by each multivibrator output pulse, produces a square wave at  $f_c$  (approximately 2 kc). Amplifier design is most convenient and economical at a medium audio frequency; the particular frequency chosen is relatively immune to interaction with the 2.4-kc spacecraft power system. The peak in system frequency response shifts somewhat with signal amplitude because of phase variations with amplitude from such effects as minority carrier storage, inherent phase characteristics of the twin-tee filter, and slight asymmetry in the clippers preceding each stage of the compression amplifier. The synchronous detector interprets this center-frequency shift as amplitude nonlinearity. The synchronous multivibrator is adjusted to the system center frequency under minimum signal conditions, that is, with an input current at the low end of the dynamic range of the detected signal to take greatest advantage of the noise-rejection properties of the filter, which are most needed at low levels.

Measurement timing must satisfy three main conditions. First, the measurement must finish with accurate data available at the moment the RT-DAS samples the output of the A/PW converter. Regardless of the data rate at which it is operating, the RT-DAS always reads out the A/PW 10 bits after it steps the instrument. Thus, sampling occurs either 300 ms after stepping (at the high data rate,  $33\frac{1}{3}$  bits/sec), or 1200 ms after stepping (at  $8\frac{1}{3}$  bits/sec).

Second, the high-voltage modulator must be gated on, but only long enough for its dc output to make a close approach to its asymptote, so as to conserve spacecraft power. The necessary compromise between the requirements of low peak power consumption and short HV rise time to achieve the required accuracy dictated an average modulator dc rise-time constant of about 20 ms. A turn-on period of 80 ms thus allows an approach to within 2% (predictable deviation). Some circuits in the measurement chain have a certain settling time, but the effect of these is secondary, i.e., if sufficient time is allowed for window accuracy, measurement chain accuracy may be assumed.

These two conditions impose the following circuit and timing requirements: (1) measurement time should be no longer than 300 ms; (2) it should be no shorter than 80 ms, and some delay between stepping the instrument and gating on the modulator is advisable to prevent the possibility of switching transients and power wastage. The analog storage circuit should have a reasonably low, predictable decay over a time period of 1200 ms less the measurement interval.

Conditions (1) and (2) suggest a delay of about 200 ms between stepping (2 ms) and measurement gating (80 ms). The resulting 282-ms total measurement time allows the analog storage decay to be neglected at the higher bit rate, because a capacitor storage circuit designed for reasonable accuracy at  $1200 - 282 = 918$  ms is certainly accurate at 18 ms. This duration also allows for some increase or decrease in measurement time due to delay-circuit component changes. Note that any uncertainty in the measurement-time interval in excess of 300 ms has a much greater effect on accuracy than the same uncertainty has below 300 ms. At the higher spacecraft rate, if component changes were to increase the measurement period to 320, 340, or 360 ms, the window voltage at the 300-ms A/PW readout time would be (respectively) about 95%, 87%, or 63% of nominal. On the other hand, even a 100-ms error in the negative direction results only in a negligible storage error.

Figure 3, the timing diagram for a typical step, is intended primarily to illustrate a flux measurement and, except for the last three waveforms, it also applies to calibration. Reference time  $t_0$  is the point at which the 10-ms step P1 pulse comes from the spacecraft. Depending on the spacecraft bit rate, the read command occurs either 300 or 1200 ms after  $t_0$ .

Step P1 triggers the 2-ms clock MV1, shown as line b on the diagram. The clock falling edge indexes the mode counter and triggers the 200-ms delay MV2 (line c). The trailing edge of the delay level starts the measurement at  $t = 202$  ms by causing the gate MV3 (line d) to enable the modulator and synchronizing flip-flop.

Both the dc and the ac components of the high-voltage output rise at a rate determined by the modulator-output impedance and capacitive loading (e). For the first part of the measurement interval, therefore, the synchronous detector and analog storage outputs (f and g) are time-compressed nonlinear profiles of particle density from 0 up to nominal step energy; however, they soon level off to the final value. Termination of the measurement gate at  $t = 282$  ms turns off the modulator and synchronizing flip-flop and disables the analog-transfer diamond so that the storage capacitor contains the collector-current analog as measured at the end of the gate interval. Storage-time constant is determined primarily by the

storage capacitor and the current drain in the A/PW converter (the diamonds by comparison exhibit negligible drain at turn off). The converter input current, approximately 5 ms, corresponds to a  $dv/dt$  of 106 mv/sec across the 47- $\mu$ f storage capacitor; the correction for storage decay at the lower bit rates is therefore  $0.92 \text{ sec} \times 106 \text{ mv/sec} = 98 \text{ mv}$ , or about 2% of full scale, and is negligible at the higher bit rate.

**b. Measurement Program.** Figure 4 shows the instrument program or measurement-step sequence; the logarithmically scaled ordinate is energy-window level. High-voltage output rise and fall times make it advantageous to follow the energy-level order shown for each measurement mode. This makes it unnecessary to charge or discharge output capacitances over wide voltage ranges between steps. The last step in each half sequence generates a redundant reset that clears all counters to ensure continuity of program cycles. Internal logic is such that the counters would normally recycle without this reset.

The entire sequence is divided into two cycles, primarily to enhance distance resolution. However, this also results in circuit economy and simplicity. A single-cycle alternative at first appears to be more economical in terms of hardware, e.g., increasing the window counter to 5 bits by incorporating cycle flip-flop F10 as the least-significant bit. Under such an arrangement, the window voltage control would be governed by F10 and by the 16 decoded outputs of the four more-significant bits, and the measurement portion of the sequence consists of a 32-window sequence in the all-collector mode and a second runthrough in the sequential-collector mode. However, insertion of the two-level self-check steps would then require either another flip-flop or a drastic increase in complexity and hardware in the mode-counter gating circuits.

The principal advantage of two program cycles is better distance resolution of plasma profiles. During planet encounter, for example, at the lower spacecraft data rate, a complete 23-min sequence of measurements is taken over a distance of about 4000 mi; however, one cycle of the presently adopted sequence makes available a rough (in terms of energy resolution) profile in 2000 mi of travel.

The linearly scaled ordinate in the figure shows a hypothetical set of instrument analog outputs. In this example, the energy spectrum of the incoming proton stream is peaked at about 400 ev, and sequential-collector measurements show that bulk direction is off the probe axis so that collectors 1 and 2 are nearly equal in partial

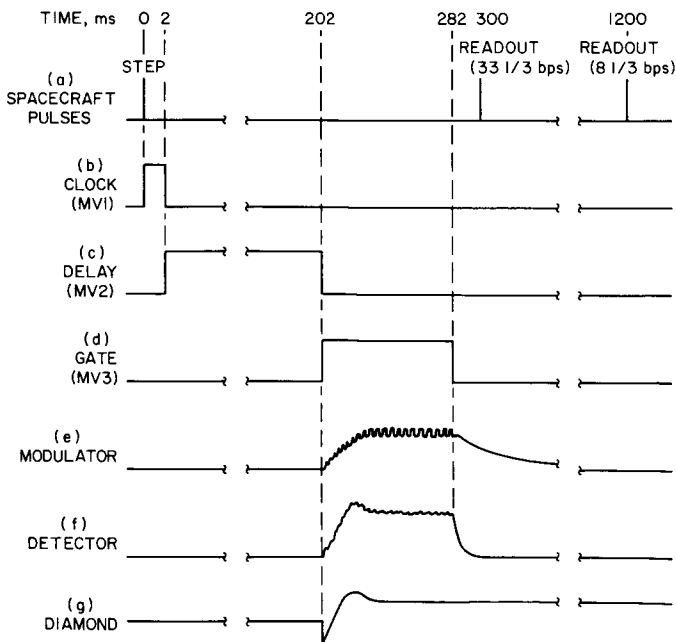


Fig. 3. Single-step timing

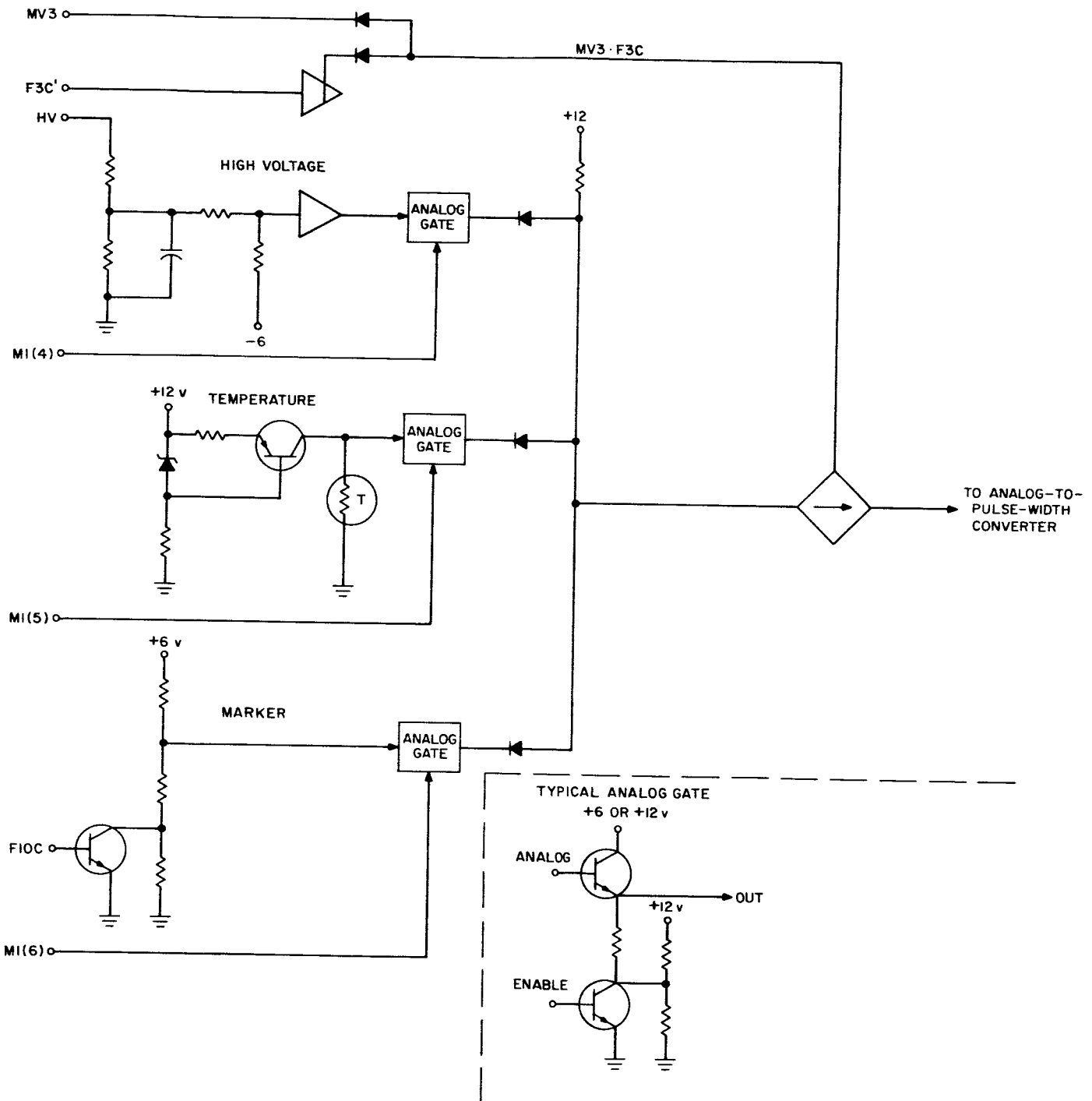


Fig. 5. Calibration system

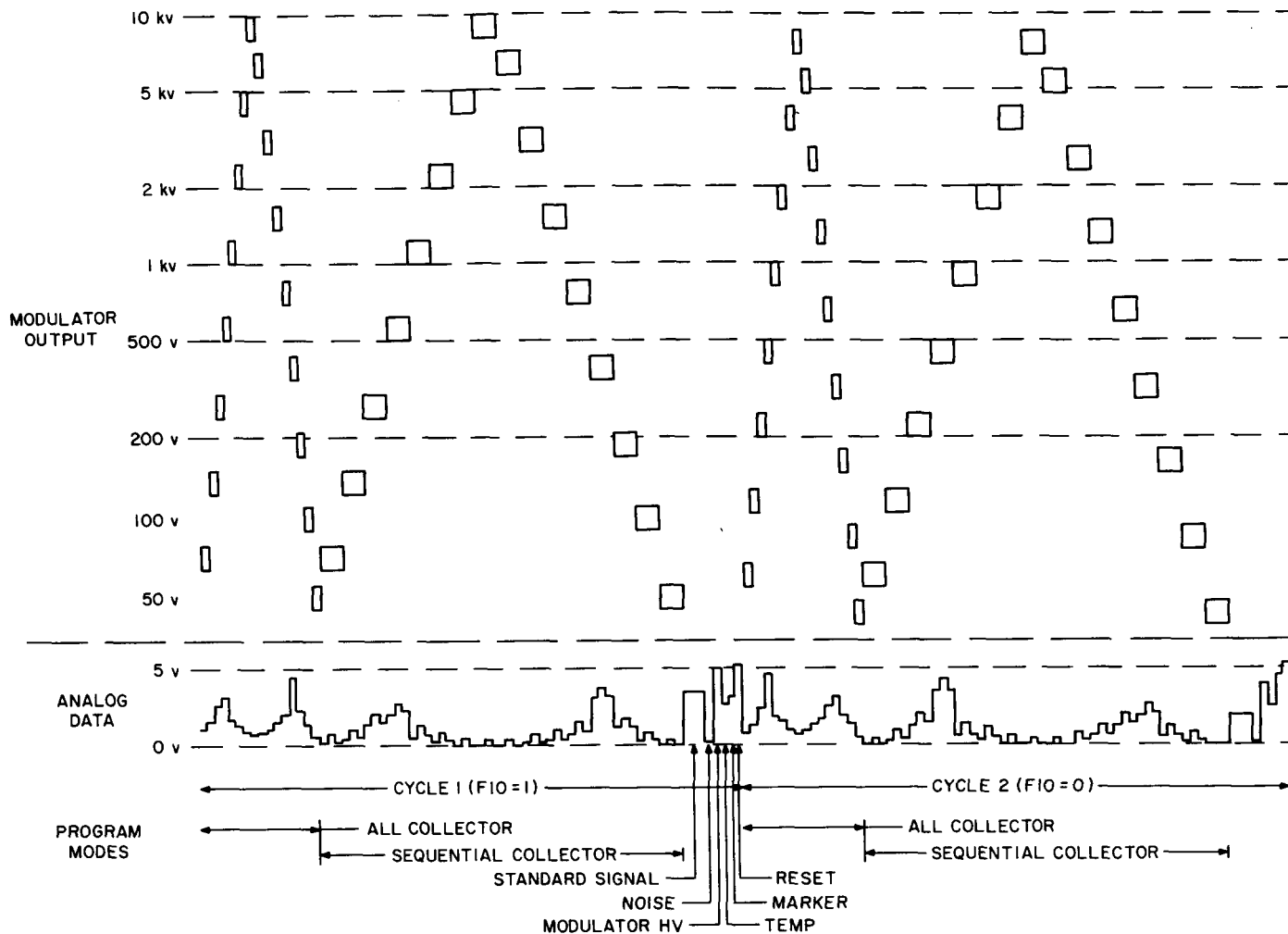


Fig. 4. Plasma-probe measurement program

shadow (collector selection order is 2, 3, 1). The counter in the spacecraft DAS that performs the digital conversion of the A/PW output interprets this level as  $000_8$  (i.e., it counts to capacity, clears, and is inhibited from further counting until read out); thus, the reset step serves as a convenient cycle or half sequence marker.

### 3. Calibration Modes

Although the standard signal and blank or noise-check steps are self-check features of the instrument performed with no high voltage at the modulating grid, they are discussed as measurement modes rather than calibration modes because they use the measurement chain. A standard signal current is injected into the measurement chain through each of the preamplifiers in turn; F10 changes the standard signal-current amplitude on alternate half sequences. The two standard signal input levels are

$3 \cdot 10^{-11}$  and  $4 \cdot 10^{-9}$  amp peak-to-peak, respectively, for the 0 and 1 states of F10. These levels correspond approximately to the  $1/4$  and  $3/4$  points along the logarithmic dynamic range of the measurement chain and provide a good basis for checking the overall transfer function. The noise check is identical to the preamplifier 2 standard-signal step except that no signal is applied.

Figure 5 shows the calibration system in simplified form. During the calibration portion of the program, this section supplies to the A/PW converter a series of four analog levels. The first two levels correspond to mean modulating-electrode dc and instrument temperature, the third level is a sequence marker, and the final calibration step generates a maximum-level analog which is essentially meaningless but may be found useful in data reduction as a half sequence marker.

These levels are sequenced by the 4 to 7 counts of the mode counter. Average modulator dc is obtained by the voltage-divider and capacitor combination shown in the figure; three stages of current amplification supply the divided level to the calibration output diamond. The energy window sampled in this step is either number 27 or 28 (counting from the lowest window), depending on the state of F10. Therefore, there is about 19% of variation in the high-voltage monitor input for alternate half sequences. However, the monitor circuit cuts off somewhat below these levels, effectively expanding the ratio of the telemetered HV samples to approximately 2:1.

The temperature analog comes from a sensistor driven by a constant-current source. A voltage divider to a positive supply generates the marker. One leg of the divider is switched by F10 to vary the marker amplitude for alternate half sequences. The high-voltage temperature and marker levels are exclusively (nonadditively) mixed to feed the calibrate diamond; the diamond input is pulled down from +6 v to the value of the active input. In the final calibration step, reset, there are no pulldowns and the diamond thus receives maximum level.

The prelaunch calibration of the instrument is accomplished by injecting an accurately calibrated current into the three preamplifier test jacks on the sensor and recording the instrument's response. In addition, measurements of the suppressor and high voltage are required. These measurements are made with the instrument mounted on the spacecraft and all other spacecraft systems operating normally.

## D. Construction

### 1. General

The subassemblies of the plasma instrument are an externally mounted sensor and electronics units. Connections between these units and between the instrument and the spacecraft are effected through multiple plugs and jacks and conventional cable harnesses. There are five coaxial cables connecting the sensor to the electronics; two are used to supply modulator and suppressor-grid voltages to the sensor, and the remainder convey the collector signals to the three preamplifiers.

Including the sensor, the instrument weighs 6.5 lb. Total power consumption is 2.67 w average and 3.2 w peak. The instrument contains 1300 electronic components.

### 2. Modules

The electronics modules consist of rectangular metal frames to which are mounted the circuit boards and necessary connectors. Each frame was milled from a block of magnesium and contains an inside flange. Circuit boards may be mounted on one or both sides of this flange. The boards are etched on both sides and have through-plated holes (rather than eyelets), which are rigid enough to accomplish crossover. Components are hand-soldered to one side of the board only. The boards are coated with an epoxy compound (Solithane 113) to protect the components.

### 3. Sensor

The instrument sensor (Unit 32A1) consists of a cup-like shell and a number of grids and collectors. This shell consists of two parts: a cylindrical wall and a circular back plate. Both pieces are gold-plated magnesium. The wall-cylinder section includes an outer flange for mounting it to the spacecraft and inner flanges for grid support. The outer and shield grids operate at ground potential and are mounted directly to the flanges, while the modulator and suppressor grids are electrically isolated from the shell by standoffs. The variable-modulator voltage and -150-volt suppressor bias enter through connectors on the outside of the wall. All grids are constructed of gold-plated tungsten-wire mesh. The three collector electrodes mounted to the inside of the back plate are 120-deg sectors, each separated from its neighbor by  $\frac{1}{16}$  in. Connectors on the outside of the back plate, in addition to carrying the collector signals to the preamplifiers, allow direct electrical access to the collectors for test purposes. The sensor is  $4\frac{1}{2}$  in. in depth and 6 in. in outside diameter (excluding the mounting flange), and the front cover has a  $2\frac{1}{2}$ -in.-diameter viewing aperture.

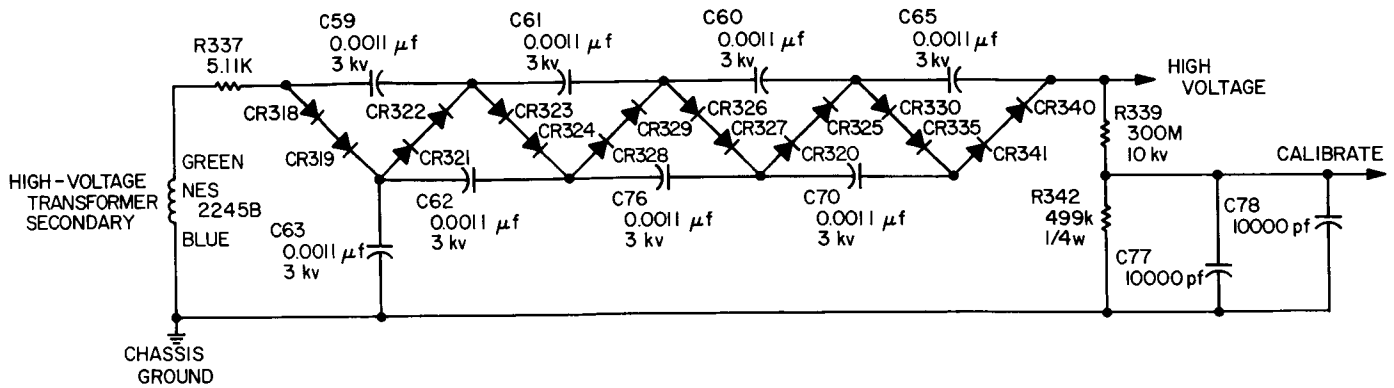
### E. Results on Mariner IV

The instrument aboard *Mariner IV* failed eight days after launch because of the opening of R339 in the voltage-multiplier circuit. As Fig. 6 illustrates, this resistor serves as a bleeder resistor for the multiplier capacitors. Without the proper discharge path, the modulating-grid voltage remains high throughout the entire program cycle and, as a result, the instrument is ineffective to low- and medium-energy plasma.

The failure of R339 in this application is caused by a radial ac field which sets up between the resistor element and the surrounding circuits and chassis. This electrostatic field strips the thin-film resistive element off the ceramic base.



HIGH-VOLTAGE RECTIFIER



NOTE: CR318 THRU CR330,  
CR335, CR340, CR341 ARE 1N3286

Fig. 6. Voltage-multiplier circuit

## VIII. MAGNETOMETER

*David D. Norris*

*Jet Propulsion Laboratory*

*Pasadena, California*

*James L. Lawrence*

*Analog Technology Incorporated*

*Pasadena, California*

*James S. Bunn*

*Jet Propulsion Laboratory*

*Pasadena, California*

### A. Instrument Objectives

#### 1. Scientific Objectives

There were three reasons for making magnetic-field measurements during the Mars mission:

1. To establish whether a planetary field exists and, if so, to determine the characteristics of the field (magnitude, direction, multipolarity, and orientation relative to the planetary rotational axis).
2. To investigate the nature of the boundary between planetary and interplanetary magnetic fields.
3. To measure the magnitude and direction of the steady and slowly varying components of the interplanetary magnetic field and to determine its variation with heliographic latitude and longitude.

To meet the experimental goals, the magnetometer must have the following operating characteristics:

1. Three outputs proportional respectively to the three mutually perpendicular components of the magnetic field, with a sensitivity threshold of  $\leq 0.25$  gamma (1 gamma =  $10^5$  gauss).
2. A frequency response of 1 Hz maximum.
3. A dynamic range of  $\pm 360$  gamma.
4. A 9-bit conversion, plus one sign bit.
5. A known zero offset less than 1 gamma.

#### 2. Engineering Objectives

The magnetometer data acquired during the early portion of the mission was a valuable source of information on the spatial orientation of the spacecraft prior to Canopus acquisition. The magnetometer experimenters

were able to advise the spacecraft engineering team as to the spacecraft orientation based on the magnetometer data output and knowledge of the geomagnetic field at the location of the spacecraft.

### B. Description

#### 1. Derivation of Magnetometer Action in Metastable Helium

The phenomenon of optical pumping in metastable helium\* underlies the operation of the low-field vector helium magnetometer. The transmission of the  $1.083\text{-}\mu$  resonant radiation through a helium plasma is dependent on the angle between a collimated light beam and the magnetic field present in the plasma. If a light detector is used to monitor the intensity of the affected light beam, the signal ( $S$ ) from the detector is experimentally found to be

$$S = k \cos^2 \Theta \quad (1)$$

where  $\Theta$  is the angle between the light beam and the magnetic field and  $k$  is a constant dependent upon parameters of the measuring system.

The basic components in the magnetometer sensor are shown in Fig. 1. The helium lamp is the source of  $1.083\text{-}\mu$  resonant radiation. The light beam is collimated and then passes through a linear polarizer and a quarter-wave plate. The polarizer and quarter-wave plate combine to polarize the light circularly. The circularly polarized light passes through the helium-absorption cell in which a glow discharge maintains a body of metastable atoms.

\*Colegrove, F. D., and Franken, P. A., "Optical Pumping of Helium in the  $^3S_1$  Metastable State," *Physics Review*, Vol. 119, No. 2, July 15, 1960, pp. 680-690.

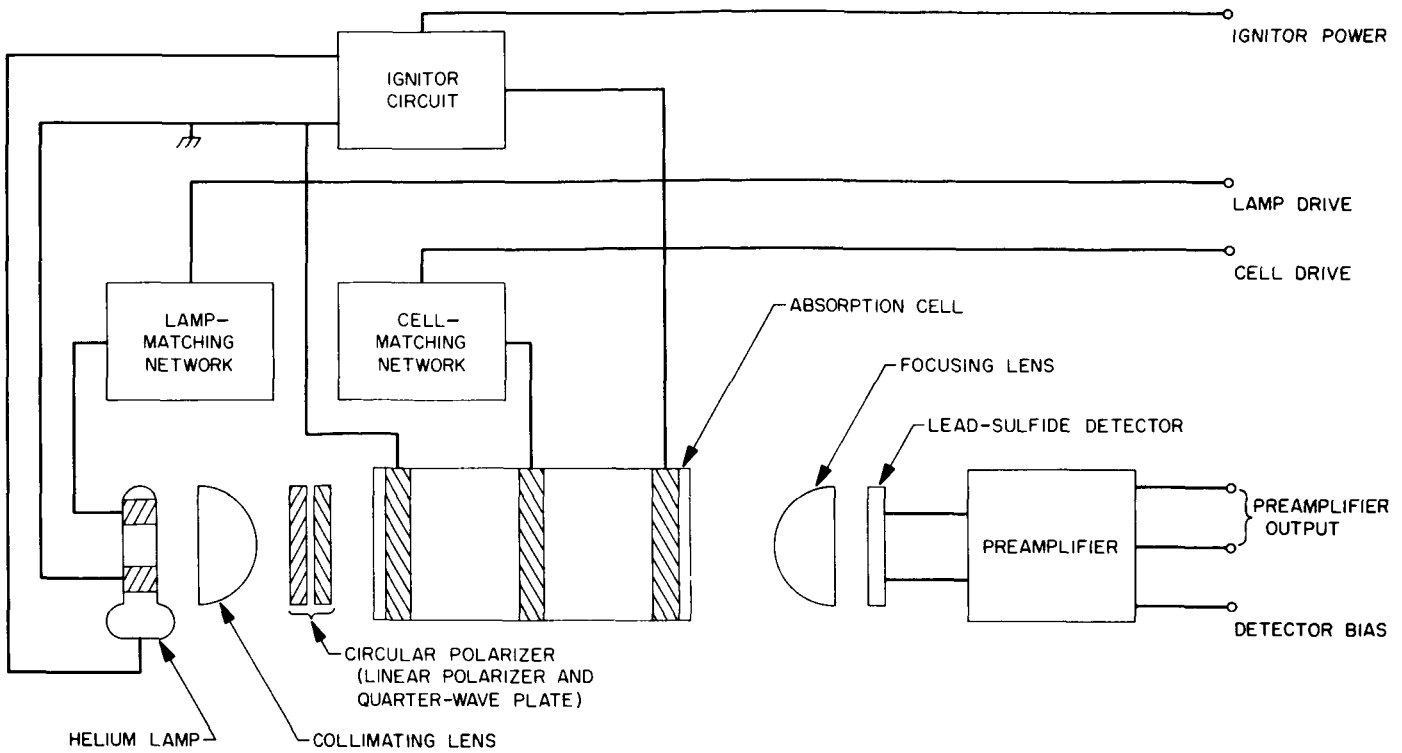


Fig. 1. Magnetometer sensor

The light not absorbed in the cell is focused onto a lead-sulfide detector.

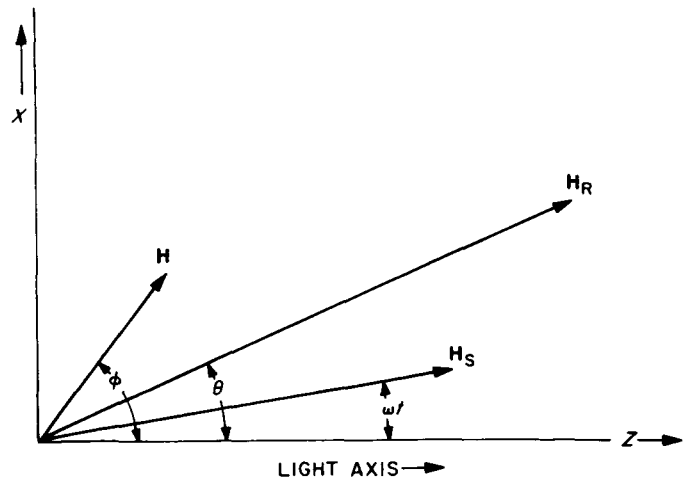
The sensor elements are surrounded by a triaxial set of Helmholtz coils used to generate a magnetic sweep vector and to null out the ambient magnetic field at the sensor. Two orthogonal coils are driven, respectively, by sinusoidal currents 90 deg out of phase. The resultant field at the center of the coils is constant in amplitude, but rotates at the frequency of the driving currents.

The lamp and cell electrodeless discharges are maintained by RF power, and the discharges are initiated by a high-voltage igniter supply.

The transfer characteristics of the sensor can be found by using Eq. (1) and the vector diagram of Fig. 2.

It follows from this diagram that

$$\cos \Theta = \frac{H_s \cos \omega t + H \cos \phi}{\sqrt{(H_s \cos \omega t + H \cos \phi)^2 + (H_s \sin \omega t + H \sin \phi)^2}} \quad (2)$$



- H MAGNITUDE OF THE AMBIENT MAGNETIC FIELD
- H<sub>S</sub> MAGNITUDE OF THE SWEEP VECTOR
- H<sub>R</sub> MAGNITUDE OF THE RESULTANT OF H AND H<sub>S</sub>
- φ ANGLE BETWEEN THE LIGHT AXIS AND H
- θ ANGLE BETWEEN THE LIGHT AXIS AND H<sub>R</sub>
- ωt ANGLE BETWEEN THE LIGHT AXIS AND H<sub>S</sub>

Fig. 2. Vector diagram

When the magnetometer is operated in a low magnetic field, the sensor is used as a null detector, and feedback currents are applied to the coil system to reduce the ambient field at the sensor to a small residual "error" field ( $H$ ). The null-sensing, servo-operation ensures that  $H \ll H_s$ , which simplifies Eq. (3). Terms in  $(H/H_s)^2$  may be discarded without introducing appreciable error. Using this approximation in combination with Eq. (1) and (2), the sensor signal becomes

$$S = \frac{k}{2} \left[ 1 + \cos 2 \omega t + \frac{H}{H_s} \cos \phi (\cos \omega t - \cos 3 \omega t) - \frac{H}{H_s} \sin \phi (\sin \omega t + \sin 3 \omega t) \right] \quad (3)$$

The term  $H/H_s \cos \phi \cos \omega t$  shows that the Z component of the ambient field causes a perturbation synchronous with the Z component of the sweep vector. Similarly, the term  $H/H_s \sin \phi \sin \omega t$  shows that X-axis component of the ambient field causes a perturbation synchronous with the X component of the sweep vector. Because  $H/H_s$  is small compared to unity, the ac portion of the signal is mostly the second harmonic of the sweep frequency.

Figure 3 is a simplified block diagram illustrating the processing of the error signal to give voltage outputs proportional to the components of a field at the sensor. The oscillator provides a sinusoidal current to drive one coil at the sensor to produce the Z component of the sweep vector. The oscillator output is phase-shifted 90 deg to provide a sinusoidal current to produce the X component of the sweep vector. The output from the sensor is amplified, filtered to remove the second harmonic, and then fed to the Z and X demodulators. The Z and X demodulators are driven synchronously with the oscillator

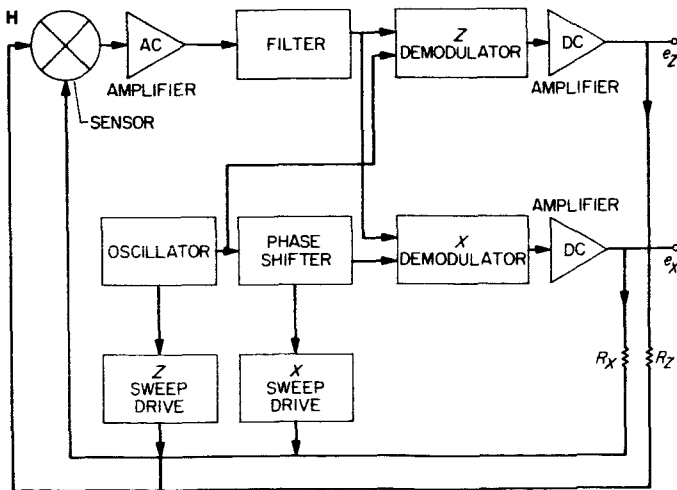


Fig. 3. Magnetometer sensor, simplified block diagram

and phase shifter, respectively. The Z demodulator detects the error signal associated with the term  $H/H_s \cos \phi \cos \omega t$  from Eq. (3), and converts this ac error signal to a dc voltage which drives the Z-axis dc amplifier. The Z-axis output,  $e_z$ , is applied to a resistor,  $R_z$ , in series with the Z-axis coil. The current through the coil,  $e_z/R_z$ , produces a magnetic field to buck out the Z component of the ambient field. Because the field of coil is linear with current, the output  $e_z$  is directly proportional to the field along the Z-axis.

The X-axis error signal,  $H/H_s \sin \phi \sin \omega t$ , is processed similarly to the Z-axis signal to produce an output voltage proportional to the X component of the field. Three-axis magnetometer action is achieved by adding a third coil (Y-axis) and commutating both sweep drive and demodulation on alternate cycles between X- and Y-axes.

## 2. Triaxial System Block Diagram

The complete triaxial block diagram is shown in Fig. 4. The system function as before with the exception that the X- and Y-axis sweep drives are commutated. The Z-axis sweep-vector component is continuously applied to its coil and the quadrature component of the sweep vector is applied to the X- and Y-axis alternately. Because of this, a rotating sweep vector is generated alternately in the Z-X and Z-Y sensor planes. To extract the information for the X and Y planes, demodulators are employed, internal to the amplifier loop, which are driven synchronously with the commutators in the X and Y sweep-drive circuits. In this manner, the X-axis error signal is gated to the X-axis demodulator when the sweep vector is rotating in the Z-X plane and the Y-axis demodulator blocks the signal from the X-axis demodulator during this period.

In the block diagram, the 50-Hz sweep frequency is generated by a high-gain amplifier with a twin-tee notch filter in its negative feedback loop. A positive feedback loop and level control around this amplifier provides a sinusoidal wave of extremely low distortion. The resultant wave form is applied through a buffer amplifier and scaling resistor to the Z-axis sweep coil. It is also phase-shifted and applied to a buffer amplifier for the X- and Y-axis. The X and Y sweep drive-coil resistors are split and commutation is provided by inverted-mode transistor choppers placed at this point. The commutator and demodulator drive is obtained by dividing the 50-Hz oscillator output by Z and applying the 25-Hz square wave, with proper phasing, to the X and Y commutators.

The commutated sweep vector is applied to the sensor Helmholtz coils and the  $H$ -field vector components are

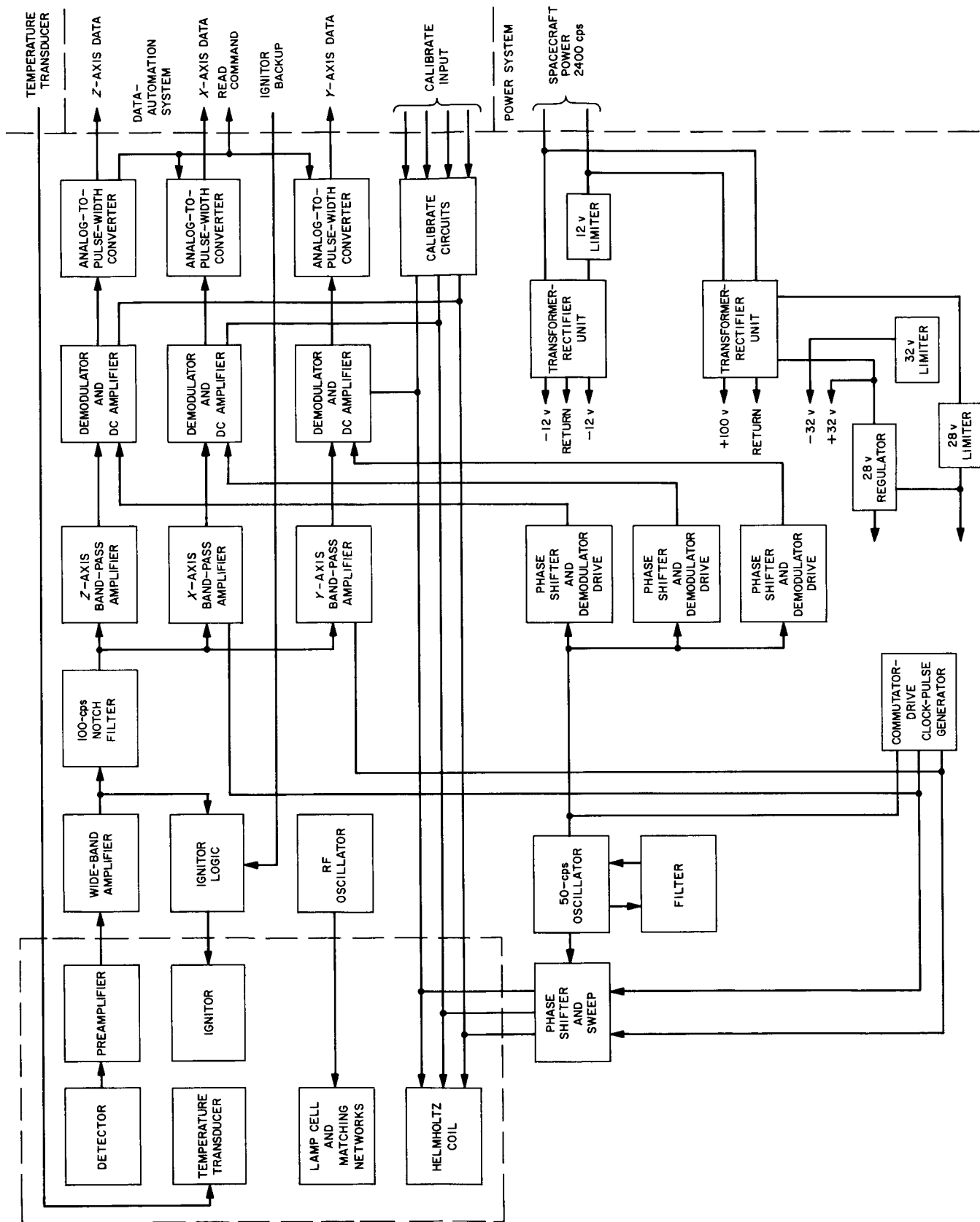


Fig. 4. Magnetometer sensor, functional block diagram

resolved as described in the preceding text. The PbS detector is followed by a high-input impedance, wideband preamplifier with a gain of 10.

The preamplifier is followed by a wide-band amplifier with automatic gain control (AGC). Using AGC to control the second harmonic component is an expedient way to maintain the loop-gain ( $AB$ ) of the system relatively constant. The nominal wide-band amplifier gain at 25°C is 20. The wide-band amplifier is followed by a twin-tee notch filter to remove the second harmonic component.

Synchronous demodulator transistors follow the 100-cps notch filter for gating of the X- and Y-axis signals. Each axis is provided with a tuned bandpass amplifier following the demodulation. This is accomplished by amplifiers with 50-Hz twin-tee filters in the negative feedback loop. The low-pass equivalent transfer function of the bandpass amplifier is

$$K = \frac{50}{S(0.032 + 1)} \quad (4)$$

Since there are two twin-tee filters in the forward loop, equalization is provided to maintain the phase relation of the 25-Hz component to the 50-Hz component relatively constant. This is essential to avoid crosstalk between the X- and Y-axis. (Effects of small phase shifts and cross

talk errors on the output signal on a given axis are attenuated by the loop gain preceding the demodulators.)

The bandpass amplifiers on each axis are followed by the demodulators and filter amplifiers. The combined transfer function of the lag network and integrator amplifier is

$$K_{(s)} = \frac{500}{S(750) + 1} \quad (5)$$

The nominal loop-gain expression is

$$AB = \frac{4000}{(S750 + 1)(S0.032 + 1)} \quad (6)$$

At gain crossover, the phase margin is about 90°.

The effective crossed-loop transfer function is given by

$$\frac{E}{H} = \frac{0.0166 \text{ volts}}{S.3 + 1 \text{ gamma}} \quad (7)$$

which provides a system bandwidth of 0.6-Hz.

### 3. Instrument Physical Description

Figure 5 is a photograph of the magnetometer sensor and electronic modules. The module on the left contains the magnetometer power supply, ignition logic, RF power

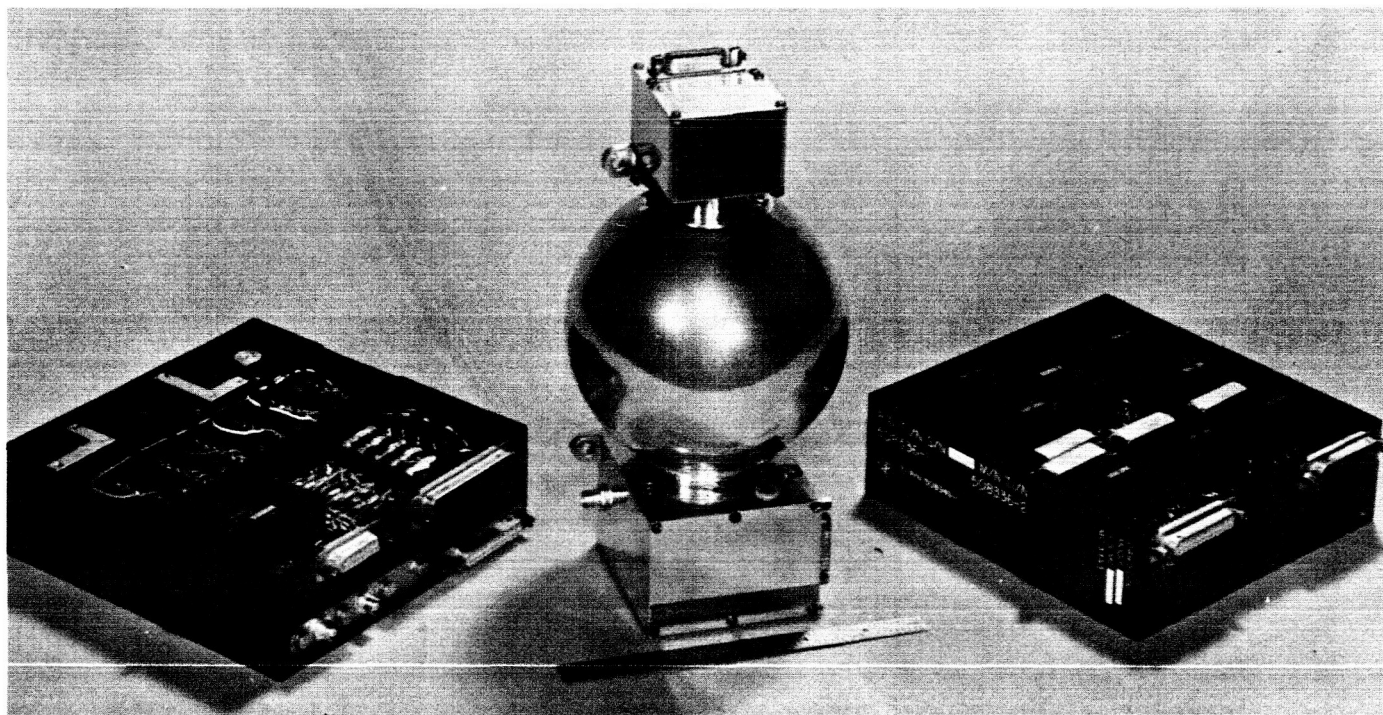


Fig. 5. Magnetometer

supply, and analog-to-pulse-width converters. The module on the right contains the basic signal-chain circuits and ancillaries. The spherical portion of the sensor is the Helmholtz coil housing.

The sensor weighs 1.25 lb, and the two electronics modules together weigh 5.0 lb. The average power input to the instrument is 7 w. During the 10-sec ignition periods, the instrument power consumption increases by 3 w.

The majority of the packaging is of welded-cordwood modular construction. Exceptions to this are the power supply, which is two-dimensional construction, and the sensor. The sensor packaging is hybrid because of the nature of the components employed. The preamplifier is soldered cordwood, and the igniter circuits are two-dimensional. All sensor components had to be nonmagnetic. The instrument contains 823 electronic components.

## C. Design Evolution

### 1. Design Reviews

In the period from March through September 1963, a series of design and method reviews were held. Extensive testing was performed on the magnetometer breadboard to determine the capability of the instrument to meet the operational design performance requirements. The packaging design was reviewed to determine whether or not the hardware would comply with the reliability requirements for the *Mariner* project. Evaluation of the design analysis and breadboard testing of the instrument resulted in a number of design changes in circuits, optical and thermal components, electronic packaging, and mechanical design.

### 2. Sensor Design

The original sensor design used plastics in both the optical system and the packaging design. Because of the deleterious effect of high vacuum on plastic materials, it was necessary to replace such unsuitable materials with materials of proven reliability.

The collimating and imaging lenses were originally f/0.8 Fresnel lenses made of Lucite. There is some evidence that Lucite will craze in a vacuum. Hence, the lenses would become opaque. The Fresnel lenses were replaced by f/0.5 plano-convex, aspherical, crown-glass lenses. The increased speed and transparency of these lenses resulted in an increase in the optical efficiency greater than 2.

The polarizer initially employed was a standard Polaroid HR polarizer, which is basically a thin sheet of iodine-

stained polyvinyl alcohol sandwiched between two sheets of cellulose acetate butyrate. The cellulose acetate is butyrate to make it more flexible, but plasticizers such as butyrate are known to outgas in high vacuum, which could cause degradation in the transparency of the polarizer. Therefore, unsupported sheets of polyvinyl alcohol were bonded between plates of glass for support and to minimize exposure to vacuum. This glass-encapsulated unit was the one used in the instrument.

The quarter-wave plate used in the original design was made by adjusting two sheets of stressed cellulose acetate with respect to each other in such a way as to achieve one-quarter-wave retardation. The birefringence in plastics is generally due to stresses in the material. Such stresses are not necessarily stable with time, especially at high temperature, and measurements made on quarter-wave plates approximately six months old indicated a degradation of as high as 40%, although the measurements are suspect because of the unknown history of the quarter-wave plates under test. Unsupported mica sheets were obtained and adjusted with respect to each other to achieve less than 1% linear polarized light when properly adjusted with a linear polarizer. The mica sheets were encapsulated between plates of glass to reduce any possible degradation in vacuum.

The polarizers and quarter-wave plates were fabricated and built into an integral circular polarizer and supplied to Texas Instruments for inclusion in the final magnetometer assembly.

The behavior of the lead-sulfide detector used in the breadboard design indicated that it was the limiting factor in obtaining the best system signal-to-noise ratio at the operating-temperature extremes. Attempts to find a replacement detector were futile. A decision was made to concentrate effort on applying the lead-sulfide detector to the best advantage. The only variable parameters were the detector biasing and the preamplifier input impedance. Testing indicated that the breadboard detector was biased close to optimum, but at low temperatures the detector impedance went above 10 M $\Omega$ . The breadboard preamplifier, which had an input impedance of  $\frac{1}{4}$  M $\Omega$ , loaded the detector output, and so, in the redesign of the preamplifier, the input impedance was increased to 20 M $\Omega$  to reduce detector loading. An AGC amplifier stage was included in the wide-band amplifier to control the signal level over the operating-temperature range so that the effect of the detector responsivity variation on loop gain would be minimized.

### 3. Sensor Design — Packaging

The initial sensor design used phenolic and fiberglass as basic structural materials. This design was reviewed and several major problems were uncovered which led to sensor redesign. With nonconductive base materials, the local heating due to power dissipation in the helium lamp caused the temperature gradient to be as high as 15°C/in. Since there was no provision for distributing heat from the lamp, thermal control could have been achieved only by using Sun energy. Under these conditions the sensor would have experienced large temperature excursions during the flight from Earth to Mars.

The basic mechanical features of the redesigned sensor are shown in Fig. 6. The igniter and preamplifier housing are 0.030-in.-wall aluminum boxes, and the optics housing is a cylinder with 0.010-in. wall thickness. The mounting rings on the Helmholtz coils are used as part of the mechanical structure, and all mating surfaces are joined through Indium foil washers to increase the thermal conduction at the interfaces. The ground electrode on the helium lamp is a brass yoke and is bolted directly to the igniter housing to provide maximum heat transfer away from the lamp. Thermal control is accomplished by heat from the lamp which is conducted uniformly through the metal structure. The sensor is now essentially Sun-independent and will have an estimated change of 30°C between Earth and Mars.

The spherical Helmholtz coil form was developed at Texas Instruments and consists of bonded fiberglass string which is formed on a sphere of cerrobend. Once the coils have been wound and bonded in grooves in the cerrobend and the epoxy fiberglass spherical surface is formed over the cerrobend ball, the cerrobend is melted away in boiling water, and the spherical shell containing the Helmholtz coils is left as an integral unit.

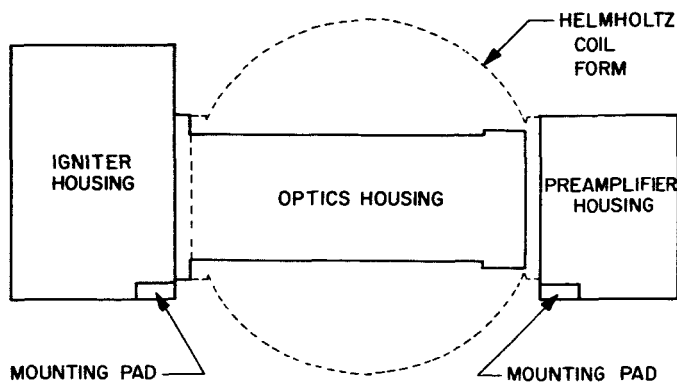


Fig. 6. Redesign magnetometer sensor

Review of system design, circuit design, and operational testing of the magnetometer breadboard uncovered the following problems:

1. Low sensor-preamplifier input impedance.
2. Inadequate system thermal null stability and offsets.
3. Excessive decoupling networks throughout the system.
4. Sweep vector asymmetry.

**a. Sensor Preamplifier.** The function of the preamplifier is to provide a buffer between the detector used in the sensor and the signal cables connecting the sensor to the magnetometer electronics in the bus.

The noise contribution of the amplifier is difficult to specify, because the detectors that were used vary considerably in source impedance and noise characteristics. Moreover, parts must be made of nonmagnetic material.

The preamplifier of Fig. 7 was designed to replace the original preamplifier. The philosophy underlying the design of this preamplifier is that an overall feedback loop should be incorporated that establishes the dc and ac characteristics of the amplifier. Through this design approach, large coupling and bypassing resistors are avoided, bias networks are minimized, and yet excellent operating point stability is obtained.

**b. System Null Stability.** The primary sources of electronically caused offsets were ground loops, pickup, equivalent dc amplifier input drift, offset caused by the demodulator driver, and insufficient loop gain preceding the dc amplifiers.

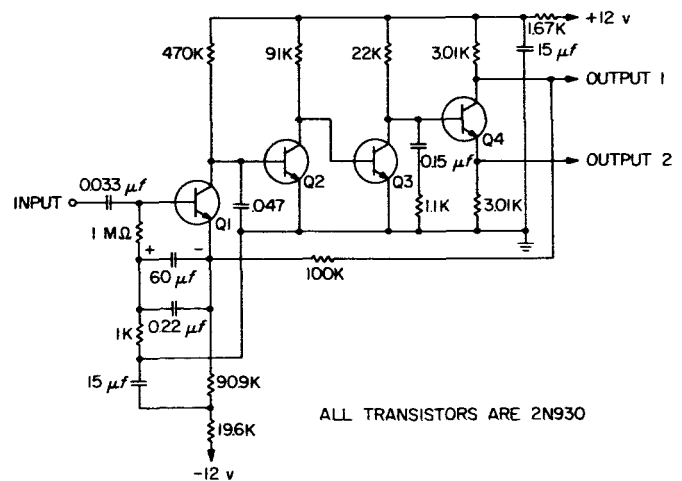


Fig. 7. Magnetometer preamplifier



An estimate was made that the loop gain preceding the dc amplifiers would have to be at least 4 to reduce the effect of their equivalent input drift on the system null stability. Although the design specification was modified to include this carrier-section requirement, evaluation of the breadboard magnetometer revealed a problem. A periodic waveform with a peak-to-peak magnitude of several gammas was observed in the system output. It was determined that this waveform was the residual second-harmonic component. This was to be expected because the second-harmonic component is several orders of magnitude larger than the frequency of interest (first harmonic), and the integrating network offers only 6 db/octave attenuation. Increasing the carrier-section gain would increase this component still more and, in addition, would have caused saturation of the bandpass amplifiers because of limited dynamic range. A twin-tee feedback element was then added to the bandpass amplifier, which provided increased reduction of the second harmonic component, reduced the output ripple, and subsequently allowed the carrier-section gain to be increased.

The shielding and grounding philosophy was reviewed and modifications were recommended. These modifications were incorporated in the breadboard, and comparison of the demodulator waveforms before and after the modifications were incorporated showed an appreciable reduction in noise. Offset measurements made by flipping the sensor in zero magnetic field showed a decrease in zero offset by an order of magnitude.

**c. Dc Amplifier.** The dc amplifier provides the filtering necessary to extract passband signals from the various frequencies generated at the synchronous demodulator. The original amplifier is shown in Fig. 8.

An undesirable feature of the amplifier are the balancing controls, R1 and R2, which are used to balance the amplifier input differential stage by unbalancing the emitter currents of the differential stage. These emitter

currents should be balanced to reduce the equivalent input drift of the amplifier as temperature varies, particularly important because this amplifier is operating from high source resistance. Therefore, it was recommended that the reference-base-return resistor (R12 of Fig. 8) be voltage-referenced to balance the amplifier. Figure 9 shows how this was accomplished.

**d. Demodulator and Driver.** The magnetometer uses synchronous demodulators to translate the carrier-centered information back to its original low-frequency bandwidth. Transistor switches are used for this function.

The basic requirement for the transistor demodulator circuits is that they be capable of switching a signal of about 6 v peak-to-peak without introducing offset signals (at the input of the dc amplifier) of more than 10 mv over the operating-temperature range.

The original circuit proposed is that shown in Fig. 10. The circuit connects the carrier-input signal to the pre-amplifier input for one-half of a carrier period, then isolates it for the remaining half period. The resultant waveform is then low-pass-filtered by the dc amplifier to obtain the passband signal components. The major problem in this circuit is that large offset voltages (50 mv or more) can be expected because of the tolerances accumulated in the demodulator-driver components. The driver will also be subject to differential variations in the absolute magnitude of the +12 and -12 v supplies.

It was recommended that a shunt demodulator and suitable driver replace the series device. The design of Fig. 11 was subsequently generated. This demodulator has an offset voltage of about 0.3 mv at room temperature and varies less than  $\pm 0.2$  mv from  $-20$  to  $+55^\circ\text{C}$ . Use of the shunt demodulator greatly simplified the driver, as can be seen by comparing Fig. 11 with Fig. 10.

**e. Excessive Decoupling.** The original design philosophy used by Texas Instruments designers included decoupling of every stage of every amplifier with an RC network on both the plus and the minus 12-v supply. Because of the low reliability of tantalum capacitors and the high density of packaging, JPL requested that Texas Instruments change their decoupling scheme to block-by-block Zener-diode decoupling. The result was the elimination of 80 capacitors and 80 resistors with no degradation in system performance.

**f. Igniter Reliability.** The circuit in Fig. 12 was originally intended for lamp and cell ignition. The theory of

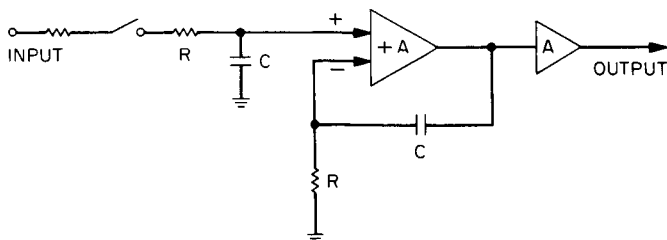


Fig. 8. Original magnetometer dc amplifier

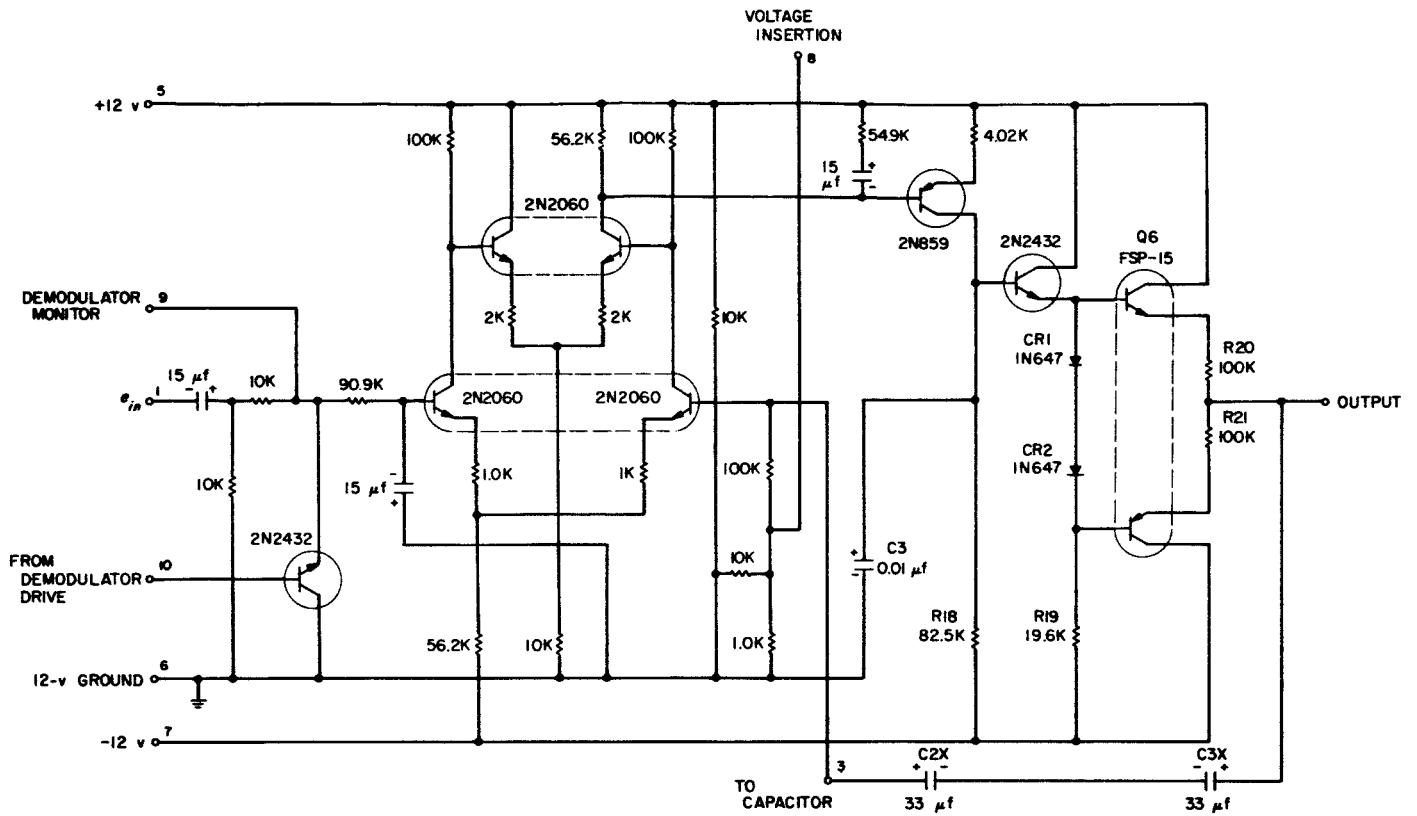


Fig. 9. Revised magnetometer dc amplifier

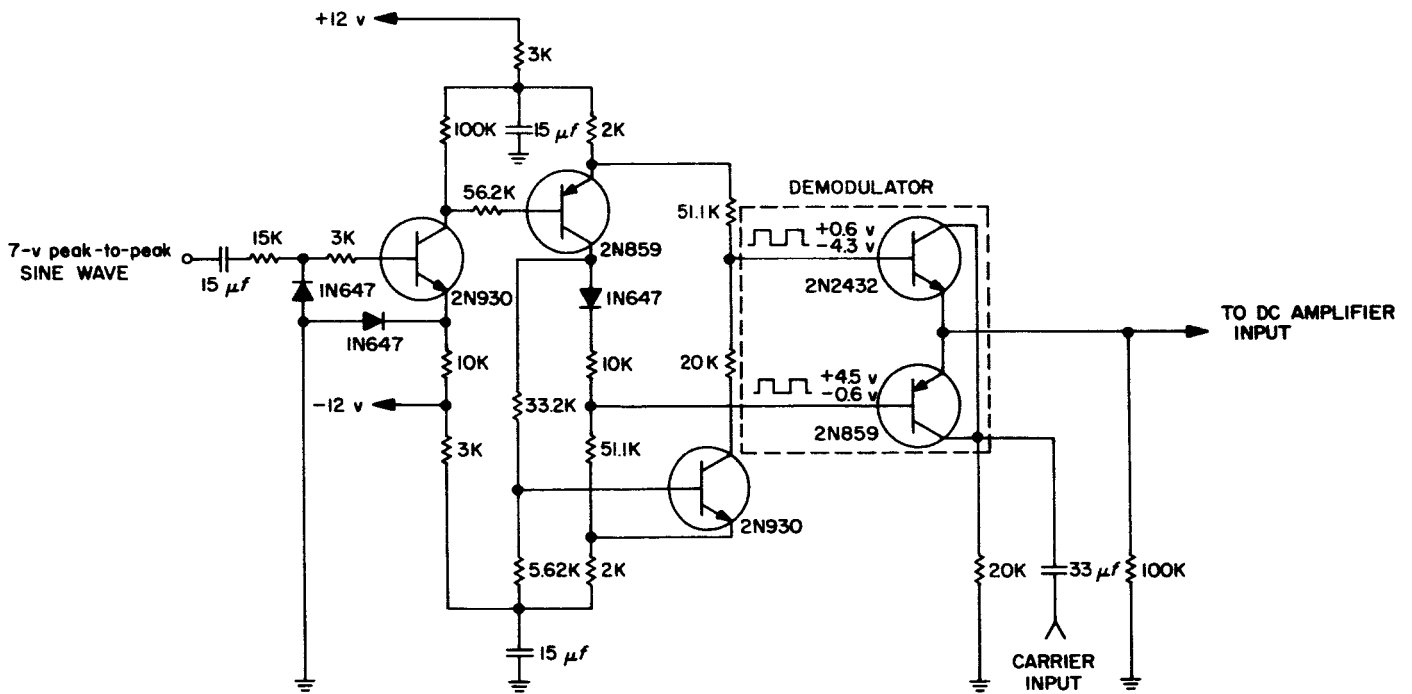


Fig. 10. Original demodulator/drives

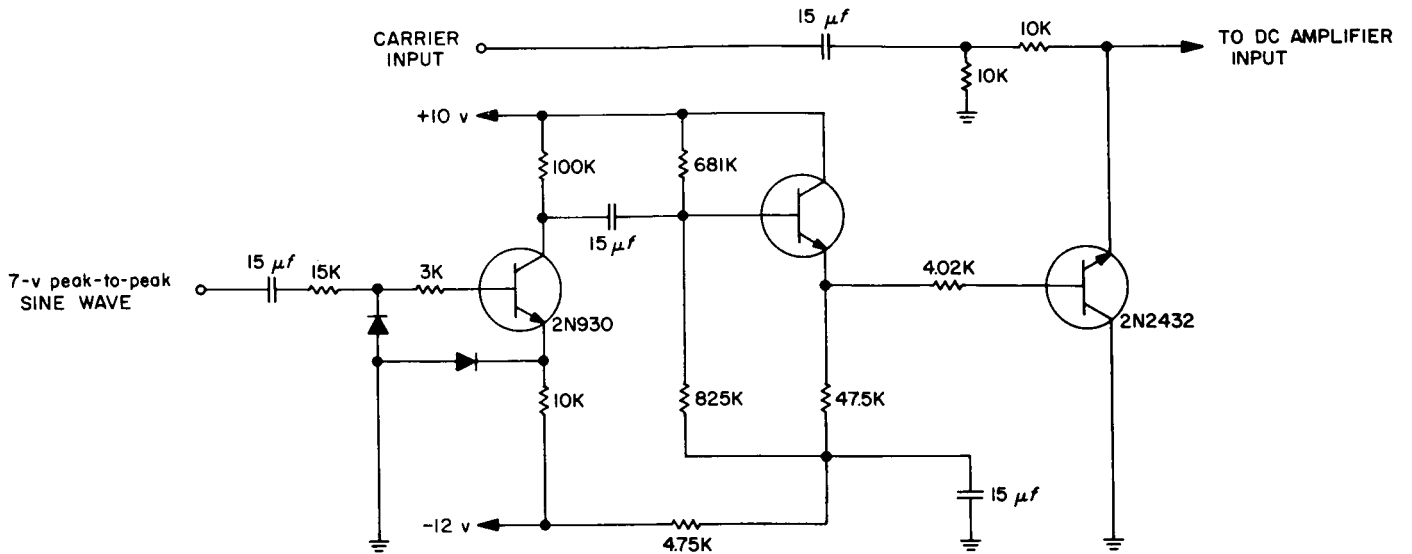


Fig. 11. Revised demodulator drives

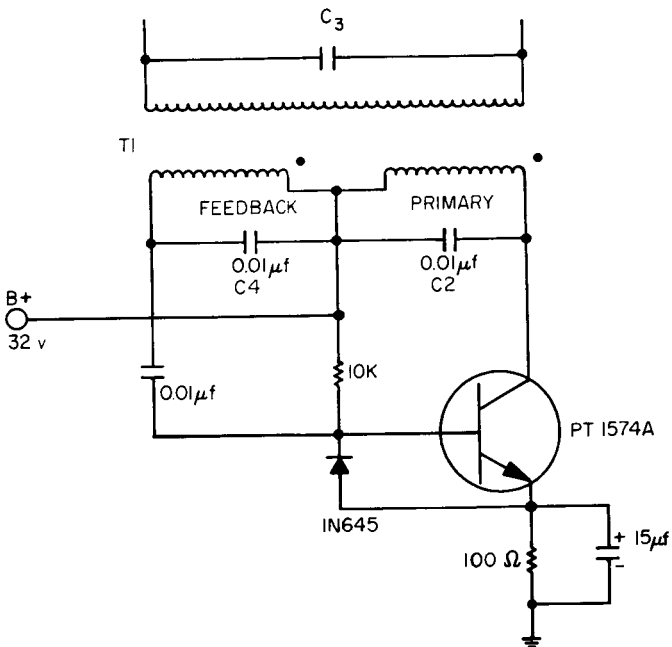


Fig. 12. Original igniter circuit

operation for Fig. 13 is the same as for the circuit in Fig. 12, with two notable exceptions. There is no form of active current limiting for Q1. The maximum collector current, at any instant, is dependent upon base current and beta of Q1. The operating point of the circuit is unstable because beta is subject to change with temperature and age. The operating frequency is dependent upon

C2 and C4. For the component values shown in Fig. 13, the frequency of operation is 100 kHz.

*g. Sweep Vector Symmetry.* If the sweep-vector amplitude does not remain constant as it rotates (e.g., if the magnitude of X component is larger than the Z component) then the input to the system electronics contains even harmonics beyond the second harmonic. The filtering in the electronics is designed primarily to remove the large second-harmonic component, and, as a consequence, the higher harmonics can be so large that the integrator will not attenuate ripple on the output. This ripple appears as noise to the data system. The problem was observed on the breadboard system and was corrected on the breadboard by reducing the sweep-vector asymmetry to below 1% by balancing the amplitude of the X, Y, and Z sweep drivers to better than 1%.

To reduce the sweep-symmetry problem and simplify the sweep circuits, the separate commutated X and Y sweep drivers were replaced by a single sweep driver with commutated outputs. As a result of this change, there was no need to balance the X and Y amplifiers.

*h. Electronics Packaging Design.* Because of the high packaging density anticipated for the magnetometer at the outset of the project, the packaging philosophy for the electronics modules was centered around welded cord-wood construction.

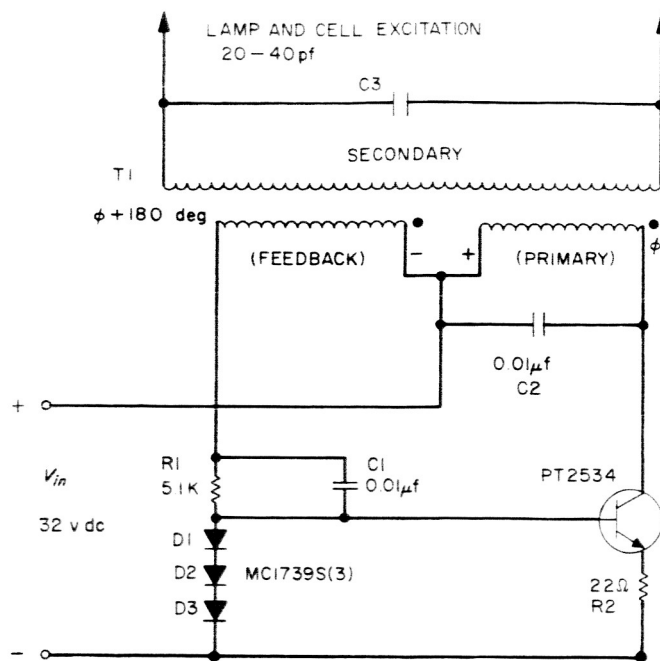


Fig. 13. Revised igniter circuit

#### D. Subsystem Operation

Failure of helium lamps and cells both in component testing and in unit testing indicated the need for a program to increase the reliability of these devices. New lamps and cells of improved design were developed and fabricated and the sensor design was altered to employ the modified units.

Failure of either a lamp or cell results from a loss of helium gas so that a glow discharge can no longer be sustained. Tests indicate that the gas has not leaked out of the glass container, but is trapped in the glass near the inside surface of the container.

Based on the experimental results on the rate of gas loss, a decision was made to increase the volume of the lamp (no space was available in the sensor to increase the volume of the cell) and to increase the pressure at which the lamps and cells were filled.

After installation of redesigned lamps and cells in all the sensors, the instrument lamp and cell ignition potentials were monitored to evaluate performance characteristics of these new components. This test does not give absolute information on the helium pressure because when the units are sealed off, impurities are driven out of the glass and these impurities affect the ignition potential. It is, however, a good figure of merit, and it is

encouraging to note that the most stable units in tests conducted from the time of installation to final testing at AFETR were those in *Mariner IV*. It should also be noted that by pressurizing both the lamp and cell above the optimum operating pressures, initial degradation in the lamps and cells will enhance system operation.

#### 1. Systems Testing

Because the full scale of the magnetometer range is approximately 0.01 that of Earth's field, either magnetic shielding or a coil system must be used to buck out the geomagnetic field during testing of the instrument. For instrument evaluation during spacecraft testing, magnetic shielding was not practical, so a coil system was employed. Figure 14 shows the Helmholtz coils that were used for system testing. The basic coil form is a 38-in.-diameter mahogany sphere with grooves cut in it into which the coils were wound. The coil constant of the triaxial coil array is gauss/amp. The coil was placed over the omniantenna waveguide and centered on the magnetometer sensor. The 120RC11 OSE console contained the support electronics for the coil system. Though there were numerous problems in spacecraft

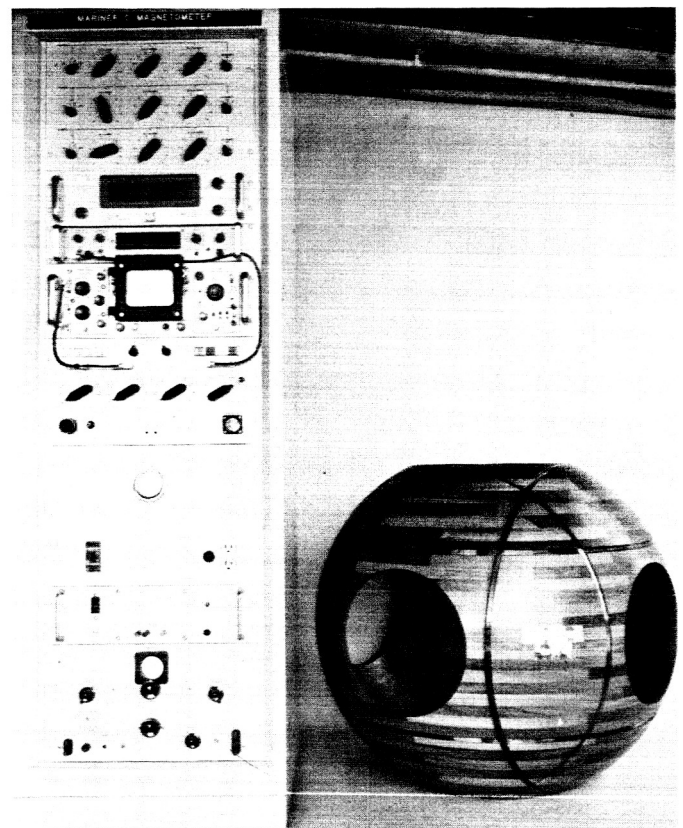


Fig. 14. Helmholtz coil system

magnetometer testing because of activity around the spacecraft and the high 60-Hz magnetic field at the various test locations, the nulling capability afforded by the coil system and support electronics allowed verification of the instrument performance through the DAS. Use of the spacecraft magnetometer for current-loop magnetic mapping of the spacecraft, a power-supply interference problem was detected and subsequently corrected.

## 2. Bench and Environmental Testing

An integrated test console was used to perform all bench testing, environmental testing, and instrument calibration. Figure 14 shows the test console also being used with Helmholtz coils in systems testing of DAS and power-supply interface circuits.

Figure 15 is a cross section of the fluxtank (magnetic shield) designed for thermal-vacuum testing of magnetometers. The tank consists of two coaxial cylindrical shells both with 0.060-in.-thick Mumetal walls. The field in the sensor test volume is less than 30 gamma when lid No. 1 is in place. This tank has been successfully used for the thermal-vacuum test of both prototype and flight

magnetometers and is now being used to support the magnetometer life test.

Figure 16 is a cross section of the fluxtank developed to support both bench testing of the *Mariner* magnetometers and calibration verifications at ETR. This tank also consists of inner and outer cylinders, but the inner shield is mechanically independent of the outer shield to minimize mechanical stresses.

Tests conducted using a *Mariner-Mars* helium magnetometer show that

1. The field in the shielded volume varies less than 0.1 gamma in 12 hr.
2. The field in the test volume is 14 gamma (i.e., the shielding factor is 3600).
3. The incremental shielding is approximately 2000 (a truck passing within 10 ft of the shield causes about 0.1 gamma disturbance).

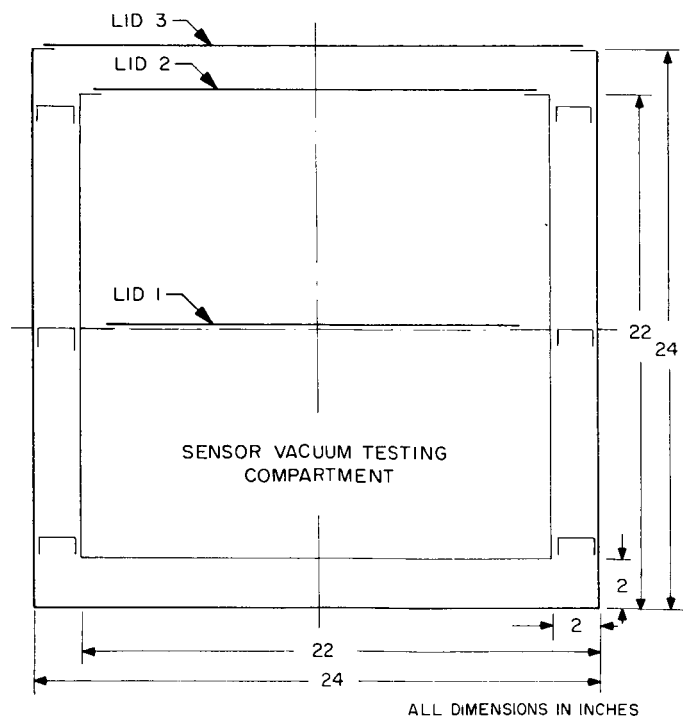


Fig. 15. Cross-section of fluxtank for thermal-vacuum testing of magnetometers

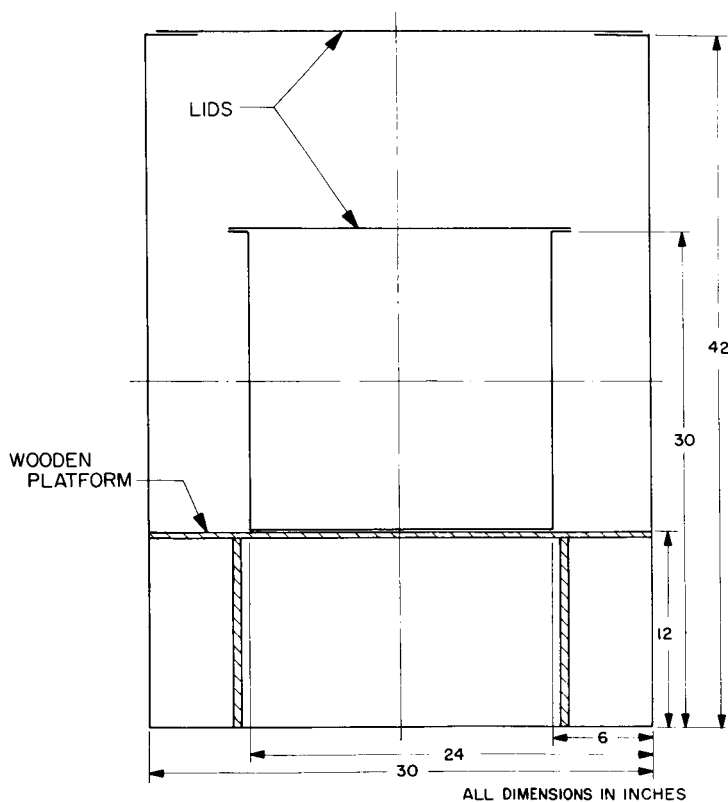


Fig. 16. Cross-section of fluxtank for bench test and calibration verification

**3. Instrument Calibration**

The *Mariner-Mars* flight magnetometers were calibrated in the magnetically shielded room at the JPL Mesa Magnetic Facility. Calibrations were performed over sensor temperatures of from  $-45$  to  $+25^{\circ}\text{C}$ , and electronics temperature ranges of  $+5$  to  $+45^{\circ}\text{C}$ . The chosen temperature ranges included all anticipated flight temperatures. The parameters that were given most serious study during calibration were

1. Offset.
2. Scale factor.
3. Linearity.

Table 1 shows the tabulated results of offset measurements vs temperature.

Because of magnetic-field drift in the shielded room and instrument noise, the offset uncertainty is approximately  $\frac{1}{2}$  gamma.

The instrument scale factor was nominally 1.01 v/60 gamma and was stable over temperature on all axes

**Table 1. Offset vs temperature (in gamma)**

Unit: MC-2	Test Date: 7-18 to 7-20-64			
Sensor	X	Y	Z	Electronics
+25° C	+0.2	+0.8	-0.2	+45° C
	+0.1	+0.6	-0.1	+25° C
	+0.4	+0.6	+0.2	+ 5° C
0° C	+0.1	+1.3	-0.7	+45° C
	+0.1	+1.4	-0.3	+25° C
	+0.2	+1.2	-0.3	+ 5° C
-25° C	-0.2	+1.4	-0.7	+45° C
	-0.1	+1.4	-0.5	+25° C
	+0.2	+1.4	-0.5	+ 5° C

of all units. The linearity of all units was approximately 0.1%. Both the scale-factor and linearity measurements were made at the outputs of the analog-to-pulse-width converters, so the instrument calibration is referenced to the DAS input.

## IX. TELEVISION SYSTEM

*J. Denton Allen and L. Malling*  
*Jet Propulsion Laboratory*  
*Pasadena, California*

### A. Introduction

The purpose of the Mars photographic system was to perform a preliminary topographic reconnaissance of portions of the surface from a flyby spacecraft system. The system consists of a single television camera employing a slow-scan vidicon tube and a narrow-angle Cassegrain telescope. Approximately 9 hr prior to the spacecraft's closest approach to Mars, power was applied to the camera initiating the picture-taking mode. On-board storage of the picture data began when the planet came into the camera's field of view and was complete when approximately 22 pictures were taken. Picture-data recording required approximately 25 min, during which time the terminator passed and illumination levels were too low for the vidicon sensor. After the brief encounter period, the picture data were transmitted to earth receivers at a rate of  $8\frac{1}{2}$  bits/sec. Each picture was digitized on board with conventional pulse-code modulation (PCM) and six binary bits per picture element.

Each picture, consisting of approximately 250,000 bits, required  $8\frac{1}{2}$  hr for transmission. The entire series of pictures was transmitted twice to provide information for bit error-corrections, if needed.

### B. TV System Parameters

Inasmuch as a planetary mission is power-limited, a low communication bit rate results, necessitating trade-offs with respect to the total information that could be communicated after the encounter period. The three most important factors that must be weighed are

1. Total area coverage for the mission.
2. Ground resolution.
3. Area coverage per picture.

The scientific objectives can be stated in general as

1. Obtaining photographic resolution a minimum of 10 times greater than Earth-based observations.
2. Covering the planet from limb to terminator.
3. Being able to locate the pictures on Mars from Earth-based data.

With the above in mind, the following system parameters were chosen:

1. 200 TV lines with 200 elements per line.
2.  $0.22 \times 0.22$  in. raster size.
3. 12 in. focal length f/8 telescope.
4. 48-sec picture repetition time, recording two of every three pictures.

The above system at the nominal miss distance yields a 5-km optical-surface resolution. A "kell" factor of 0.7 was assumed in both the horizontal and vertical resolution numbers because of the sampling nature of the scan lines and the digitizing process.

The camera took still pictures with a single optical electrical transducer, so the image had to be completely erased after each frame-readout process. For this reason, the image that was shuttered onto the vidicon faceplate was read out in 24 sec, leaving an additional 24 sec to prepare or prime the vidicon for the next exposure. The prime is accomplished by flooding the cathode side of the photoconductive target with electrons, thus reducing it to cathode potential.

### C. Camera Mechanization

#### 1. Optics

The optics subassembly consists of a shutter/filter assembly and the telescope. The telescope (Fig. 1) is an f/8 Cassegrainian system of 12-in. equivalent focal length. The primary mirror, made of beryllium, has a diameter of 1.62 in. and an f-ratio of 2.47. The beryllium secondary provides an amplification of 3.0. An all-metal system was chosen because of the constraints imposed by the space environment and a desire for minimum weight. An all-beryllium system was originally considered. It is desirable to have the mirrors, the mirror support, and spacing structure fabricated from materials exhibiting high thermal conductivity and similar thermal expansion coefficients to minimize mirror distortions and focal shift due to temperature changes in the optical system.

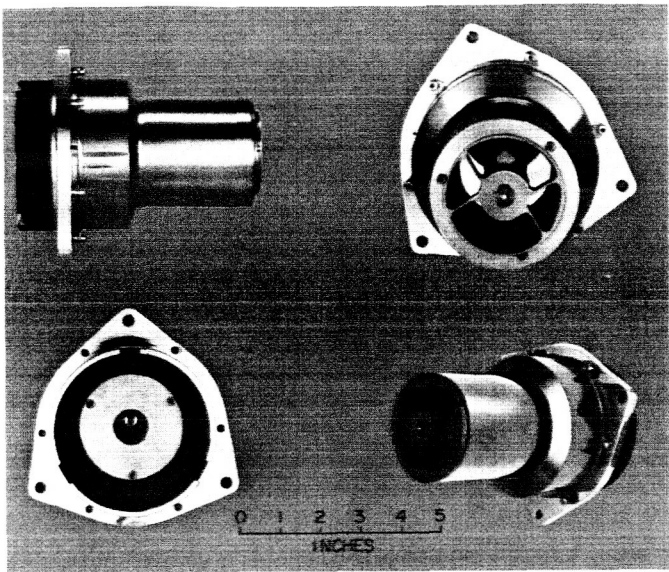


Fig. 1. Telescope

It was decided that fabricating the optical support structure from beryllium metal produced an unwarranted risk because of the brittleness of beryllium. There was concern that such a structure might not survive launch vibration. Beryllium was used for the mirror structure because of its stiffness, a requirement in producing high-quality mirrors. Beryllium copper was, therefore, chosen for the support structure.

The shutter (Fig. 2) consists of a single rotating disk containing four openings where filters are inserted. The

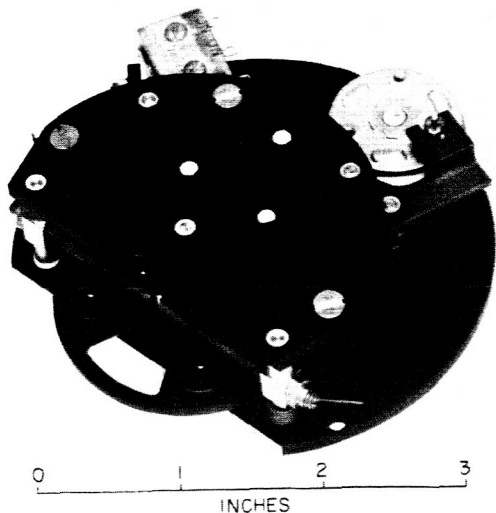


Fig. 2. Shutter

filter is introduced into the light path by a pulse applied to a rotary solenoid and removed by a second pulse. Therefore, two pulses are required per exposure. A nominal 200-ms exposure time was planned with an 80-ms emergency-mode capability if illumination levels were much higher than anticipated. Four filters were used in the disk: two in the blue-green transmission region and two in the orange-red region. The colors appear alternately as the disk revolves. A microswitch senses the condition of the shutter and provides telemetry information as to which filter is in position for each exposure.

## 2. The Vidicon

The vidicon tube (Fig. 3) was chosen as the camera photo sensor because of ruggedness, light weight, small size, simplicity, and capability of operating unattended. An all-electrostatic version was selected because it was 2 lb lighter than an all-magnetic type.

The vidicon has a specially developed target surface that allows an image to be stored for the required

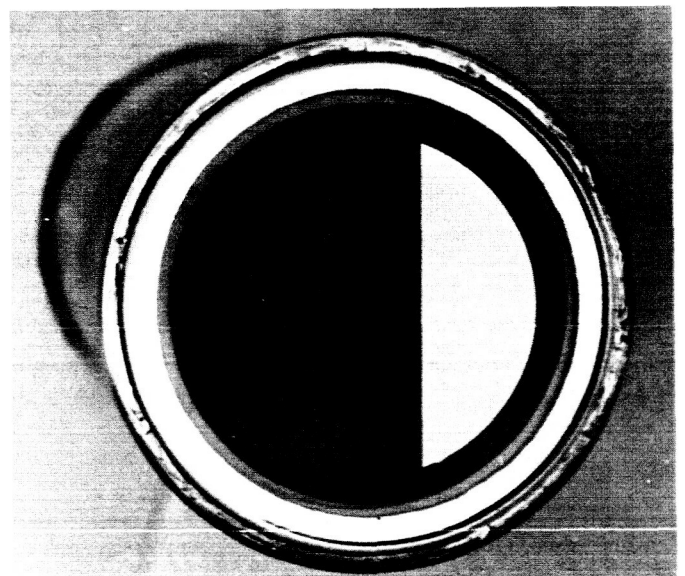
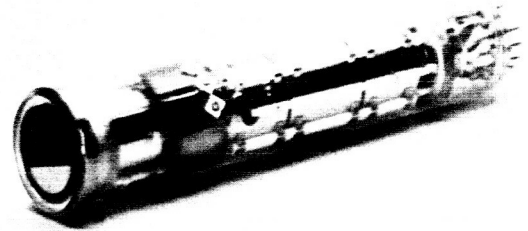


Fig. 3. Vidicon



24-sec frame-readout time with negligible degradation. Other equally important properties are

1. Sensitivity.
2. Dynamic range.
3. Shading characteristics.
4. Aperture response (resolution).
5. Erasure properties.
6. Geometrical fidelity.
7. Target noise.

The ideal sensor would be one having a noise-free linear-transfer characteristic over the entire expected illumination range with aperture response characteristics meeting the resolution requirements of the mission. The vidicon is considered to be presently the most successful electro-optical transducer for the space environment and the missile launch requirements. Knowing and understanding its limitations are extremely important in designing a spacecraft-borne television system.

The major problems encountered in system design and development were directly associated with the vidicon tube. Factors that had to be considered in design and manufacture of the tube included

1. All-electrostatic operation.
2. Ruggedness.
3. Sensitivity.
4. Dynamic range.
5. Spectral response.
6. Erasure characteristics.

An all-electrostatic vidicon was successfully developed by General Electrodynamics Corporation of Garland, Texas. This tube was of sufficiently rugged design, and was fitted with an RCA storage target, tested, and flown on the early *Ranger* missions.

The basic tube was, therefore, believed to be a proven space component. The target supplied on the *Ranger* vidicon, which was developed at RCA, was an antimony-sulfide oxygen-sulfide material known as ASOS. The ASOS surface exhibited fundamental operating difficulties at low temperatures which required further development work. As a result, GEC experimented with a selenium compound. The selenium target material developed with a new processing technique is said to be able to withstand

temperatures to 100°C. The *Mariner* tubes were tested from -40 to +80°C with no apparent degradation. This target material was found to be quite successful for the *Mariner* application. Some difficulty was experienced in reproducing the sensitivity, dynamic range, dark current, and erasure characteristics. This was eventually solved by instituting process controls at a point where acceptable tubes were being produced.

The vidicon thus selected for use was a GEC 1351A with the modified selenium target. Difficulty was encountered late in the development when vibration testing on the structural test model spacecraft revealed levels on the scan platform much higher than anticipated. Vibration testing of the 1351 vidicon indicated it was marginal and could not be relied upon to meet the new-type approval vibration requirements. It was found that the tube exhibited self-resonances in the 200-Hz range where input accelerations of 10 to 20 g rms was expected. The tube was found to be extremely rugged in the axial direction but suffered damage in the radial direction.

Two courses of action were initiated at this point. Further techniques for making the tube more rugged had been developed by GEC for ½-in. vidicons used in the Saturn booster fuel-tank studies. These techniques were incorporated into the *Mariner* vidicon along with careful weld control and 100% inspection on all subsequent tubes. The final version of the *Mariner* vidicon was assigned the number 1343-010.

A new mounting technique was also developed for the tube, as illustrated in Fig. 4, to provide damping in the radial direction. Bearing surfaces spring-loaded in the axial direction consisted of teflon-to-teflon or teflon-to-glass. The tube was surrounded by a polyurethane foam material for support and damping. Focal-plane position was maintained by axial spring loading. A low-force centering spring was used in the radial direction. Testing then proceeded on all flight cameras and the type-approval camera with no further difficulties encountered.

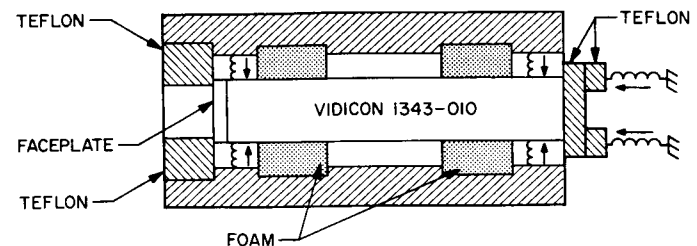


Fig. 4. Vidicon mounting

## D. Camera Electronics

The electronics were divided into two major sections: equipment associated with the camera head (Fig. 5) and equipment mounted remotely in the main part of the spacecraft (Fig. 6). The camera head was mounted on a scanning platform, so its weight had to be kept to an absolute minimum. The electronics associated with the head consists of a 110-kHz oscillator, a tuned preamplifier, and voltage-distribution and filtering circuits. The camera head, including the telescope and shutter, weighs approximately 3.5 lb. The 110-kHz oscillator serves to modulate the vidicon beam, giving rise to an RF carrier amplitude-modulated by the video information (dc to 7 kHz). This AM carrier is then coupled to the main electronics area for signal processing.

### 1. Bus Electronics

Most of the electronics equipment is located in the part of the spacecraft known as the bus. This equipment is used to perform the following four functions.

*a. Video Signal Processing.* These circuits perform amplification, demodulation, and conversion to 6-bit PCM digital. The digital circuits perform a simple amplitude-to-time conversion wherein a fixed-frequency clock is gated by the time conversion, counted, and subsequently shifted out as a digital word. A 6-bit digital word is thus created for each picture element or 200 times per TV line.

*b. Sweep Circuits.* Line and frame sweep potentials from external synchronous information are generated by the sweep circuits. These circuits consist essentially of constant-current integrators with differential drive to the vidicon deflectrons.

*c. Control.* The control circuits accept line- and frame-synchronizing inputs and convert them to the many control functions required for camera operation. A typical camera-operation sequence is as follows. The frame pulse initiates the logic-control circuits and starts the vertical sweep. Line-synchronizing data is received continuously and is scaled to provide various control functions. The readout frame consists of 200 lines requiring 24 sec. Upon completion of a readout frame as determined by the line counter, the target erase or prime mode is initiated. The prime mode, which lasts for 12 sec, is performed by increasing vidicon-beam current, scanning vertically with a 4-kHz sine wave and increasing the scan-voltage amplitudes. These functions occur simultaneously because they are initiated from the same switching logic. The scan-rate and beam-current increase ensures that the

target area is discharged to cathode potential. Increasing the scan size ensures that all residual charge arising from lateral leakage is adequately discharged.

To cover the wide illumination range anticipated, an automatic video gain technique was developed. Digital encoding is performed over a fixed voltage range; namely, the range capability of the final video amplifier which is coupled to the analog-to-digital converter. For illustrative purposes it can be assumed that the converted range is 6 v and that this 6 v is divided into 64 levels. The quantization signal-to-noise ratio then becomes a function of the peak-to-peak video level. An eight-step video gain control is used to maintain the peak-to-peak video level between 2 and 6 v. Gain switching is performed by a video-level sampling circuit that switches gain according to the video level in the amplifier chain.

Another function of the control circuits was to determine when the planet was in the camera's field of view and to issue a signal to the data automation system to start recording pictures. This function, known as narrow-angle acquisition, is performed by integrating the TV video signal. Upon reaching a preselected threshold, it issues the command. This function was performed as a backup to an entirely separate sensor on the platform known as the narrow-angle Mars gate.

Power was turned on and the camera started taking pictures approximately 9 hr prior to narrow-angle acquisition. This was done to allow adequate time for synchronization. Prior to narrow-angle acquisition, the gain-control circuit was inhibited, however, to prevent the gain from going to maximum inasmuch as no light was entering the camera.

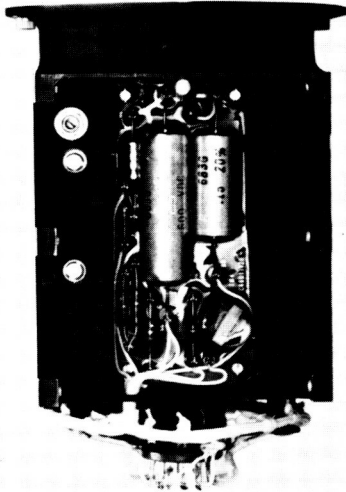
*d. Power Conversion and Distribution.* The power-conversion circuits use the 2400-Hz square-wave power from the spacecraft power subsystem and convert it to some 13 separate potentials required for the vidicon tube and the electronics. A current-limiting circuit is employed to limit the current to 160% of nominal in the event of a failure in the camera system. This technique is employed throughout the spacecraft system to provide some degree of subsystem-to-subsystem power isolation.

### 2. Test and Calibration

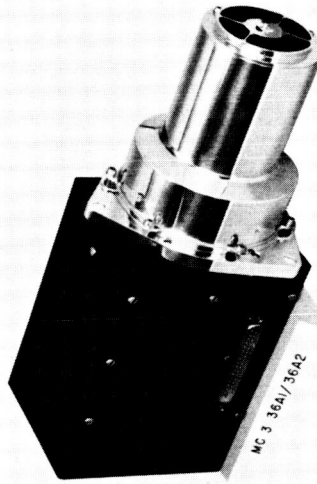
Test and calibration are touched on very briefly here inasmuch as this subject represents a fairly lengthy paper in itself. The use of a vidicon television system as a spacecraft scientific instrument presented a number of new problems with respect to test and calibration. First of all,



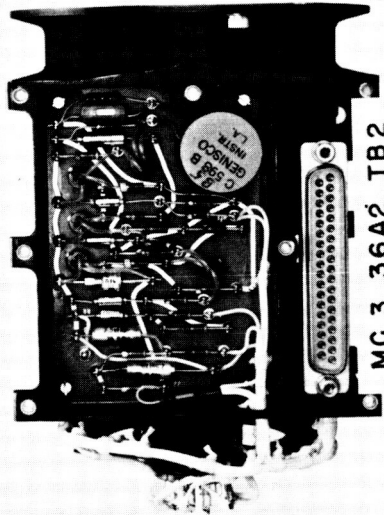
MC 3 36A2 SHUTTER



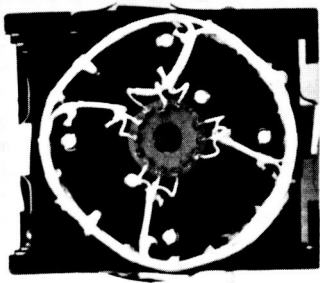
MC 3 36A2 TB4



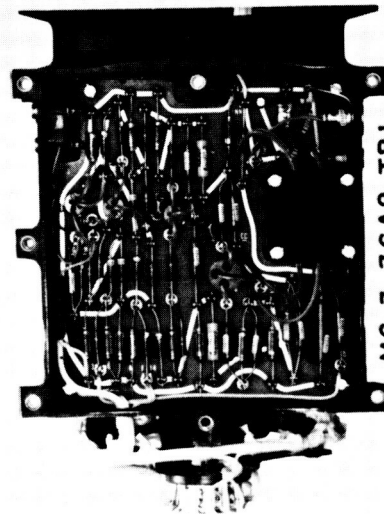
MC 3 36A1/36A2



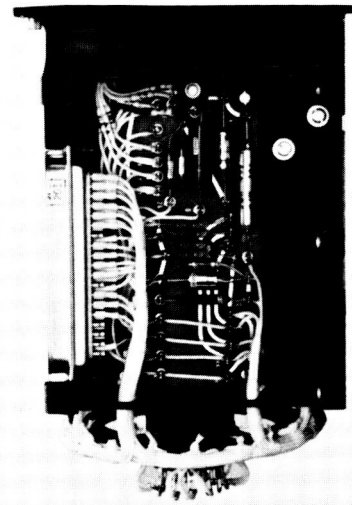
MC 3 36A2 TB2



MC 3 36A2 TUBE SOCKET



MC 3 36A2 TB1



MC 3 36A2 TB3

Fig. 5. Television camera head

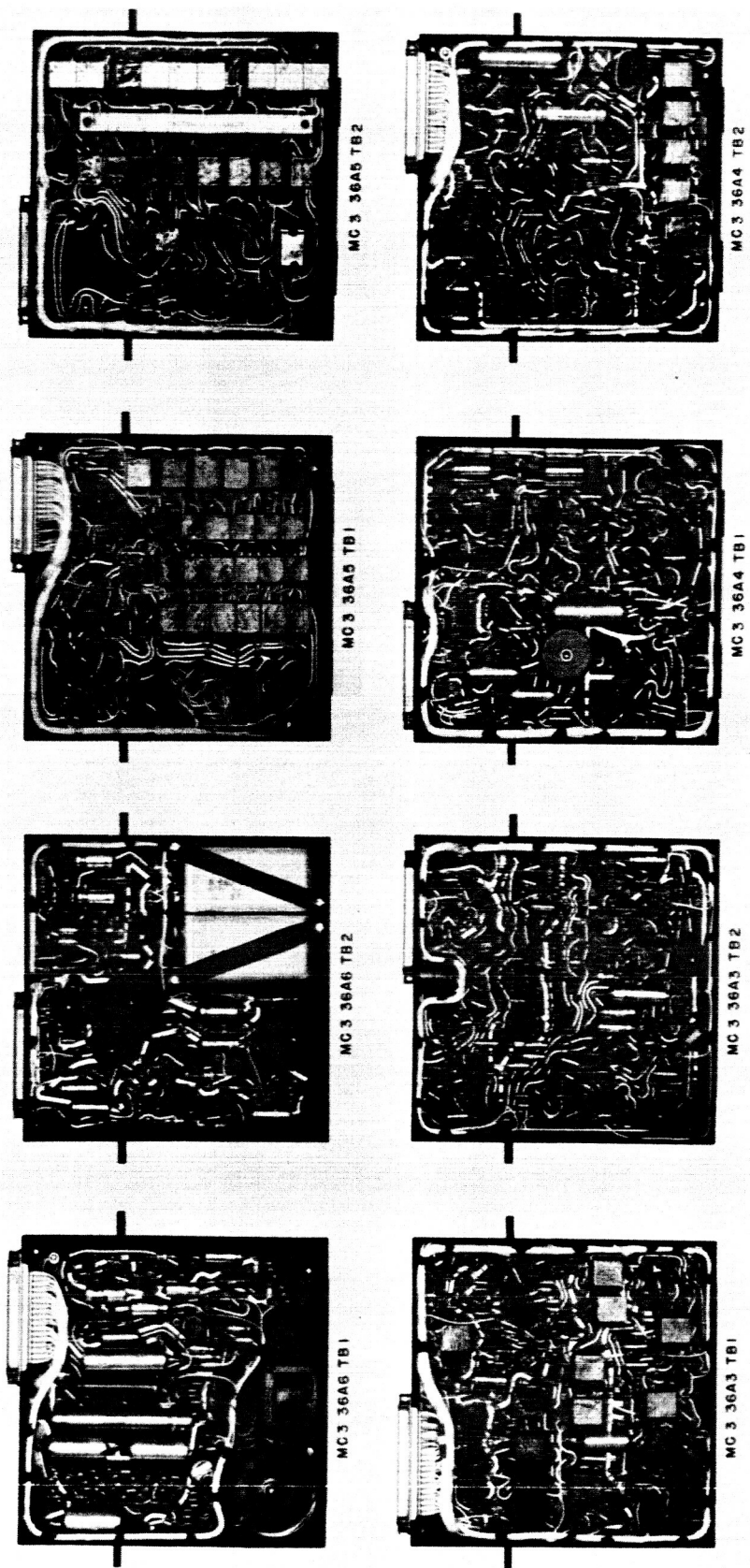


Fig. 6. Television camera electronics

the camera had to qualify environmentally for a spacecraft mission. This environment consisted of the launch, which is mainly shock, acceleration, and vibration, plus the cruise environment, which is thermal/vacuum. The ability of the camera to withstand such an environment is, of course, determined by the quality of the electronic and mechanical design. The camera as an electronic system was designed to operate from  $-40$   $+75^{\circ}\text{C}$  without adjustment and with negligible degradation.

The following calibration data were obtained on each flight camera:

1. Sine-wave resolution (high- and low-contrast ratio).
2. Geometrical properties.

3. Shading properties.

4. Illumination transfer characteristic and resultant system gamma.

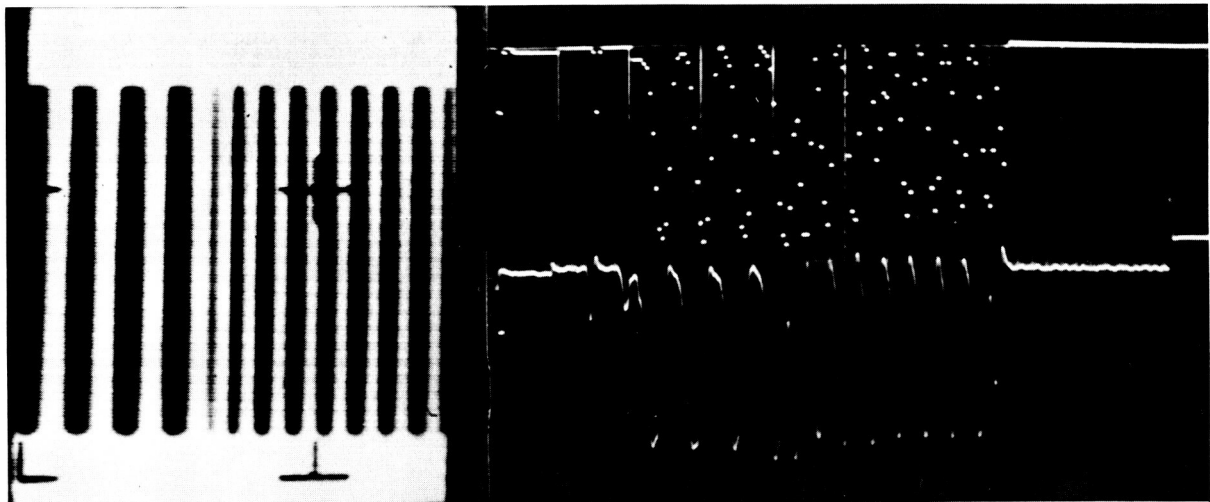
5. Flat-field switching levels.

6. Grey-shade capability.

These data were obtained with a 40-in. focal-length optical collimator with color spectrum and illumination levels approximating those known of Mars.

Sine-wave resolution measurements were made with the use of sine-wave test slides of varying spatial frequencies at two contrast ratios. Typical sine-wave response photos are shown in Fig. 7. Geometrical proper-

(a) TYPICAL SINE-WAVE RESPONSE CHARACTERISTIC



(b) BLOWUP OF "A" TRACE IN (a)

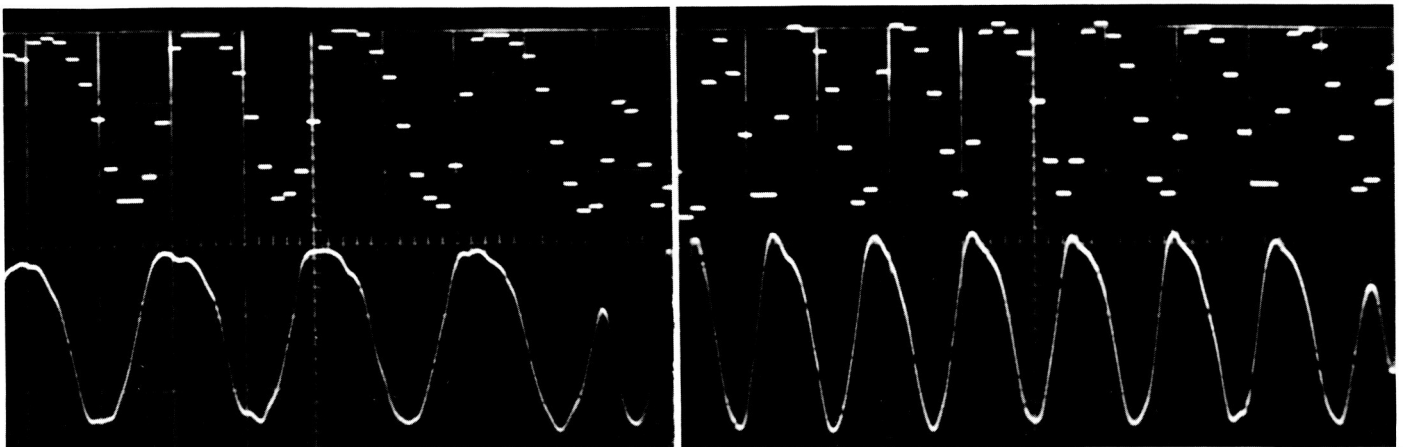


Fig. 7. Sine-wave response characteristics

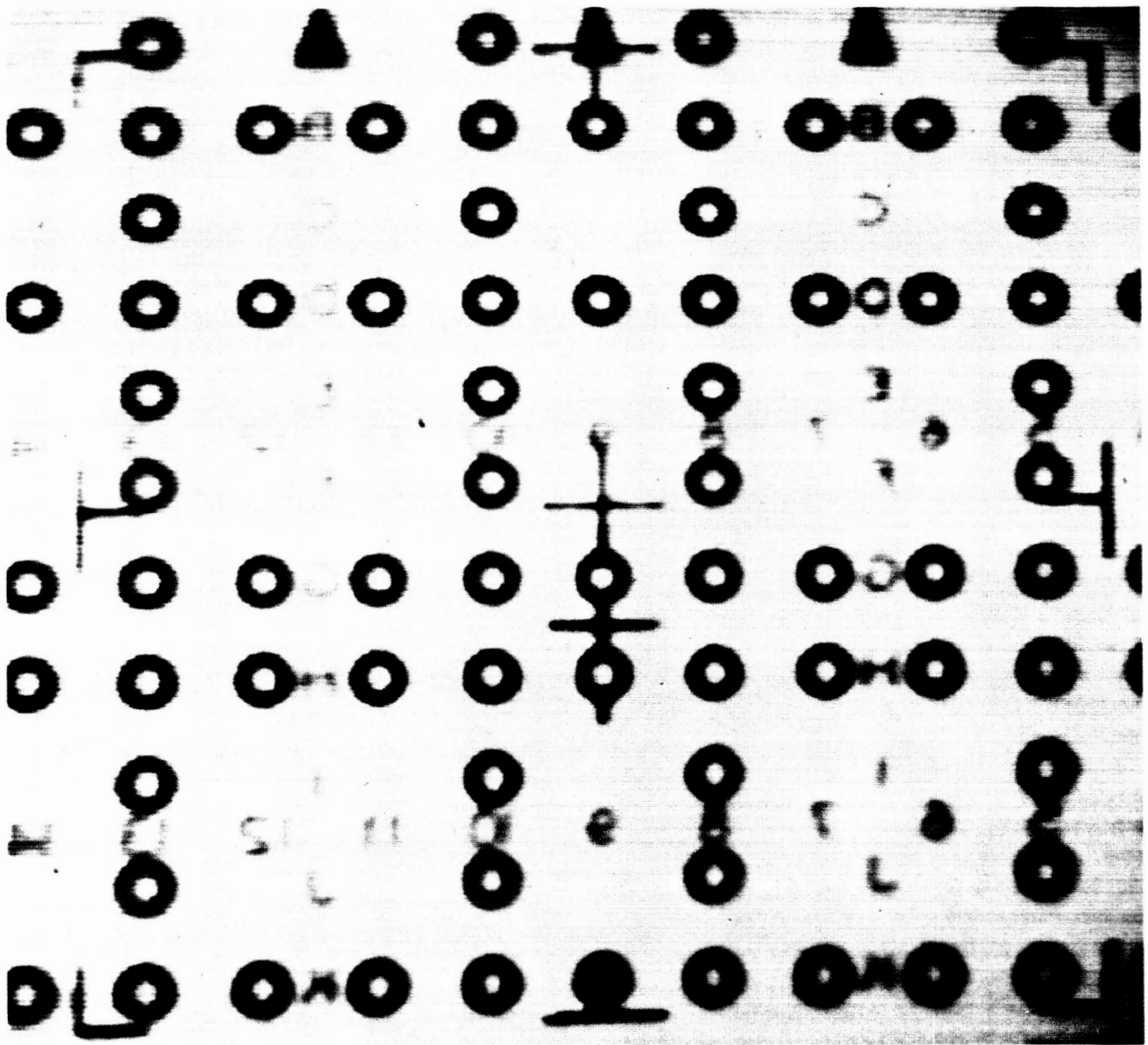


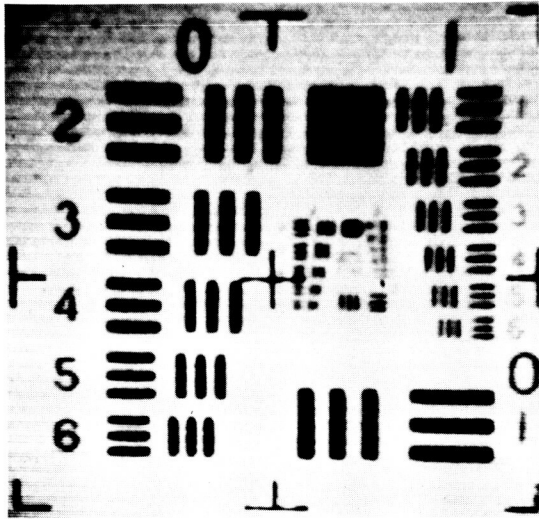
Fig. 8. Retma ball chart

ties are obtained using a standard ball chart (Fig. 8) in conjunction with fiducial marks on the vidicon faceplate. Shading characteristics are measured at three illumination levels using flat-field illumination. The illumination transfer characteristic is measured with flat-field illumination, the intensity of which is controlled by inserting neutral-density filters in the collimator. Inconel neutral-density filters having excellent spectral-response characteristics are used. The gain-switching and narrow-angle acquisition levels are measured in the same general way as the illumination-transfer characteristic using neutral density filters. Gray-shade capability is measured

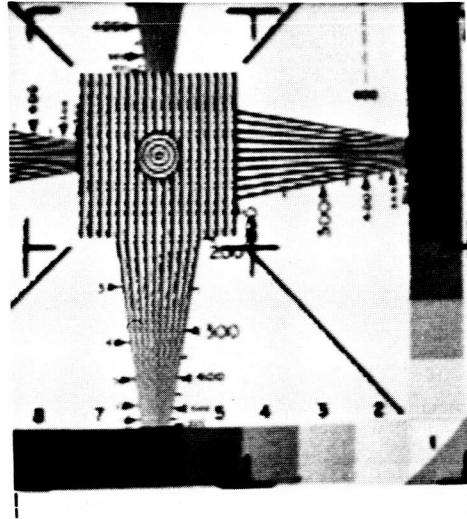
with a test slide having 10 gray levels of linear density or logarithmic transmission. Figure 9 shows a set of typical photographs illustrating the general capabilities of the system.

In general, the purpose of the calibration procedures is to document the camera's transfer function with respect to contrast, spatial frequency, and illumination as inputs and the digitized video information as output. It is desirable to measure this transfer function independent of the data-handling and display techniques. Digital techniques that circumvent the problems associated with

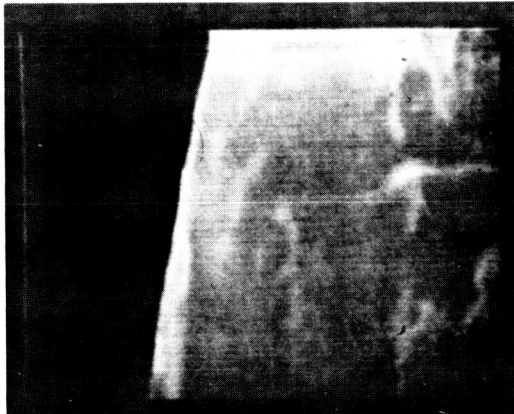
AIR FORCE RESOLUTION CHART



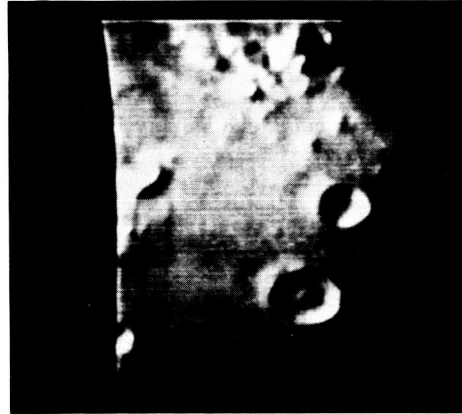
RETNA TEST PATTERN



LUNAR LIMB USING 60-in. TELESCOPE AT MT. WILSON



LUNAR CRATERS AT THE TERMINATOR USING 60-in. TELESCOPE AT MT. WILSON



LUNAR TEST SLIDE



LUNAR TEST SLIDE

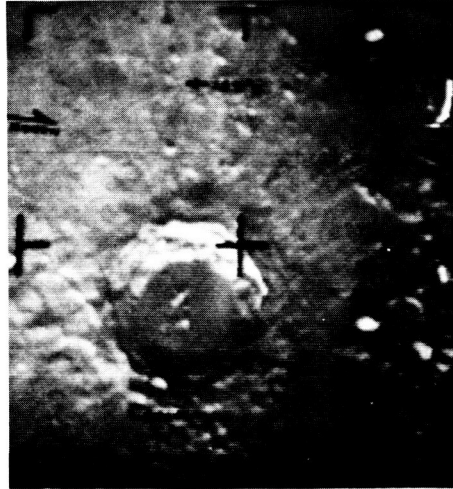


Fig. 9. Typical performance photographs

phosphors and film characteristics were used for data display. The primary quantitative display was in the form of a  $200 \times 200$ -element matrix where each picture element is a decimal number from 1 to 64 representing the 6-bit digital word corresponding to a picture element. Qualitative displays were made with a kinescope film recorder. The pictures shown in Fig. 9 were made with the kine recorder process on 35mm film.

### **E. Summary**

The Mars TV system was designed to take approximately 20 photographs on the Martian surface from the limb to the terminator. This brief flyby period, lasting

about 25 min, occurred after an eight-month flight through interplanetary space from Earth to Mars. The camera was energized 9 hr prior to encounter by a ground command. Upon obtaining narrow-angle acquisition, the pictures that had been digitized to 6 bits per element were coupled to an on-board data system where the data rate was converted from the TV rate of 83.3 kilobits/sec to 10.7 kilobits/sec. The 10.7-bits/sec data were then recorded on magnetic tape. After completion of the picture-taking mode, the camera was deenergized and the tape recorder played back the data for transmission to Earth receivers at 8.3 bits/sec. At this bit rate it requires 8.3 hr to obtain one picture. The full set of pictures was read back twice.



## X. DATA-AUTOMATION SYSTEM

*W. J. Schneider and D. L. Nay*

*Jet Propulsion Laboratory  
Pasadena, California*

### A. Description of Mission

The science mission to Mars consisted of two parts: (1) the interplanetary cruise portion when fields and particles instruments alone were active and (2) the planetary encounter portion when the encounter instruments in addition to the cruise instruments were active. Two physically and electrically independent data systems were used to accommodate these two distinct portions of the mission and to reduce their interdependence. A real-time data-automation system was used to put the cruise science data into format for real-time transmission to Earth. A non-real-time data-automation system both controlled the spacecraft encounter sequence and put the

television data into format for recording and subsequent transcription to Earth.

Figure 1 depicts the nominal mission sequence. Except during maneuver portions of the interplanetary cruise, only the RT equipment operated and the spacecraft transmitted in Data Mode 2, which consists of 20 engineering measurements of 7 bits each and 28 science measurements of 10 bits each. Five hundred and forty minutes before closest approach, non-real-time power was turned on, activating the planetary scan, video storage recorder, and the NRT data system. When the planet came within the field of view of the planetary scan system, the data system issued the switch to Data Mode 3 command. Data

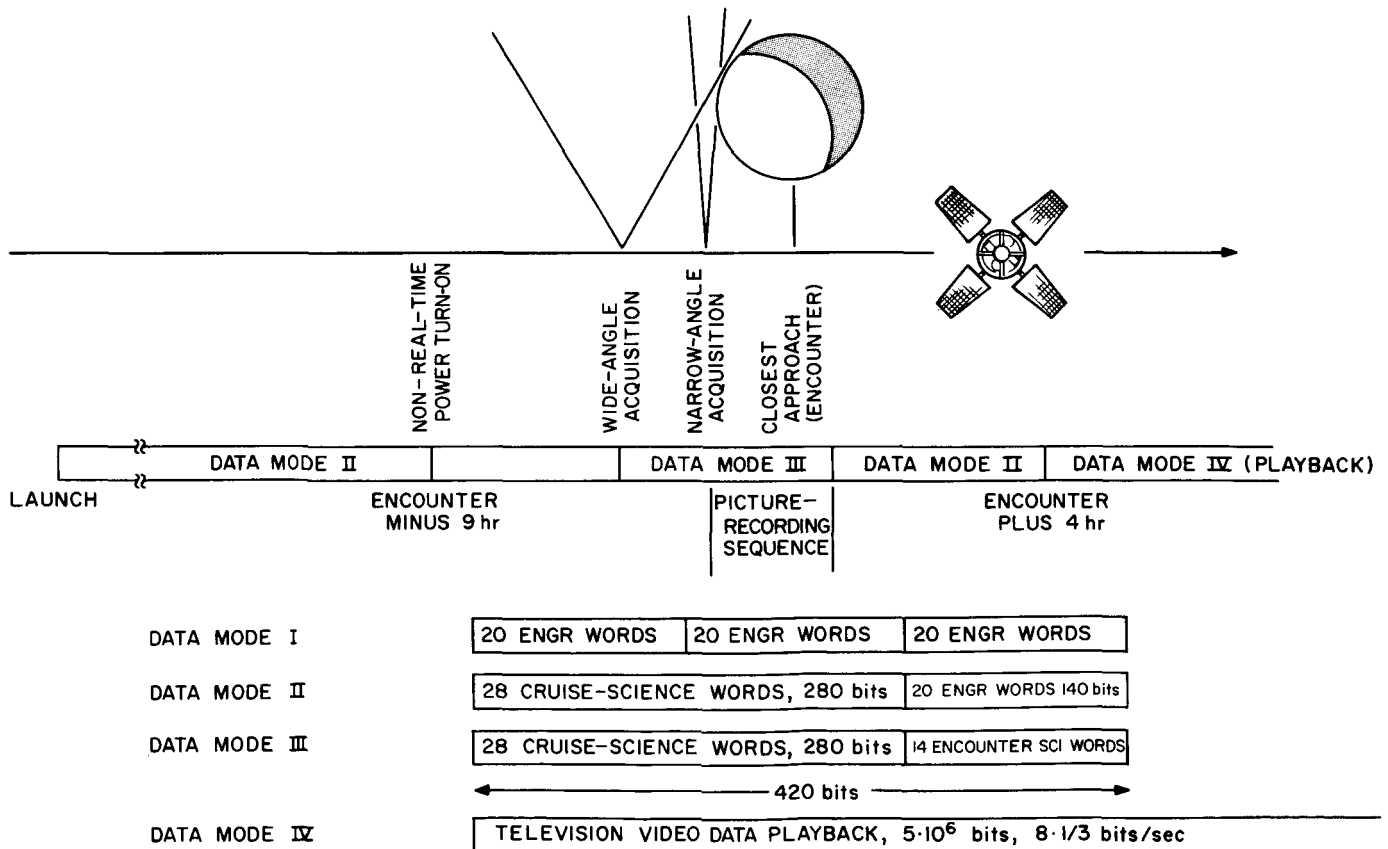


**Fig. 1. Nominal flight sequence**

Mode 3 consisted of 42 science words of 10 bits each. When the planet came within the narrow field of view of the television system, the data-automation system initiated the recording of TV pictures and continued until the tape recorder had fully recorded all 21 pictures. The data encoder then issued a switch to Data Mode 2 command. The recorded pictures were later played back, independent of the data-automation system.

### **B. Real-Time Data Handling**

Data from the science-payload instruments were gathered by the science-data system and presented to the data encoder in a serial format. The real-time data format is shown in Fig. 2. The format consists of forty-two 10-bit words. Seven of these words were used to indicate the status of the data system itself. For example, words 1 and 2 contained a pseudorandom sequence which identified the start of the data frame, while word 28 indicated the state of the internal frame counter.

Five of the instruments produced analog-voltage outputs. These voltages were quantized by a two-step process. A voltage-to-pulse-delay conversion was made within the instrument followed by a pulse-delay-to-time conversion made within the data system. In the case of the magnetometer, three bipolar voltages, corresponding to the X, Y, and Z magnetic-field magnitudes had to be measured simultaneously. The parallel conversions were made in three separate registers. Each conversion consisted of a sign bit and 9 data bits. The registers were then read out serially.

The remaining instruments produced digital-data outputs. Digital data was transferred to the data system serially by the cosmic-ray telescope and in parallel by the cosmic-dust detector. The trapped-radiation detector output consisted of the actual counts from each of its five particle detectors. These detector signals were commutated into a data-system accumulator on a frame-by-frame basis. An adaptive-scale switching technique was employed to accommodate the widely varying count rates. The ionization chamber discharge pulses were also accumulated in a data-system register. When less than eight pulses occurred in a frame, this data word was altered to include time of occurrence as well as pulse-count data.

### **C. Encounter Sequence**

The encounter-orientated equipment was set into operation when non-real-time power was turned on. The data-

automation system immediately established its normal sequence (Fig. 3) of operations. Shutter and line commands were issued to the television and the tape recorder received stop commands and data, but no start commands.

As the spacecraft approached the planet, the scan system sensed it and issued a "planet-in-view" signal to the data system. The data-automation system responded by issuing a "switch-to-Data-Mode-3" command to the data encoder. As the planet entered the narrow field of view of the television sensor or the narrow-angle Mars gate, a planet-in-view signal was issued. This signal caused the narrow-angle Mars gate sensor flip-flop to be set. It could also have been set by a ground command.

The narrow-angle Mars sensor flip-flop was set asynchronously to the established sequence. The equivalent synchronous flip-flop, narrow-angle acquisition was set through the transfer gate. The narrow-angle acquisition flip-flop initiated the picture sequence as follows:

1. It prevented further movement of the scan platform by issuing a scan-inhibit command,
2. It enabled the tape-recorder-start commands,
3. It enabled the data-frame counter to count picture sequences, and
4. It caused a back-up gain increase command to be issued to the television system.

The picture-encoding and -recording sequences were allowed to continue until at least 18 but not more than 22 picture sequences were completed. The completion of 22 pictures or the receipt of an "end-of-tape-loop" signal between the completion of the 18th and 22nd pictures caused the termination of the sequence and a subsequent "switch-to-Data-Mode-2" command.

### **D. Video Data Handling**

The data-automation system gathered video data from the television equipment and put it into the required format for recording by the video storage recorder. Although this requirement was conceptually simple, it became functionally complex when the detail requirements of the individual systems were considered.

The design of the television system was the result of careful consideration of the number of pictures, spatial resolution, brightness range, and storage capacity. The final design called for 20 pictures to be taken. Each picture was to contain 200 lines of 200 elements. The ele-

LEGEND  
 CALIB COS RAY DATA-AUTOMATION SYSTEM ENCODER MAGNETOMETER MOST-SIGNIFICANT BIT  
 NRT NON-REAL-TIME PARTICLE FLUX PLASMA PSEUDONOISE PRESSURE NON-REAL-TIME POWER ON REAL TIME SERIAL NUMBER TEMPERATURE TRANSFORMER-RECTIFIER  
 CALIB COS RAY DAS ENC MAG MSB NRT PF PL PN PRES Q RT SN TEMP TR

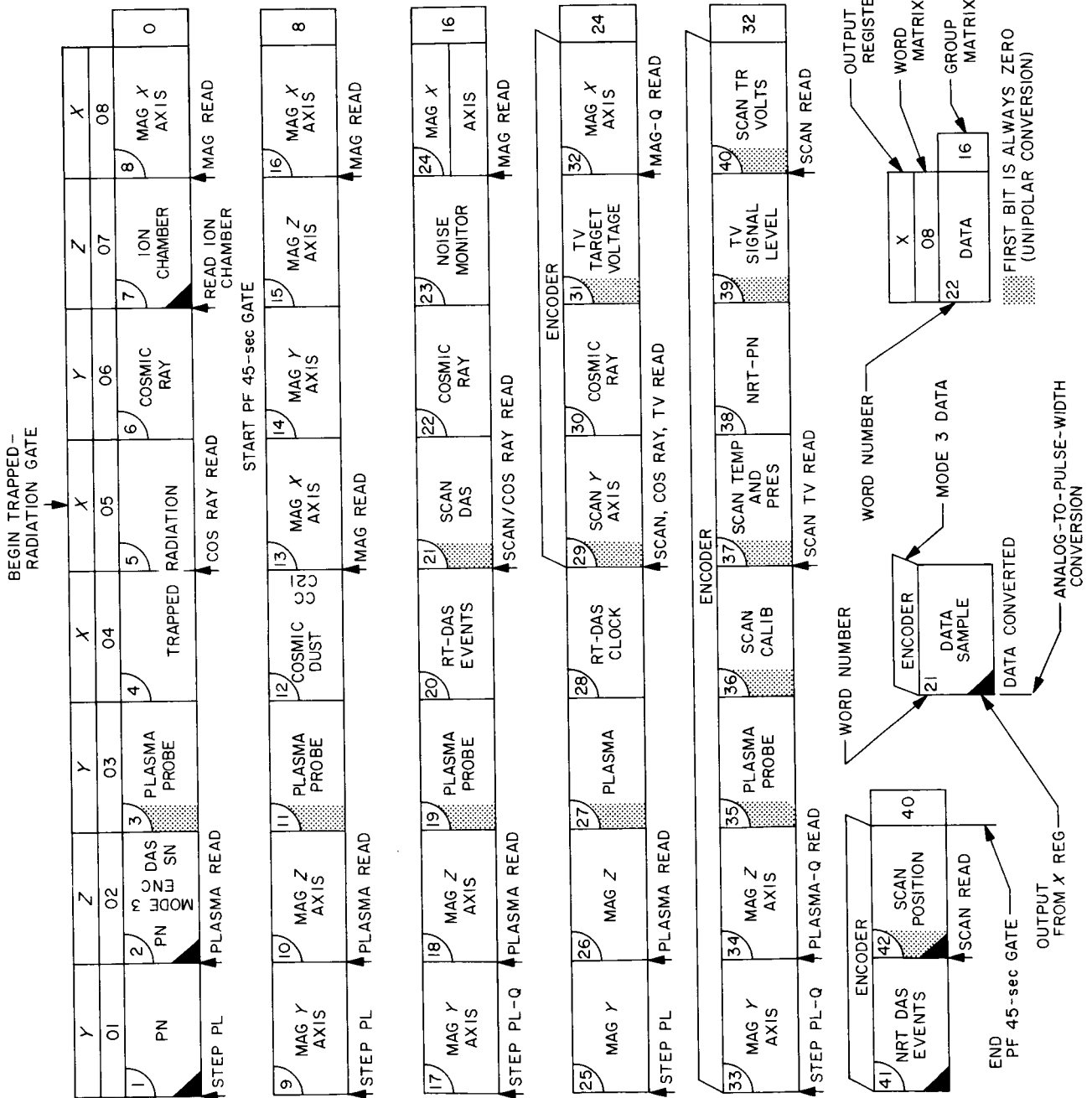


Fig. 2. Real-time data format

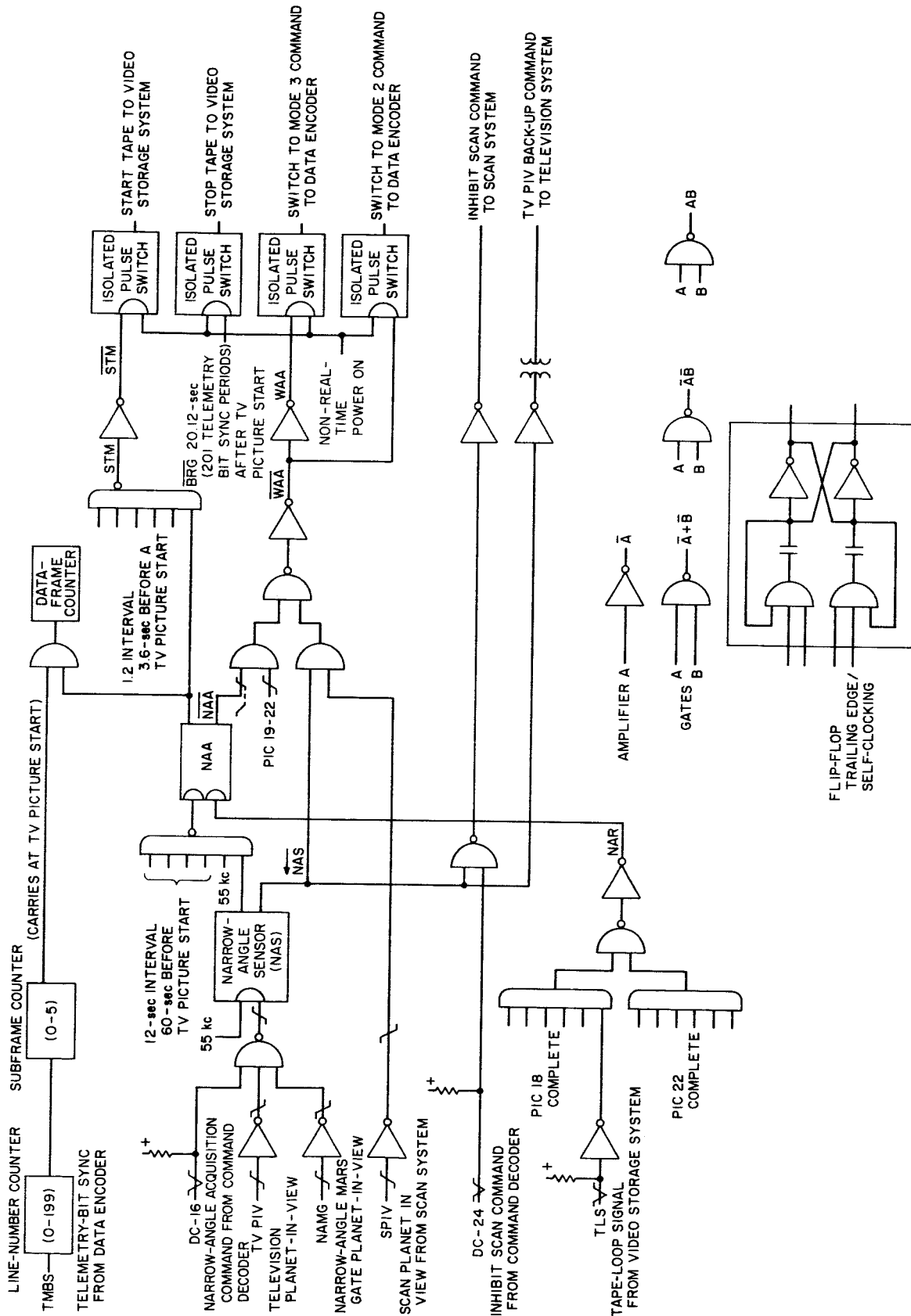


Fig. 3. Encounter sequence logic

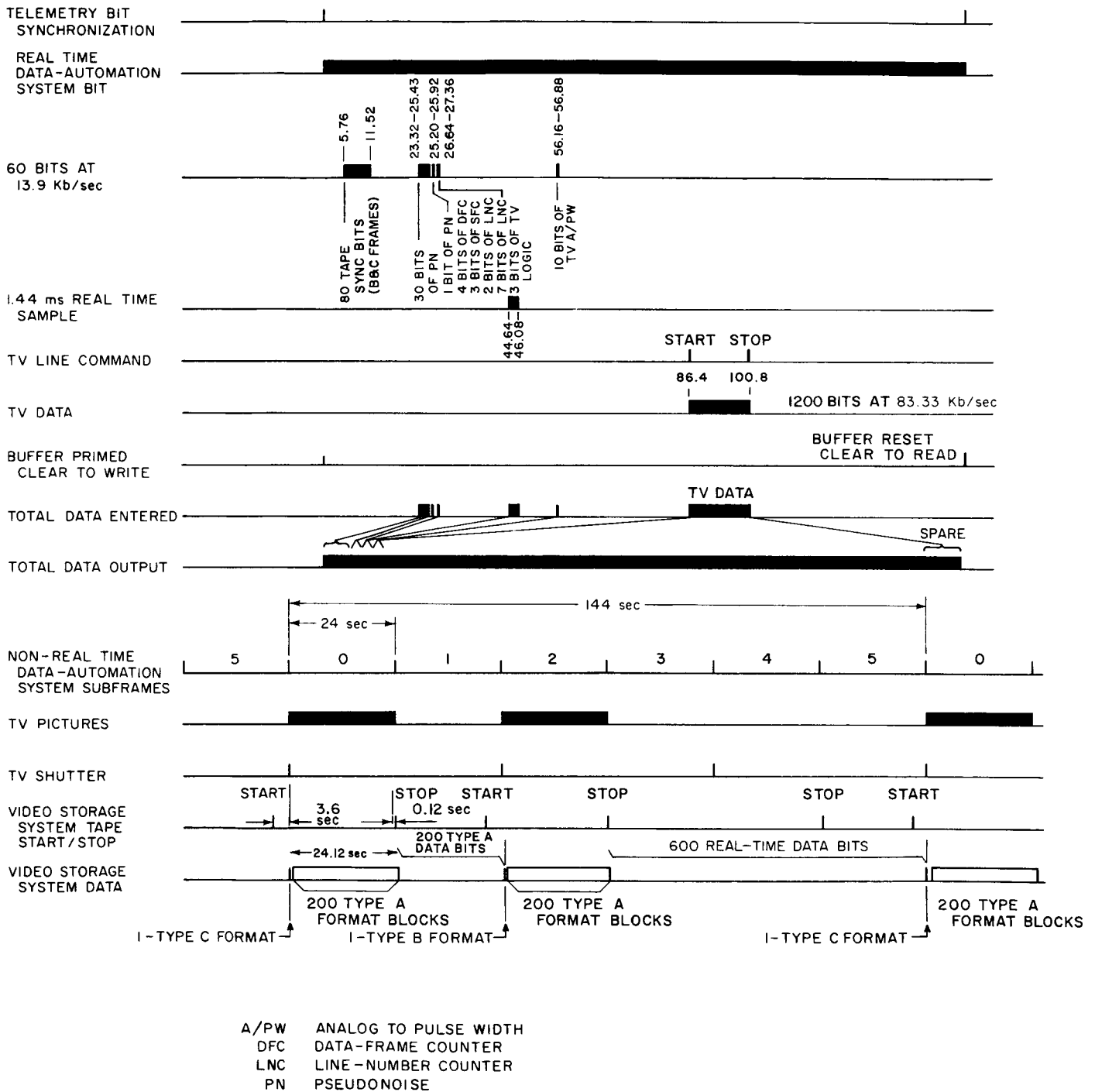


Fig. 4. Non-real-time data-automation system format

ments were to be quantized to 64 levels and expressed as 6-bit binary words. The video storage requirement was slightly more than 5 million bits of data.

The tape recorder required start commands from the non-real-time data-automation system 3.6 sec before the first data arrived to allow for tape-speed stabilization. Data and synchronizing pulses were taken to be supplied at a uniform rate of 10.7 kilobits/sec. A stop-tape-recorder command was required after each picture was recorded and termination of spacecraft Data Mode 3 was required after an end-of-tape-loop signal.

The television system required a shutter command from the data system at the start of each picture and individual start/stop commands to control the reading of each line of video data.

On receipt of a line-start-read command, the television encoded 200 words of 6 bits each—a total of 1200 bits. The data system entered these 1200 bits directly into a core memory at the 83-kilobits/sec asynchronous rate of the television encoder.

The data-automation system had the further requirement of identifying each line of the video data and of recording all real-time data produced during the encounter. These requirements were satisfied by the frame format shown in Fig. 4. Each frame was 120 ms long and was synchronous with the 8<sup>1</sup>/<sub>2</sub>-bits/sec rate of the real-time data-automation system. The corresponding real-

time data bit was entered directly into the core memory as part of the non-real-time format. The start of each frame was identified by a 31-bit pseudorandom sequence, followed by picture number, line number, television engineering measurements, and finally, the video data. At the end of each 120-ms interval, the path of this data was routed to a second core memory while the first memory was read to the video storage recorder.

The time from the television shutter command to the completion of the recording and the subsequent recorder stop command was 24.12 sec. The design of the television instrument also required that the pictures be spaced alternately by intervals of 48 and 96 sec. The output of the real-time data system, occurring between recording sequences, was stored in one of the core memories for recording during the next period of tape-recorder operation. All of the real-time data acquired during the encounter was thus stored along with the video data.

### E. Packaging

The data system was packaged as shown in Fig. 5. Five separate trays of electronics were used for the logic assemblies. In addition, a number of ancillary voltage-to-pulse-delay converters were constructed and were incorporated into the instruments that required them.

Power supplies for the real-time and non-real-time sections are electrically independent, but shared a common tray. They were of conventional construction. A

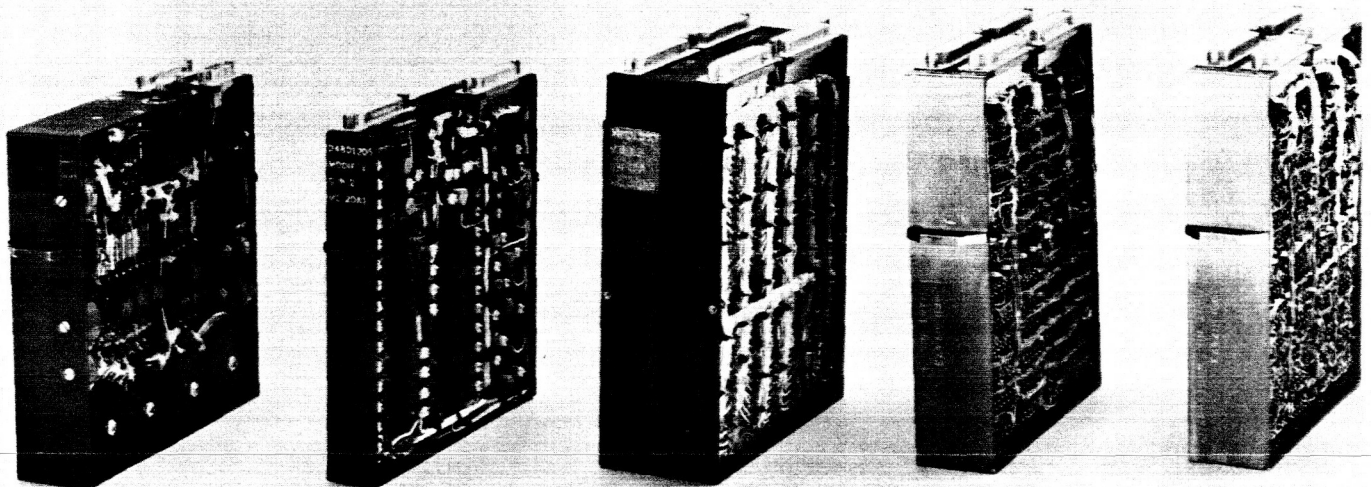
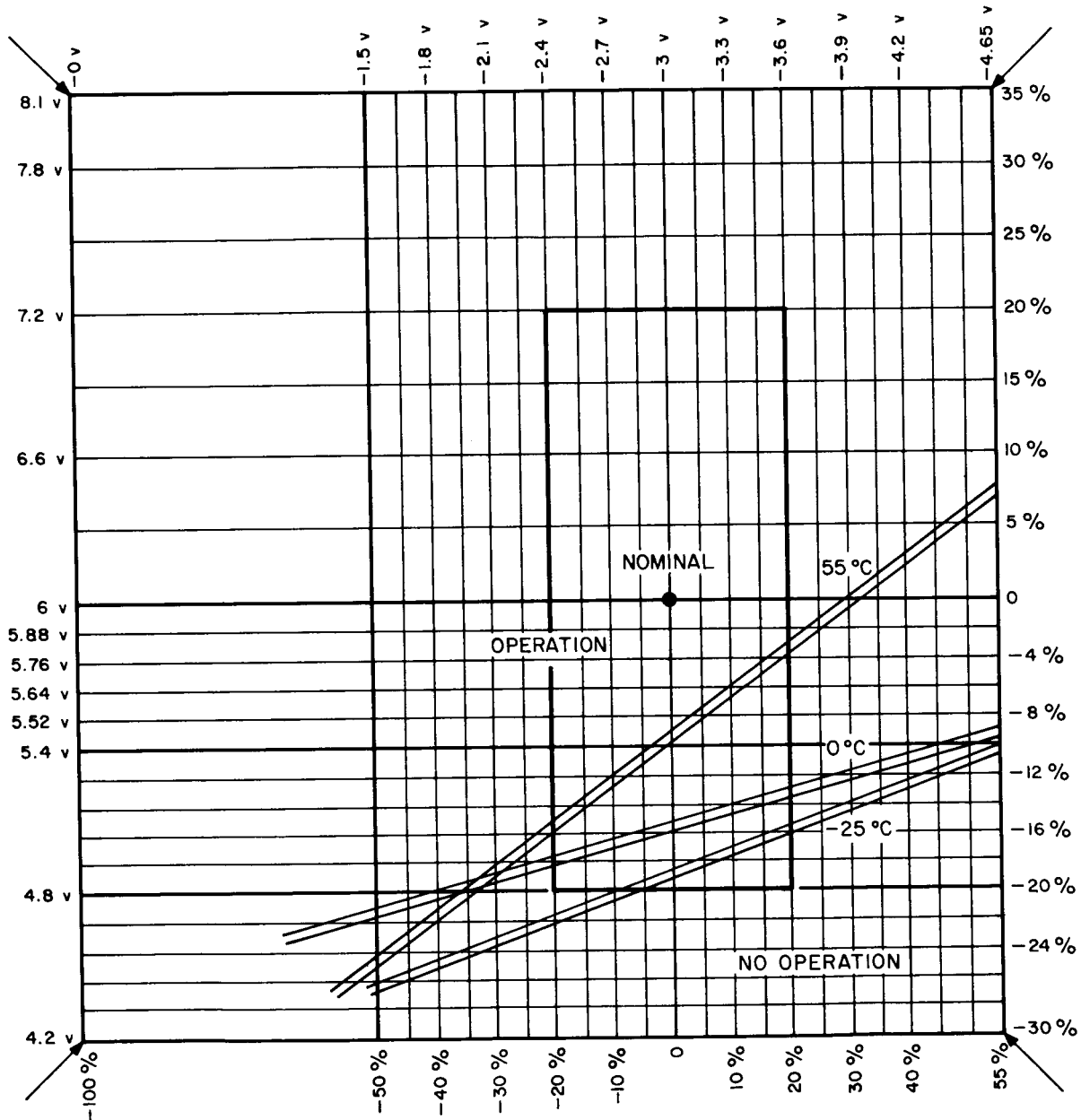


Fig. 5. Data-automation system subassemblies

DATE \_\_\_\_\_  
 TIME \_\_\_\_\_  
 TEMPERATURE \_\_\_\_\_  
 DAS SERIAL No. \_\_\_\_\_



- LEGEND:
- o DAS CORRECT OPERATION
  - No. 1 FAILURE FRAME COUNT
  - Δ No. 2 FAILURE \_\_\_\_\_
  - x No. 3 FAILURE \_\_\_\_\_
  - \* No. 4 FAILURE \_\_\_\_\_

TYPE OF MARGINS:		
RT (NRT OFF)	<input type="checkbox"/>	20-v MARGINS: (6=6, -3=3)
RT (NRT ON)	<input checked="" type="checkbox"/>	PASSED 30% <input checked="" type="checkbox"/> -30% <input checked="" type="checkbox"/>
NRT (NO RT)	<input type="checkbox"/>	FAILED AT _____
COMPLETE DAS	<input type="checkbox"/>	
COMPUTER TEST	<input checked="" type="checkbox"/>	PASSED 16% MARGIN
SPC-I TEST	<input type="checkbox"/>	OPERATOR _____

Fig. 6. Data-automation system margin check sheet

total of 331 components were required for both supplies giving an average density of six components per cubic inch.

The two electrically independent memories, used to buffer television data to the tape recorder, shared a standard tray 1-in. thick. Planar construction on a double-sided printed-circuit board with back-side magnet-wire jumpers was used. Components were mounted to forked terminals except for ribbon diodes, which were soldered directly to the printed-circuit conductors. Exclusive of the bit cores, there were 600 components yielding an average density of 16.2 components per cubic inch. When the cores were included, the density went up to 87.3 components per cubic inch.

The non-real-time logic contained 2516 conventional components packaged in welded cordwood modules with a wired interconnect. The average component density was 25.5 components per cubic inch.

Two trays were required for the real-time logic section. A total of 4911 components are used, of which more than 4000 are leadless pellets. Pellet resistors, capacitors, and diodes in the form of right circular cylinders 0.030 in. high were used. These were cast in epoxy to form circuit substrates 0.030 in. thick. Interconnections to the pellet components were formed by vacuum deposition of metals followed by dip-soldering. An average component

density of 39 components per cubic inch was achieved for the two real-time logic trays.

The complete data-automation system weighed 11.91 lb and contained 11,130 electronic components.

### **F. Testing**

The data-automation system interfaced 82 functions with the science subsystem and four other subsystems of the spacecraft. Correct operation of these functions was tested with a modified general-purpose digital computer operating through interface equipment. The computer observed the format data and the commands issued by the data-automation system with the expected events as described in its program. Any differences between the expected and observed events were indicated in the printer output.

Not only was a complete and documented test obtained, but it became possible to make "schmoo" plots of system performance. Figure 6 shows an actual plot of the operational space for the real-time data-automation system frame counter. The ordinate and abscissa were supply voltages while the contours shown corresponded to operating temperatures of 0, 25, and 55°C. These plots were made and maintained over the history of the equipment. The final plots were made a few days before launch and served as preflight acceptance criteria.



## XI. PLANETARY-SCAN SYSTEM

R. Y. Wong

Jet Propulsion Laboratory  
Pasadena, California

### A. System Objectives and Requirements

The planetary-scan system was designed and developed to support the planet-encounter requirements. Its function was to search for, acquire, and track the planet Mars so that television photographs of a portion of the planet surface could be obtained by correctly orienting the television sensor.

To develop a system capable of accomplishing these objectives, the major system requirements were established as design objectives:

1. System operating range was chosen to be 9000 to 70,000 km. Selection of this range was based on considerations of trajectory requirements. With the established aiming point of approximately 25,000 km from planet center and a 3 $\sigma$  rms target error of 15,000 km, the distance at encounter can be anywhere in range of 10,000 to 40,000 km. With an optical field of view of 50 deg, the detection and acquisition of the planet at 70,000 km provides the system 1/2 to 1 1/2 hr of planet tracking prior to the television picture sequence.

2. Planet searching and tracking speed was dependent on the magnitude of the relative motion of the spacecraft with respect to the planet during encounter period and the relative stability of the attitude-stabilized spacecraft with respect to its roll axis. It was anticipated that the spacecraft would be traveling at an approximate speed of 0.02 deg/sec with respect to the planet and that a spacecraft roll rate of not more than 0.03 deg/sec would be encountered. The searching and tracking speed of 0.5 deg/sec was selected to satisfy these requirements.

3. A planet-tracking accuracy of  $\pm 1$  deg was specified to meet the television mission requirements.

4. The system was required to have an operating temperature range of  $-40$  to  $+75^\circ\text{C}$ .

### B. Functions

A functional block diagram of the system is shown in Fig. 1. The system performs four major operations: planet searching, planet detection, planet tracking, and scan inhibit.

#### 1. Searching

When the system is energized, a signal from a one-shot multivibrator circuit presets all logic circuits and initiates the planet-searching mode. Searching is accomplished by placing a positive dc voltage at the output of the X-axis filter. This voltage, supplied by the searching driver, is phase-detected with a reference signal derived from the 400-cps motor-driving signal shifted 90 deg in phase. The phase-detected signal, 90 deg out of phase with the motor-driving signal, is amplified and used as the motor-drive signal. The system scans 180 deg in the process of searching for the planet. The scanning provides motion in one direction, while the moving spacecraft provides a motion in the other direction that is approximately perpendicular to the scanning plane. Upon completion of each 180-deg search, the following occurrences cause the motor drive to reverse:

1. The planet-searching logic is reset by a wave-shaped and noise-filtered signal initiated by limit-switch action.

2. A dc voltage of proper polarity is applied to the X-axis filter by the searching driver. A positive dc voltage is used for counterclockwise motor drive and a negative dc voltage is used for clockwise drive.

3. The dc voltage is converted to an ac signal, the phase of which is dependent upon the polarity of the dc voltage. A positive dc voltage is converted to an ac signal that is 90 deg out of phase with the reference signal and a negative dc voltage is converted to an ac signal that is 270 deg out of phase with the reference signal. The ac signal is then amplified and applied to the motor as the directional-drive signal.

#### 2. Planet Detection

A radiation detector is used to detect the presence and location of the planet. When the planet is in view of the detector, a pair of signals is generated to indicate the location of the planet and the amount of energy received. The X-axis output is used as the error signal for planet tracking while the Y-axis output determines the angular position of the planet with respect to the detector mount. Both signals are modulated by a pair of oscillator-driven

modulators prior to entering the preamplifier and amplifier. A pair of synchronous detectors is used to demodulate these signals before filtering. At the output of the preamplifier, the X-axis signal is sampled by the planet-in-view logic where noise-filtering and planet-signal identification are performed. A planet-in-view signal for the purpose of data-mode switching is delivered to the data-automation subsystem for processing, and, at the same time, the searching driver is inhibited, which changes the system from searching to tracking mode.

### 3. Planet Tracking

The X-axis output, after demodulation and filtering, is used as an error signal to track the planet. The motor driver and associated circuits, being commonly employed in both searching and tracking operations, perform the same functions while tracking.

The filtered Y-axis output signal is amplified and converted from a bipolar to a unipolar signal. This signal, together with the platform scan position output and other signals, are time multiplexed and analog-to-pulse-width converted before transmission to the data-automation system for processing.

### 4. Scan Inhibit

A scan-inhibit signal is initiated either internally or by ground command. The signal indicating that the planet is in the field of view of the television is used to stop the scanning and tracking motion prior to television picture-data recording. The scan trace across the planet after planet-tracking-motion inhibit is dependent upon the motion of the spacecraft relative to the planet.

## C. Components of the System

The system basically consists of three main types of equipment: (1) the radiation detector and optics, (2) the electronics, and (3) the motor assembly and its associated scan platform.

### 1. Radiation Detector and Optics

The presence and relative position of the planet is to be detected by a radiation detector. The detector senses radiation from the planet and transforms the radiant energy into an electrical signal indicating the planet position as well as the amount of radiation received. Three requirements are imposed on the detector for the system:

1. A definite spectral range of sensitivity corresponding to the assumed spectral radiance characteristics of the planet.

2. The achievement of a high radiant-to-electrical-energy conversion efficiency through the proper combination of characteristics of the optical system and detector.

3. A definite relationship between the detector electrical output and the magnitude and relative position of the radiation source.

To satisfy these requirements, a detector capable of operation with a minimum number of auxiliary components was needed, so a p-n junction silicon detector was selected. This detector, the output of which is self-generating, requires no bias supply. Without bias, the output is obtained with zero volt as reference, and predetection chopping of the incoming radiation signal is not needed. This compares to a biased detector which requires signal chopping to separate the signal from the bias voltage. It is known that the characteristics and performance of the junction detector are dependent on its construction, physical geometry, and electronic parameters. The detector's spectral response as well as radiation collection efficiency are determined by

$$\eta(\lambda) = [1 - \gamma(\lambda)] \{1 - \exp[-h(\lambda)d]\} \eta_c(\lambda) \quad (1)$$

where

$\eta(\lambda)$  = Radiation collection efficiency and relative spectral response of the detector

$\gamma(\lambda)$  = Relative reflectivity as a function of incident wavelength,  $\lambda$

$$\gamma(\lambda) = \frac{(n-1)^2 + \left[\frac{\lambda \cdot h(\lambda)}{4\pi}\right]^2}{(n+1)^2 + \left[\frac{\lambda \cdot h(\lambda)}{4\pi}\right]^2}$$

$n$  = Refractive index of the detector

$h(\lambda)$  = Absorption coefficient as a function of incident energy wavelength

$1 - \exp -h(\lambda)$  = Factor accounting for incomplete radiation absorption

$d$  = Thickness of the bulk material

$\eta_c(\lambda)$ , the carrier collection efficiency is the sum of the p-layer efficiency  $\eta_n(\lambda)$  and n-layer efficiency  $\eta_p(\lambda)$  or

$$\eta_c(\lambda) = \eta_n(\lambda) + \eta_p(\lambda)$$

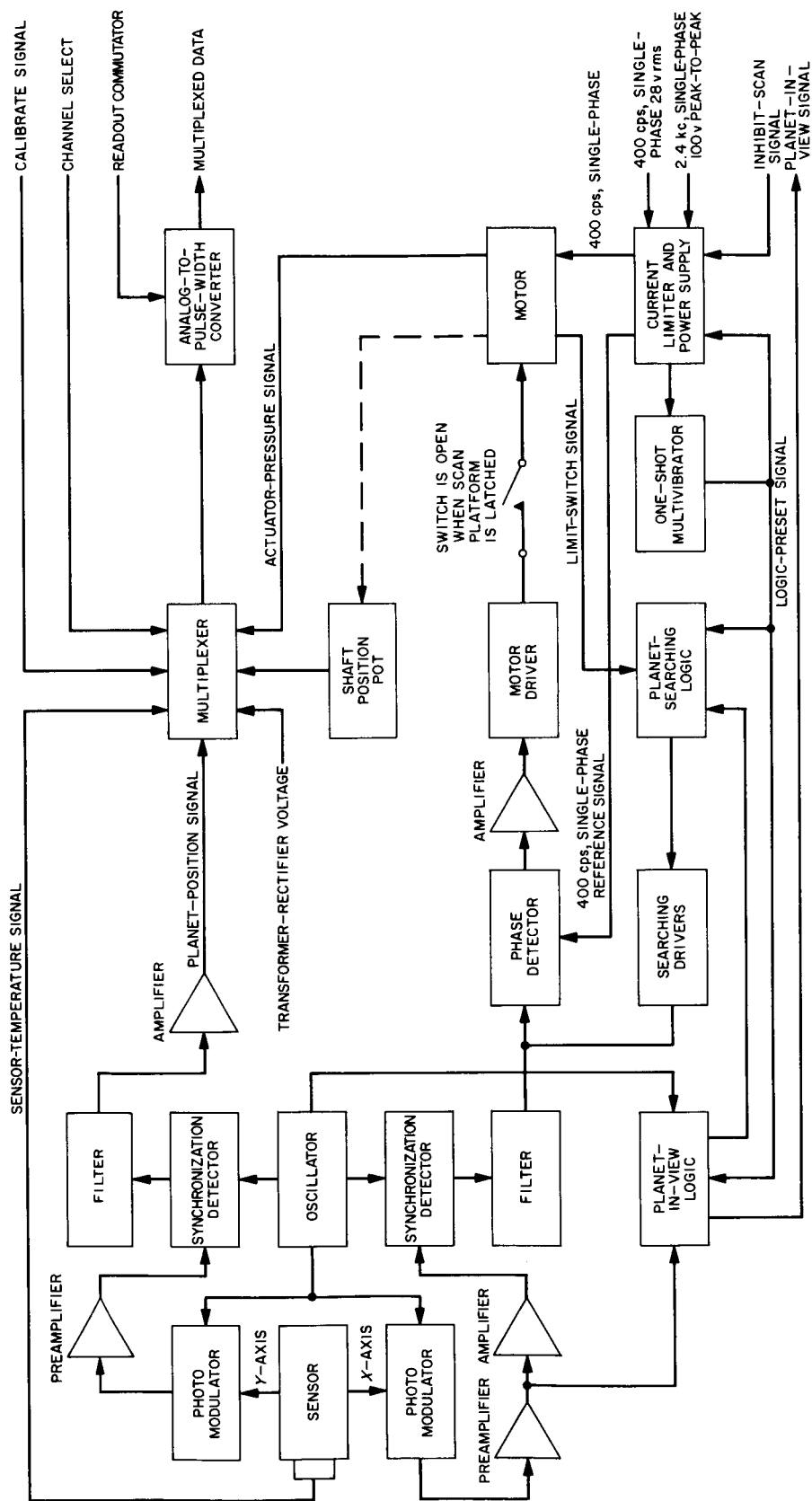


Fig. 1. Scan-function block diagram

where

$E_r$  = monochromatic energy flux at  $\lambda = 0.55\mu$  corresponding to visual albedos  $\alpha = 0$  deg,  $\Delta = 1$ ,  $\gamma = 1$

$E_r = 1.52 \times 10^{-11}$  watt  $\text{cm}^{-2} \mu^{-1}$   
phase angle (Sun-planet-subsystem angle)

$\phi(\alpha)$  = phase function

$\phi(\alpha) = 0.406$  when  $\alpha = 60$  deg

$S$  = aperture area of the optics

$$S = \frac{\pi d^2}{4}$$

$S = 1.32 \text{ cm}^2$  for  $d = 1.3 \text{ cm}$

$\tau$  = transmission efficiency of the optics

$\tau = 0.80$

$K(\alpha)$  = Illuminated fraction of the planet at phase angle of  $\alpha$

$$K(\alpha) = \frac{1}{2} (1 + \cos \alpha)$$

$\gamma$  = distance from planet to the subsystem in astronomical units

$\Delta$  = mean distance from planet to Sun in astronomical units

$\Delta = 1.524 \text{ A. U.}$

$p(\lambda)$  = assumed planet spectral reflectivity

$f(\lambda)$  = spectral energy function of solar energy

$\lambda_1, \lambda_2$  = cutoff wavelengths of the subsystem

$\eta(\lambda)$  = spectral response of the radiation detector as calculated by Eq. (1)

Then  $e_x, e_y$  as a function of the planet position  $\theta$  with the planet angular semi-diameter as the parameter was calculated and plotted on Fig. 4. It is seen that the magnitude and polarity of  $e_x, e_y$  can be used to determine the position of the planet image with respect to the detector axis and magnitude of  $e_x$  and  $e_y$  can be used to determine the amount of energy received at a distance at which the planet is considered to have an apparent semidiameter of  $\beta$ . Subsequently,  $e_y$  was used to indicate the planet position and, while  $e_x$  was used as error signal, for planet tracking.

The planet angular diameter, when viewed at the closest operating range of 9,000 km, is approximately 40 deg. To accommodate a full field of view of the planet, the optical system must have an optical view of greater than 40 deg. An  $f/2.3$  optical system with a focal length of

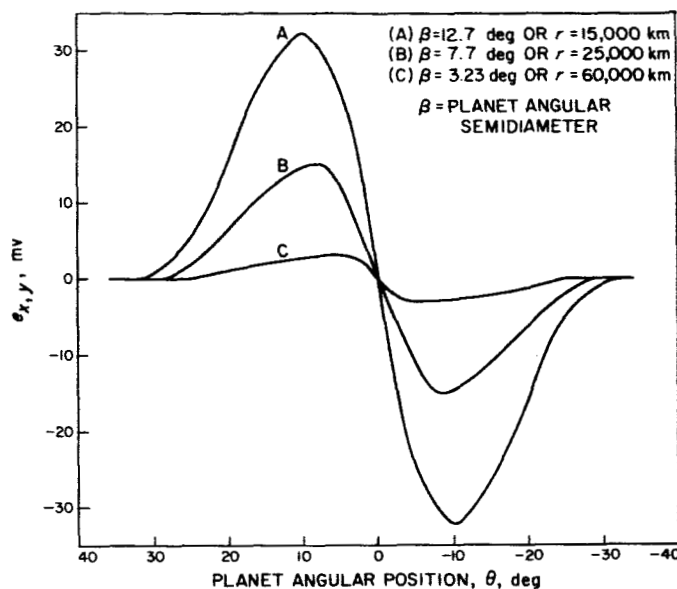


Fig. 4. Detector output as a function of planet position

30 mm and a circular field of view of 50 deg was chosen. This optical system, when operating at a distance of 9,000 km, formed a planet image of 0.89 in. in diameter. Therefore, the detector, having a sensitive area of 1.000 in. and an overall diameter of 1.125 in. was chosen to accommodate the full field of view of the planet over the entire operating range.

## 2. Electronics

**a. Signal Modulation.** To simplify the design of the electronic amplification circuits, the dc outputs of the detector are converted to an ac signal by a pair of photo-modulators, each consisting of a pair of small neon lamps and a matched pair of cadmium selenide photocells. Amplification of the resultant signal produces a low-noise ac output. This method of modulation was chosen not only for its simplicity but for its reliable operation. It also produces extremely low offset voltages over the required temperature range. Each pair of lamps is connected in parallel for redundancy and an oscillator is used to drive the lamp. Selection of the oscillator frequency of 24 Hz was based on two limitations: (1) the low-frequency limit set by design simplicity and (2) the high-frequency limit imposed by photocell time constants.

It is well known that higher-than-nominal breakdown voltage is required to fire the neon lamp in darkness or after long duration in the non-conducting state in darkness because of the time required for the gas ionization

From Eq. (1) it is possible to choose the various detector parameters to match its spectral response to that of radiation source.

The detector having a calculated spectral response,  $\eta(\lambda)$ , curve 2 of Fig. 2, was fabricated with a useful area of 1.00 in. in diameter. Two straight lines at right angles to each other are chemically etched on the surface of the detector to form four electrically isolated equal-area quadrants. The depth of the etches is such that the top layer, including the junction, is physically separated from the bottom layer. Two output-differential voltage pairs, each formed by taking the outputs of the adjacent quadrants through a resistor matrix are shown as  $e_x$  and  $e_y$  in Fig. 3. The operational concept of the detector is that the planet image is bisected by the adjacent quadrants and a null point is indicated when each quadrant receives equal energy and the detector outputs are nulled to zero volt. Since the signal of the adjacent pairs is balanced out, the differential signal indicates the angular deviation of the planet position from the null axis.

The detector output voltages  $e_x$  and  $e_y$  are related to the various parameters as follows:

$$e_x e_y = [1 - R(\theta)] [\Delta A(\theta, \beta, \phi)] \cdot \delta(\theta) \cdot E(\gamma, \alpha, \lambda) K \tag{2}$$

where

$$R(\theta) = \frac{1}{2} \left\{ \left[ \frac{n^2 \cos \theta - (n^2 - \sin^2 \theta)^{1/2}}{n^2 \cos \theta + (n^2 - \sin^2 \theta)^{1/2}} \right]^2 + \left[ \frac{\cos \theta - (n^2 - \sin^2 \theta)^{1/2}}{\cos \theta + (n^2 - \sin^2 \theta)^{1/2}} \right] \right\}$$

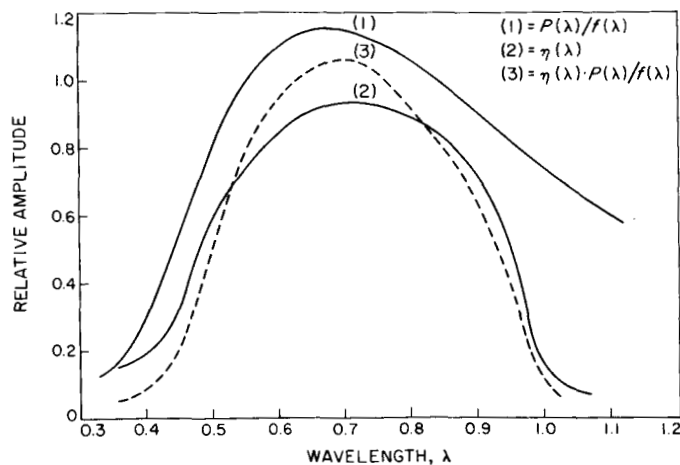


Fig. 2. Detector spectral response

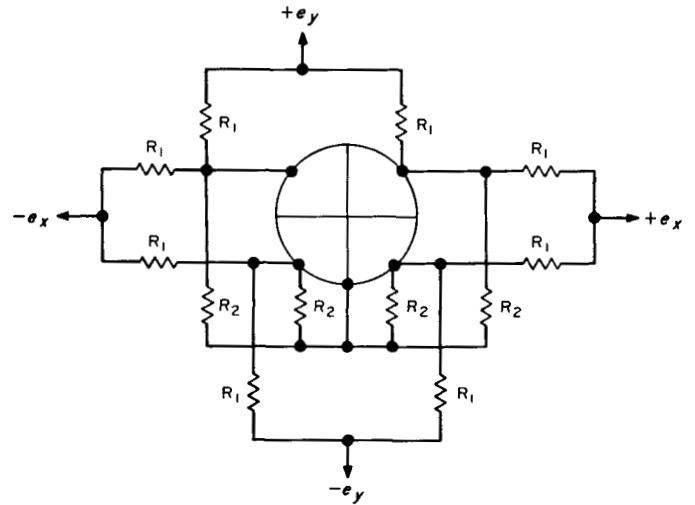


Fig. 3. Detector outputs

$R(\theta)$  = Fresnel coefficient of reflection for unpolarized incident energy as a function of incident angle  $\theta$

$$\Delta A(\theta, \beta, \phi) = \frac{1}{\pi} \left[ k_1^2 \cos^{-1} \frac{y}{\beta_1} + \cos^{-1}(k, -y) - 2 \cos^{-1} k_2 \right] - \frac{1}{\pi} \left[ y(k_1^1 - y^2)^{1/2} + (k_2 - y) [1 - (k_2 - y)^2]^{1/2} - 2k_2 (1 - k^2)^{1/2} \right]$$

= factor relating planet angular semi-diameter  $\beta$ , optical angular half field of view  $\phi$  and planet position angle  $\theta$

$$y = \frac{k_1^2 + k_2^2 - 1}{2k_2}; k_1 = \frac{\tan \theta}{\tan \beta}; k_2 = \frac{\tan \theta}{\tan \beta}$$

$$\delta(\theta) = [1 - \sin 2\theta]$$

$\delta(\theta)$  = Factor due the vignetting effect of the optics

$k$  = Detector responsivity

$E(\gamma, \alpha, \lambda)$ , the input energy from the planet, can be calculated by assuming the planet has the spectral radiance, property of  $p(\lambda)/f(\lambda)$  as shown on curve 1 of Fig. 2.

$$E(\gamma, \alpha, \lambda) = \frac{E_p \cdot \phi(\alpha) \cdot A \tau K \alpha}{\Delta^2 \gamma^2} \int_{\lambda_1}^{\lambda_2} \frac{P(\lambda)}{f(\lambda)} \eta(\lambda) d\lambda \tag{3}$$

to increase when the lamps are operating in the dark. The ionization time can be reduced, however, through the use of radioactive additive. To further insure proper operation, an applied voltage in excess of the static breakdown voltage was used to fire the lamps.

**b. X- and Y-Axis Signals.** The modulated X- and Y-axis outputs were amplified by a pair of four-stage ac preamplifiers of identical design. The preamplifier, having an impedance of  $3\text{ M}\Omega$  with the use of a field-effect transistor at input stage, has a closed-loop gain of 8,000. Sufficient feedback was incorporated in the design so that the gain of 8,000 was constant within 3% when operating in the required operating-temperature range.

The X-axis output was further amplified by a three-stage Zener-coupled ac amplifier having a gain of 1,000 and an output impedance of  $300\ \Omega$ . Use of Zener diodes as the ac interstage coupling elements minimizes the loss of gain, eliminates the need for large coupling or bypass capacitors, and provides stable operation over a wide temperature range because of the temperature-compensation effects of the diodes. The gain stability of the amplifier when operating over the required temperature range is within 5%.

The X- and Y-axis signals were then separately demodulated and filtered by synchronous detectors and three-stage RC filter networks. A field-effect transistor is used in each of the detectors to minimize the offset voltage. The ac-to-dc conversion gain of these stages was determined to be  $0.48\text{ v dc/v rms}$ .

The bipolar X-axis dc signal from the filter network was phase-detected using the 400-cps motor-driving signal shifted 90 deg in phase as a reference. A double-emitter transistor (integrated chopper transistor) is used in the phase detection to take advantage of its extremely low offset voltage. The conversion gain of this stage, including attenuation in the compensation networks, is  $0.150\text{ v p-p/v dc}$ . A four-stage amplifier with a pair of transistors in a complementary push-pull configuration at its output was designed for further signal amplification with a gain of 280.

The output of this amplifier is then transformer-coupled to the motor-driver circuit consisting of a pair of power transistors in a push-pull configuration with a gain of 10. This signal is then applied to the control winding of the motor to provide directional drive control.

The demodulated Y-axis output is amplified by a dc-coupled difference amplifier with a gain of 30. An adjustable negative dc feedback from the amplifier output to the detector Y-axis output was employed to accommodate the wide range of energy input.

To provide design data, the amount of solar energy reflected from the planet and incident at the detector was calculated by Eq. (3). To verify the validity of the calculated values, experiments were performed using the encounter data to determine the magnitude of the integrated energy in the spectral range of 0.5 to  $1.1\mu$ . With the output of the detector as a function of planet position as shown in Fig. 4, the Y-axis output can be used to determine both the angular position of the planet with respect to the detector mount and the amount of radiation energy received. Fig. 5 shows the Y-axis output as a function of the variables. These curves were generated by multiplying the Y-axis detector output  $e_y$ , in Eq. (2) by the loop-amplification factor of the Y-axis circuits. It should be noted that this signal has been converted from a bipolar signal to a unipolar signal by the dc-coupled difference amplifier.

Additional information can also be obtained from the Y-axis output curves. The slope of these curves at  $\theta = 0$  is a function of the planet angular diameter. Since the detector-to-planet distance is related to the angular diameter by the known optical geometry, the approxi-

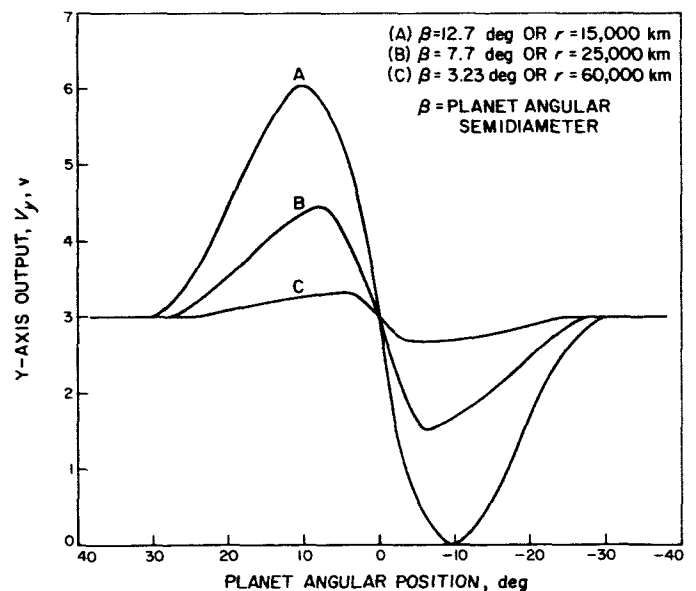


Fig. 5. X-axis output as a function of planet position

mate flyby distance can be calculated from the value of the slope at  $\theta = 0$  or  $dv/d\theta|_{\theta=0}$ .

*c. Logic and Control Circuits.* The logic and control circuits are as shown in Fig. 6. Searching and acquisition modes of operation are controlled by flip-flop C (F/F C).

When the power to the subsystem is applied, a signal from the one-shot circuit presents all the F/F's and the system is in the planet-searching mode. The clockwise and counterclockwise motor-drive signals are controlled by F/F S, which in turn, is being set and reset by the wave-shaped and noise-filtered signal initiated by limit-switch action.

The planet-in-view logic consists of the signal threshold and noise-discrimination logic circuits. The planet signal is bandwidth-limited by a filter having a bandwidth of 120 Hz. The signal is then level-detected by a Schmitt trigger with an adjusting dc biasing level. The proper threshold level is adjusted so that the dc biasing level plus noise is less than the Schmitt trigger level, a condition at which the noise alone evokes no response from the circuit. The dc biasing level can be determined by

$$E_{dc} = V_{in} - \gamma(Vn) \quad (4)$$

where  $E_{dc}$  is the biasing level,  $\gamma$  is the normal threshold level as a function of the planet detection probability,  $V_{in}$  is the Schmitt trigger level and  $Vn$  is the noise level at the filter input.

The noise-discrimination logic consists of a number of flip-flops and gates. A signal from the oscillator having the same frequency as the modulated signal—and either in phase with it or 180 deg out of phase with it—is frequency-divided by 8 through the use of F/F's L, M, and N. This signal is used to control the planet-signal sampling period. F/F's X and W are used to count the number of pulses passing through the Schmitt trigger during each sampling period. If four or more consecutive pulses are gated per period, F/F C changes its state to indicate a planet acquisition. If less than four pulses are gated, F/F's X and W are reset by a pulse from gate 4 at the end of each period, and the gating resumes in the next period.

### 3. Motor Assembly

The scan-system optics and detector assembly as well as the television camera head are mounted on a scan-platform suspended at the bottom of the spacecraft. A motor assembly having a torque load of 20 in.-lb is used

to drive the platform. This motor assembly consists of a size 8, 8000-rpm, 400-Hertz synchronous motor, reduction gearing, a shaft-position potentiometer, and scan-limit switches. Further reduction gearing is used to reduce the motor output speed to 0.5 deg/sec. A clutch assembly is provided so that driving slippage occurs when a torque load equal to or greater than 40 in.-lb is encountered. A potentiometer geared to the motor output shaft indicates the angular position of the platform. Limit switches are provided to limit the searching cycle to 180 deg. This entire assembly is housed in a sealed container and pressurized at 15 psig.

### D. Physical Characteristics

A total of 501 components were required in the fabrication of each system. Wherever possible, components having a high reliability history were chosen, tested, and screened to the existing JPL specifications. Components designed and constructed for performing special tasks were also tested and screened to specifications written for that purpose. Inasmuch as the system requires various techniques for development and fabrication (i.e., detector and optical fabrications, module and electronic packaging, mechanical, etc.), components and units were fabricated by manufacturers who specialized in these fields. The system was fabricated and packaged in the four subassemblies as shown on Fig. 7.

To conserve weight, volume, and power consumption without sacrificing reliability, thin-film microcircuit networks manufactured by Texas Instruments, Inc., were used in the searching, tracking, and planet-in-view logic circuits. These semiconductor networks, along with the other electronic logic components, were packaged in welded modules to take advantage of their physical configuration and small dimensions.

The fabricated system weighed 6.8 lb and required 2.8 w of 2.4 kHz, 50 v rms, single-phase, square-wave power and 4.5 w of 400 Hz, 28 v rms, single-phase, square-wave power for its operation.

### E. System Performance

#### 1. Planet-Acquisition Range and Acquisition Probability

A criterion for the effectiveness with which the system accomplishes its mission is the range at which the system has a high probability of detecting the planet. The maximum range at which the planet can be detected and acquired primarily depends upon whether the planet can be distinguished from the "noise" appearing with the

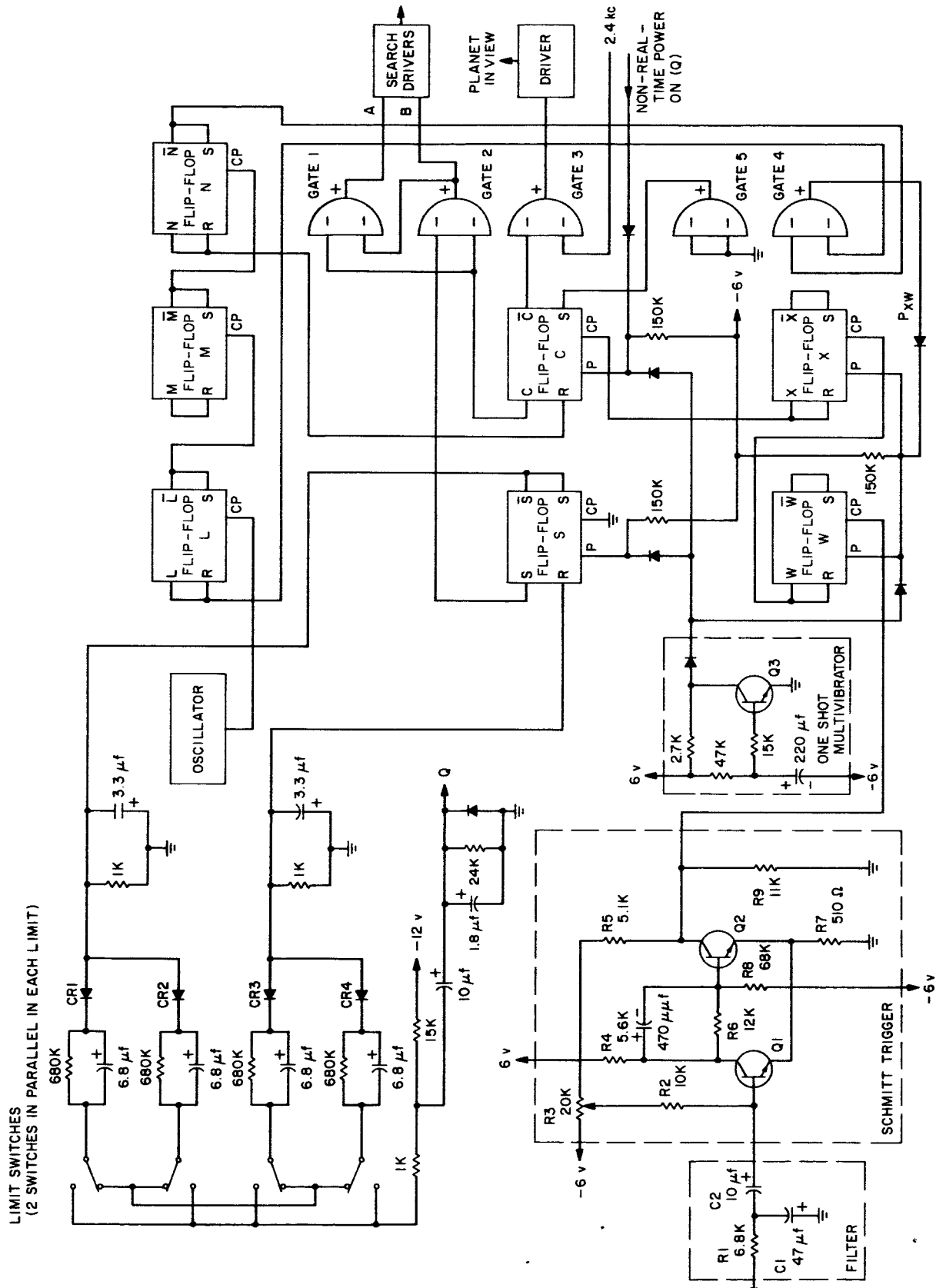


Fig. 6. Logic and control circuits



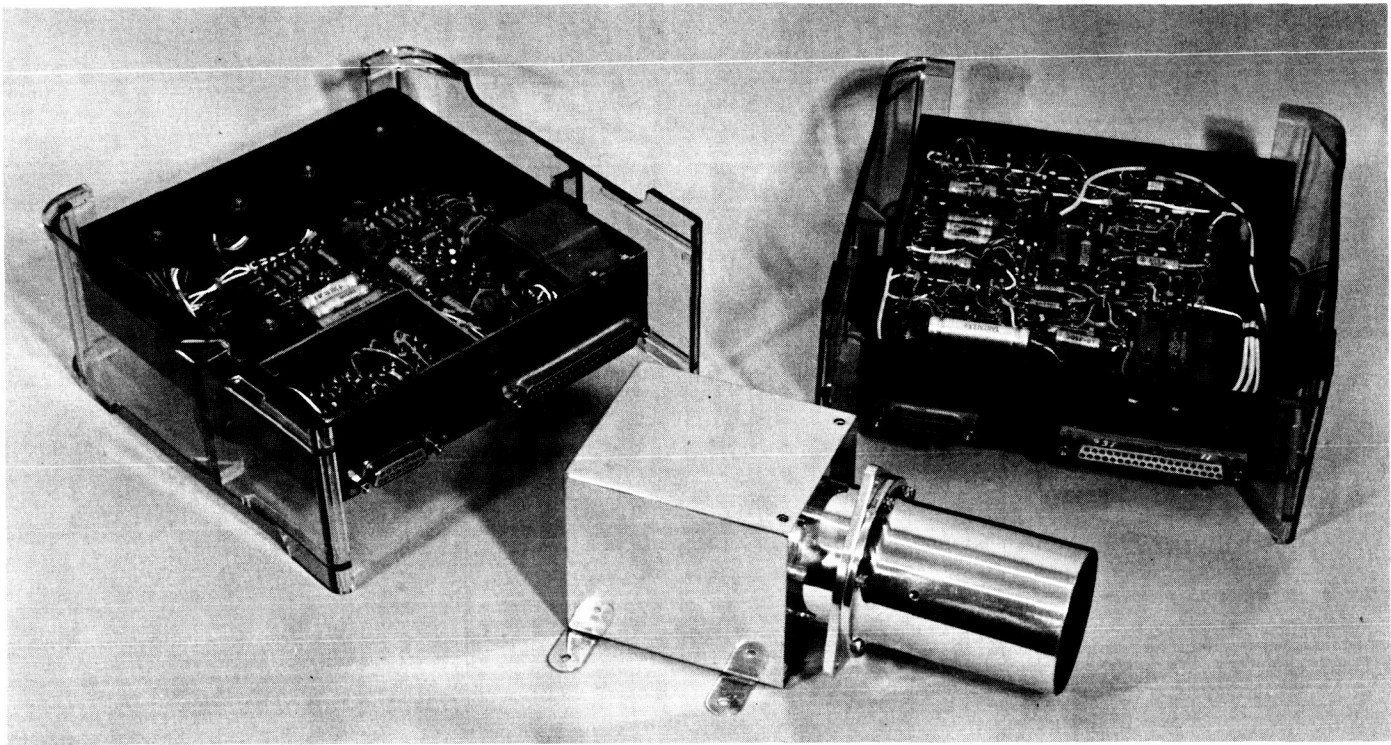


Fig. 7. Scan system subassemblies

planet signal. If the noise amplitudes are high, the chance of mistaking a noise pulse for a signal in the absence of the planet is appreciable.

An analysis employing statistical methods was used to relate planet distance to the acquisition probability with the design parameters of the planet-in-view circuits taken into consideration. The planet is considered to be detected when the signal-plus-noise voltage is higher than Schmitt triggering level.

Planet acquisition is said to have occurred when an acquisition signal was indicated by a change of logic state in the planet-in-view logics. The probability ( $P_o$ ) that the threshold of the Schmitt trigger is not exceeded in a time  $T_f$  can be determined by

$$P_o = (1 - P_n)^n \quad (5)$$

where

$$P_n = \int_{\gamma}^{\infty} x \exp\left(\frac{-x^2}{2}\right) \exp(-z) I_0 \left[ (2z)^{\frac{1}{2}} \cdot x \, dx \right]$$

$$P_n \approx (2\pi)^{-1/2} \int_{\gamma}^{\infty} \exp\left(\frac{-x^2}{2}\right) dx$$

$P_n$  = the probability that a noise pulse exceeds the threshold.

$\infty$  = normalized threshold

$$\gamma = \frac{\text{peak threshold voltage}}{\text{rms noise voltage}}$$

$n$  = number of noise pulses per false alarm time  $T_f$

The probability ( $P$ ) that at least one signal pulse exceeds the threshold:

$$P = 1 - (1 - P_s)^m \quad (6)$$

where

$$P_s = (2\pi)^{-1/2} \int_{\gamma-\beta}^{\infty} \exp\left(\frac{-x^2}{2}\right) dx$$

$\beta$  = normalized signal level

$$\beta = \frac{\text{peak signal voltage}}{\text{rms noise voltage}}$$

$m$  = number of signal pulses per detection time  $T_d$

It is seen from the operation of the planet-in-view logic that the detection time  $T_d$  and false alarm time  $T_f$  are equal to the sampling period,  $T_d = T_f = 1/f = 0.333$  sec,

and the detector must receive incident energy throughout a complete sampling period to obtain an acquisition signal. Therefore, the number of signal pulses per  $T_d$  is one ( $m = 1$ ). Because of the filtering action prior to threshold discrimination, the noise bandwidth is reduced to 120 Hz, and the number of noise pulses per  $T_f$  is therefore equal to 40,  $n = \Delta f \cdot T_f = 40$ . Figure 8 shows the probability of acquiring the planet as a function of the acquisition range with  $m = 1$  and  $n = 40$ .  $P_o$  is assumed to be 0.8 prior to noise discrimination, and its value increases to near unity through the use of the noise-discrimination logic circuits. Since the responsivity of the detector and the system circuit noise are functions of the operating temperature, the acquisition-distance curves at various operating temperatures are also shown in Fig. 8.

**2. Compliance of Design Requirements**

Analysis and testing of the system indicated that all major criteria required for a stable system have been

met. The performance under various operating and environmental conditions was evaluated by means of system testing. The system was found to be stable and operated satisfactorily under these conditions.

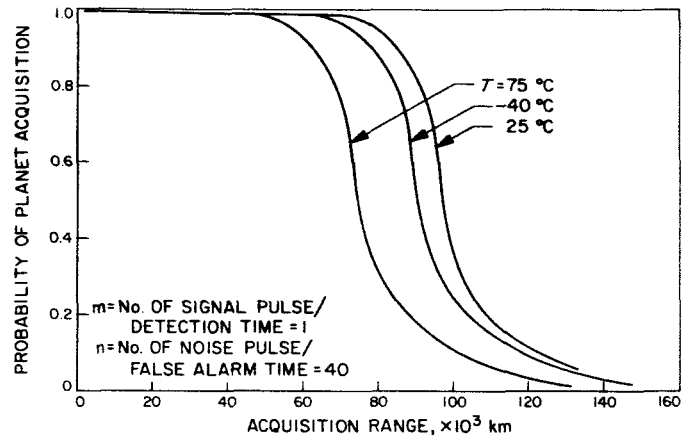


**Fig. 8. Planetary acquisition as a function of operating range**

## XII. SCIENCE DATA PROCESSING

Stephen Z. Gunter and Michael J. Sander

Jet Propulsion Laboratory  
Pasadena, California

### A. Introduction

*Mariner IV* marks a significant increase in the application of digital-computer processing to spacecraft system test and flight telemetry data. The keynote of a successful data-processing system is to provide the desired processed results within a time responsive to the user's needs. From this guiding principle the *Mariner* ground data-handling systems were evolved.

The salient features of the on-board data flow are shown in Fig. 1. Data from each instrument or ancillary were collected by the DAS and put into the required format for transmission to the data encoder. The data encoder transferred the data serially to the radio subsystem for transmission to Earth.

The data format, Data Mode 2, contained 420 bits, 140 of which contained engineering information and the remaining 280 of which contained the science data. The 140 bits assigned to engineering telemetry were divided into twenty 7-bit words. Using a hierarchy of commutation, 100 data measurements or synchronizing words were telemetered. On the other hand, since the basic science word was 10 bits and because of the varied nature of the science information, some words were combined to make a science measurement, others contained

status information, and still others were commutated by the science instrument according to the intensity of the measurement. Therefore, there was no simple scheme to process and display the science information as there was for the engineering telemetry.

The three segments of science data processing discussed include test data, flight operations support, and the master data library.

### B. Test-Data Processing

The basic test-data processing concept was to have each spacecraft subsystem acquire its particular data from the telemetry stream, and process and display the data according to individual needs. For science, this processing and display took the form of a page printing of the raw data converted to octal and grouped into four character words representing 10 bits. In place of the 15-bit PN code accompanying each frame, a high-order truncated time word derived from the ground test complex clock was inserted. At the high spacecraft bit rate of  $33\frac{1}{2}$  bits/sec, the time identification was not unique. In fact, unique identification depended on the combination of frame count and the value of the cosmic-dust detector/hit-accumulative counter. This problem of accurate and reliable time identification from ground time

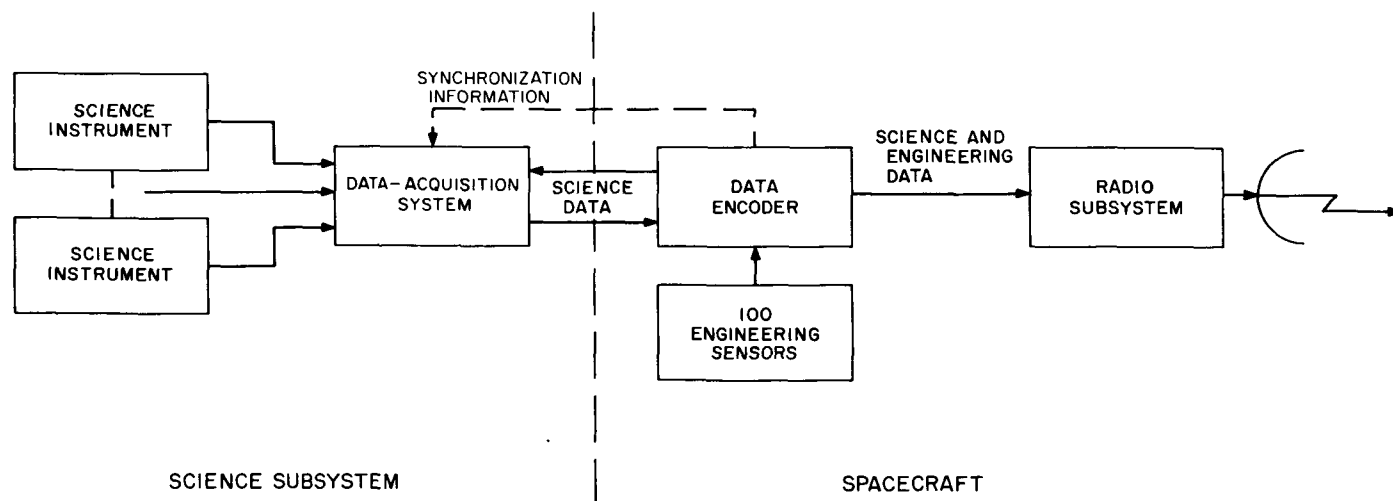


Fig. 1. Spacecraft telemetry system

sources asserted itself throughout all phases of processing without ever being completely solved. Sample 1 shows the format used for the display.

During prelaunch test operations, a data monitor reviewed each data frame primarily to note changes in the status bits or gross changes in the data. Detailed data analysis required for verification of the science subsystem status required manual processing of the data subsequent to the tests. The statistical nature of the radiation instruments' data, for example, did not lend itself to real-time instrument performance verification. Redundant to the page display was a paper-tape punch and a strip-paper printer. The punched paper tape contained the raw-data stream and later became the central source of data for machine processing.

The environmental test of the proof-test model spacecraft held in January 1964 showed that the raw-data page display was inadequate for analysis of instrument performance. The clerical manpower needed to retrieve the data and perform the necessary computations, such as count-rate determinations for the radiation instruments was unavailable. Therefore, a computer program was written that accepted the punched paper tape and prepared a science-summary listing in a format directly

adaptable to analysis. The count-rate determinations and similar processing were still done manually. However, the format simplified this task. Samples 2 and 3 show this display which was carried throughout test, flight operation, and master-data library processing. While somewhat arbitrary in design, it became the standard summary display for all science data for *Mariner IV*.

For system testing, the page display of octal data, when monitored by a trained and constantly alert data monitor, was sufficient to support the system test complex needs. The science-summary listing and accompanying detailed log of spacecraft and test-complex events and explanation of data gaps caused by processing difficulties within 12 hr of a system test's completion permitted timely analysis of instrument performance. Figure 2 is a block diagram of the processing used.

The method of data acquisition and processing so far described has been confined to supporting the cruise instrument or non-TV portion of the science subsystem. Figure 3 describes the system used for the TV data.

The TV data was recorded in a computer-compatible format on magnetic tape. Computer processing provided a tab listing of all TV elements and image data that was

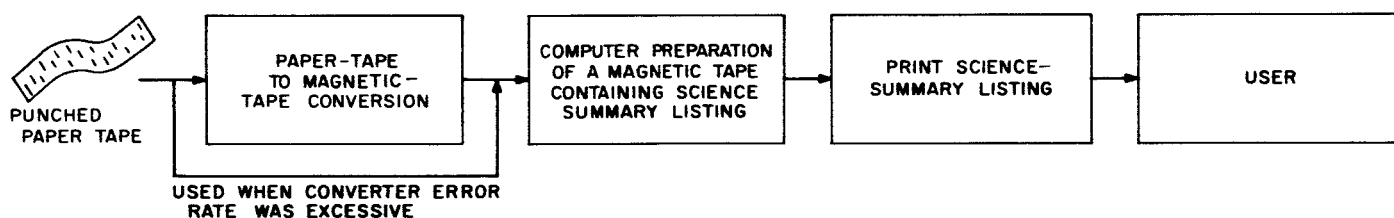


Fig. 2. Cruise data processing

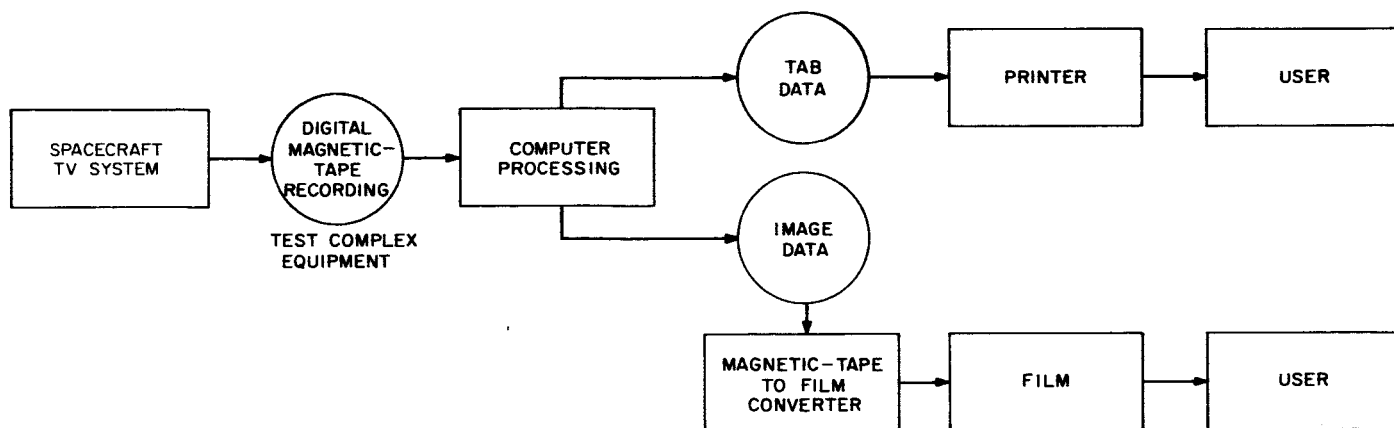


Fig. 3. TV data

converted to film. The test schedule required that the TV data be processed and distributed within 24 hr of a test's completion.

Meanwhile, a real-time computer processing and display was integrated into test operations. This system primarily displayed changes beyond a tolerance in a given data value and provided alarm monitoring when either engineering or science data exceeded predefined limits. This capability greatly enhanced real-time test monitoring and test operations, but was inadequate for science-instrument performance analysis because only gross changes in data were displayed. Correlations between performance of several instruments and long-term analysis depended on the post-test science-summary listings of all data. The real-time computer, by logging both science cruise and TV data on magnetic tape, supplanted both the punched paper-tape recording of cruise data and separate magnetic-tape recording of TV data.

When the first *Mariner* flight spacecraft left for Cape Kennedy in August 1964, the test-data processing system and procedures had reached the point of full dependence on computer-processed output for data reduction. For these operations the science-summary listing program was expanded to include averaging of data, count rate and flux determinations, and display of anomalous data, such as nonsequential frame counts. Figure 4 shows the block diagrams of the final configuration used to process this data. Table 1 lists the primary problems experienced and the solutions that were derived in test data processing.

**Table 1. Primary test-data-processing problems**

Problem	Solution
1. Unreliable techniques of data recording in a computer compatible format, i.e., punched paper tape.	1. Real-time logging of raw data on magnetic tape in a computer-compatible format.
2. Unreliable and non-unique time annotation of data	2. Reliance on frame count.
3. Varied types of computers required for processing and data sources to support constantly increasing processing requirements	3. Standardizing the science-summary data-listing format as the basic display for analysis; a succession of programs designed for the same task; and a basic TV data-processing program with a variety of input packages.
4. Multiple interfaces and insufficient recognition of the complexity of the task	4. Hard work!

Despite these difficulties, an impressive list of benefits was derived:

1. More complete and detailed user analysis of spacecraft functions on a more timely basis than had been previously possible
2. More complete recording of spacecraft functions for analysis and comparison
3. Stricter definition of spacecraft anomalies and spacecraft conditions because of the availability of more definitive and usable data
4. Training and experience in the use of processed results that were applicable to interpretation of flight data
5. Acceptance by instrument engineers of the benefits and reliability of systems test-data processing that fosters better understanding and definition of processing requirements and use of computer processing at the subsystem level of testing
6. A complete library of test data in an easily accessible form to support analysis of instrument performance throughout the test phase and during flight if anomalous behavior was experienced.

The experience gained has suggested a number of recommendations for future spacecraft projects:

1. Test data should be recorded in a reliable manner in a computer-acceptable format, magnetic-tape recording in IBM-compatible format preferred.
2. Data should be displayed in real-time with sufficient pre-processing to indicate significant aspects, such as listing and plotting of data after decommutation.
3. Since spacecraft test-data reduction requires data-reduction and analysis-computer programs as sophisticated as the flight program, more emphasis should be placed on the planning and implementation of the test-data processing system to minimize redundant efforts.
4. Unique and reliable spacecraft-generated time should accompany each frame of data.
5. A well-indexed and accessible library of data should be kept as an invaluable tool in understanding the spacecraft performance during testing.

**C. Flight-Operations Support Processing**

Monitoring and analysis of flight performance has been keyed primarily to computer processing:

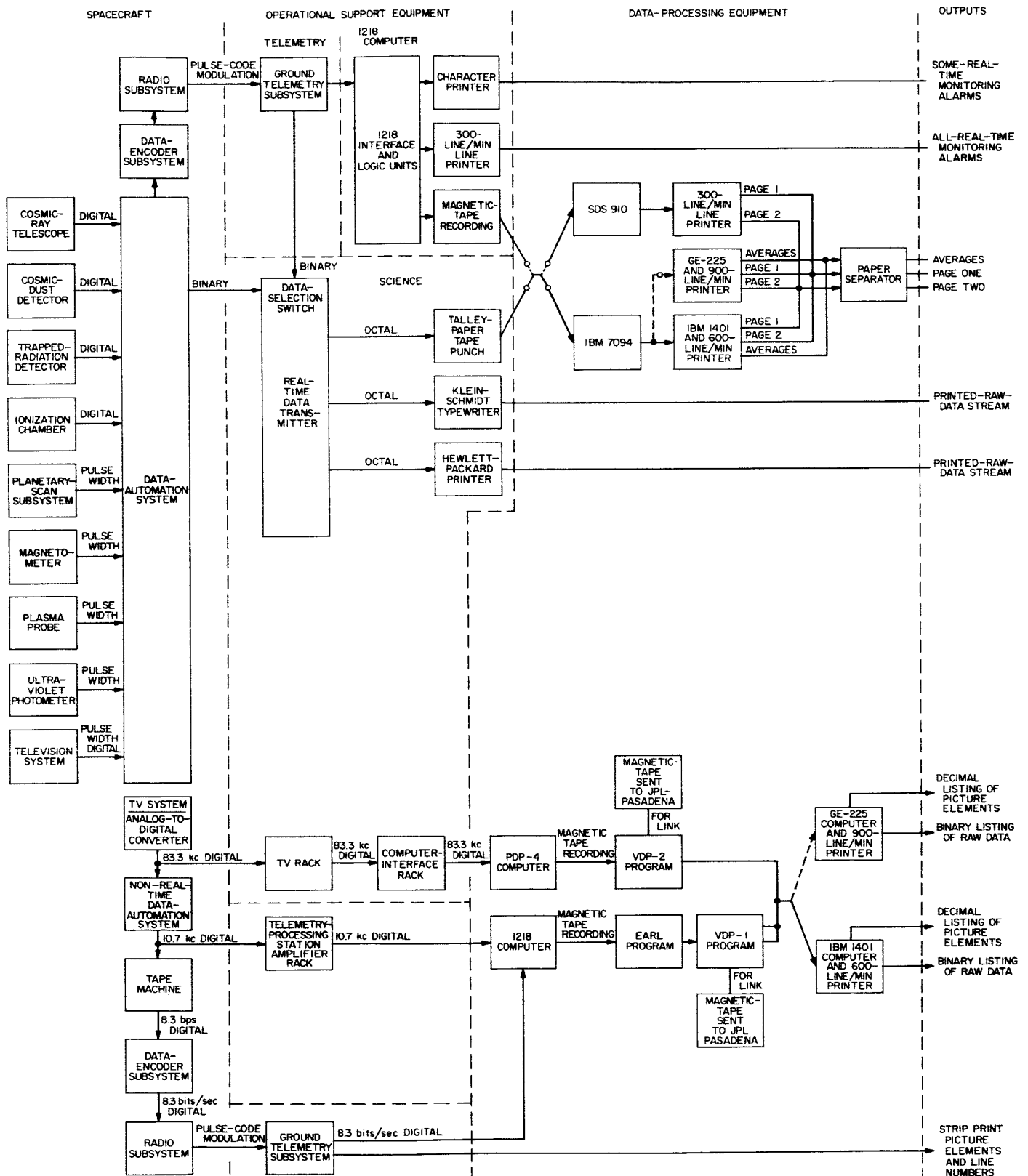


Fig. 4. Science-subsystem test-data processing

1. Real-time processing—current within 5 min of receipt from the spacecraft, the telemetry data was reduced and displayed in a manner sufficient for evaluation of the engineering performance of the spacecraft sub-systems.

2. Near-real-time processing—within 24 hr of receipt from the spacecraft, the telemetry was reduced and displayed in a manner sufficient for preliminary analysis of the scientific information.

In support of critical flight operations, however, as a redundant effort, raw data and test-complex-type raw-data displays were included. The flight data-processing system is described in Fig. 5.

Data telemetered from the spacecraft were received and recorded at the DSIF stations and simultaneously transmitted via teletype to the Space Flight Operations Facility (SFOF) at JPL. In the SFOF the received data

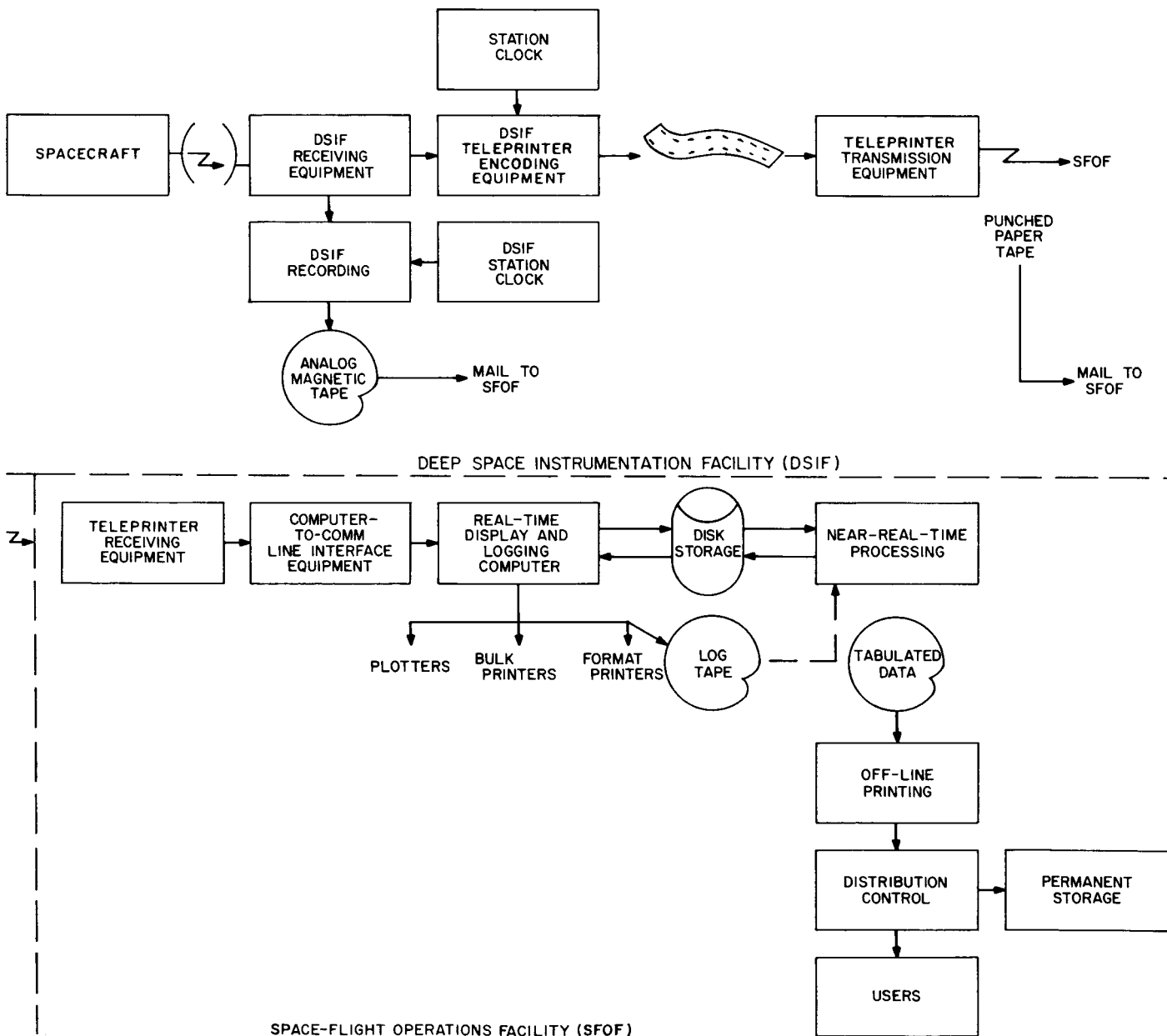


Fig. 5. Flight data processing

was processed by an on-line computer system performing two main functions: real-time display of the data and logging of the data for non-real-time processing and analysis. During normal cruise operations, the more detailed processing was accomplished off-line and distributed within 24 hr. The real-time processing and display consisted of decommutating the data; putting the data into binary, octal, or decimal format, whichever was desired; using up to a fifth-order polynomial to convert the raw data to more meaningful units; assigning time to each frame by prorating from the time words inserted in the data stream every five minutes; and logging the raw-data stream on magnetic tape.

The primary displays for science data were a 30- × 30-in. plotter divided into 12 subfields permitting representative data from each instrument to be plotted against time, and a tabular listing of all data in format for quick identification. Samples 4 and 5 represent the plotted and listed data, respectively. Engineering data was similarly displayed, with the addition of selected format printers which permit each engineering subsystem to have its data listed and isolated from the rest. Real-time data can be displayed within 3 min of receipt by the DSIF station at the 8½ bits/sec spacecraft transmission rate. Normally, the stations batch-transmit the data to take advantage of the full capability of the TTY lines, i.e., data was transmitted beginning on the hour until the backlog was depleted, requiring about 27 min.

During critical periods, the analysis processing can be accomplished on a time-sharing basis by connection to the real-time computer using a disk file as the interface. The time-sharing is illustrated in Fig. 6.

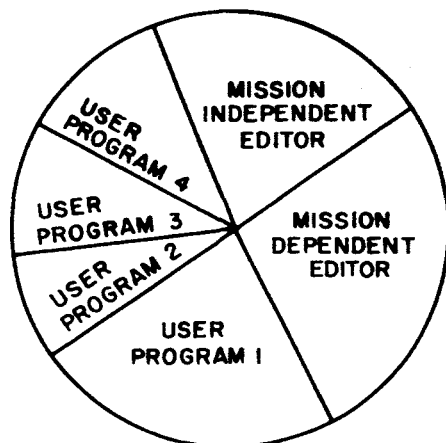


Fig. 6. Program time sharing

For every computing period, 15 to 20 min, all the programs that were enabled share the cycle and process the available data during the assigned interval. Processed data may be displayed on the real-time devices by interrupting the real-time displays, or they may be printed on plotted off-line. A massive executive program controlled the time-sharing system to assure proper interruptions and maintenance of the interrupted program in a state from which it can resume during the following cycle.

The flight-support data processing was intended to monitor the spacecraft performance in real-time and to permit preliminary analysis of the scientific information. To accomplish this, the analysis programs process the previous 24 hr of data to perform such tasks as

1. Determining counting rates for the radiation instruments.
2. Transforming the component vectors of the magnetic data to the total magnetic vector in a convenient coordinate system.
3. Providing the science-summary data listing.

Item 3 was recorded on magnetic tape and each week a data package was mailed to the *Mariner IV* experimenters. A typical data package contained

1. Plots of temperature vs time from launch for each instrument.
2. Plots of trajectory parameters vs time for the preceding week.
3. The science-summary data listing for the previous week.
4. Item 3 on magnetic tape.
5. A log of spacecraft and ground processing associated events.

The predominant science analysis so far accomplished and results released by the experimenters have been derived from the user program results and the weekly data packages.

#### D. Master Data Library

The most auspicious task undertaken by *Mariner* ground data handling was the formation of a master data library of all flight data. The objective was to retrieve from the station recorded magnetic or punched paper tapes a complete and accurate stream of spacecraft telemetry and tracking data adequately and reliably



time-annotated. This processing provided the "best record of spacecraft-transmitted data in a format for more analytical digital computer processing by the experimenters.

Figure 7 describes the master data library processing system for the spacecraft telemetry.

Briefly, after conversion to a computer-compatible format, the composite data stream consisting of spacecraft telemetry, time, and DSIF ground-station functions was identified, each data frame time-tagged, and the data put in a format for further processing. Because the time tag inserted in the data may be incorrect, a re-edit run was used to correct time according to a manual review of the data. The edit and re-edit functions were actually performed separately for each station and for each data source. After re-editing, the sources from a given station for a given tracking period were merged to produce a best-data stream for that tracking period. After the individual station merges were complete, a composite merge was performed to eliminate overlap between stations and to produce the master data library.

The extract program selects the data assigned to a given experiment from each frame and, with time-correlated comments, provides a magnetic tape in the appropriate format for each experiment. From these

extract tapes it was expected that the experimenters would perform their detailed scientific analyses. Because no absolute percentage of such as 99% or 99.5% of the transmitted data was an adequate measure of the adequacy of a given portion of the master data library, a committee composed of both the producers and users decided whether each week was satisfactory or required additional effort. The prime considerations were

1. Reliability of time tagging.
2. Inclusion of data for those periods known to be interesting.
3. Exclusion of data gaps that would prevent detailed processing such as power-spectrum analyses.

**E. Summary**

This paper has described the three major aspects of data processing for the *Mariner* project: test-data processing, flight-operations support-data processing, and master-data library processing.

In each case the extent and depth of processing has been related to the time the results are required by the user for responsive action. Problems have been plentiful, but their solutions and the experience gained has accumulated the knowledge necessary for confident planning and support of future interplanetary spacecraft missions.

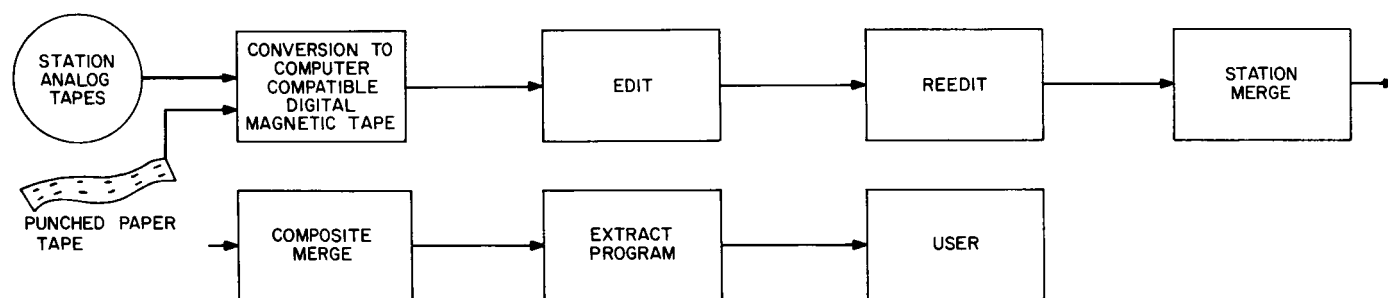


Fig. 7. Master data library processing system